The Indian Ocean Dipole: Impact on the ENSO–Monsoon Relationship

(Ashok et al., 2001, 2004, 2007)

(* Koica Training Material)

Karumuri Ashok

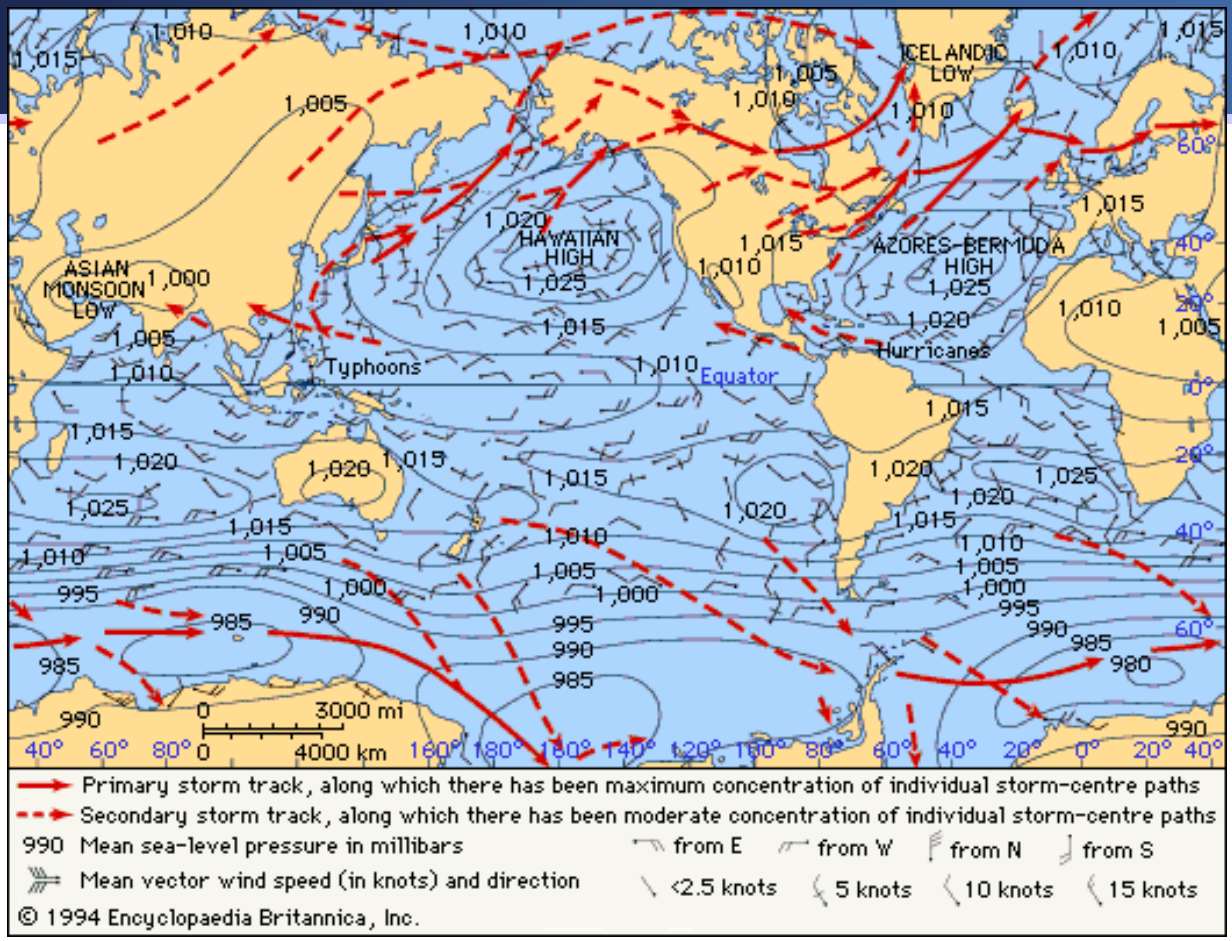

Figure 3: World distribution of mean sea-level pressure (in millibars) for July, and primary and secondary storm tracks. The general character of the global winds is also shown.(*From H.L. Crutcher and O.M. Davis, Navy Marine Climatic Atlas of the World, vol.8, NAVAIR 50-1C-54; U.S. Naval Weather Service Command*)

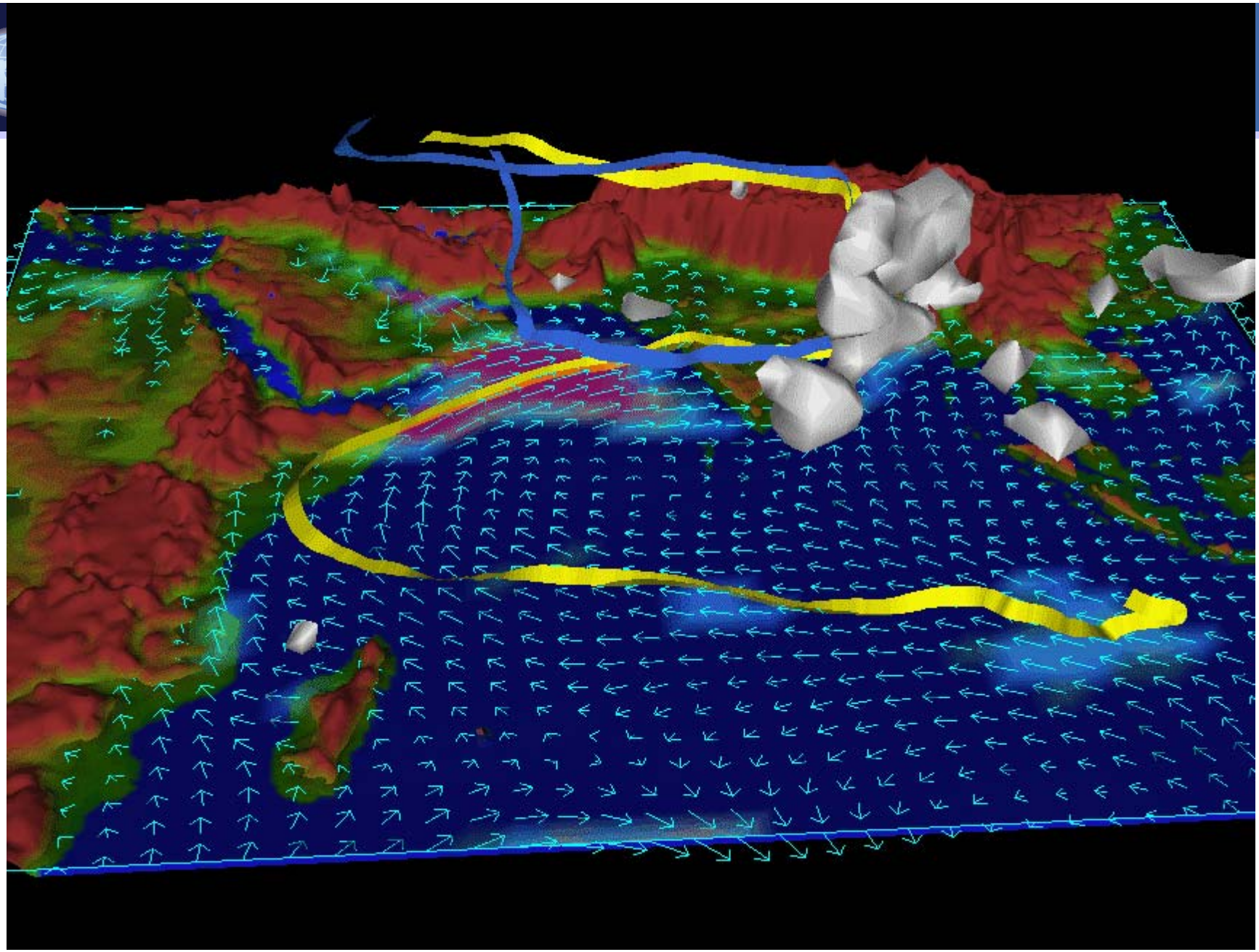

www.nassmc.org/pictures/indian_monsoon.html

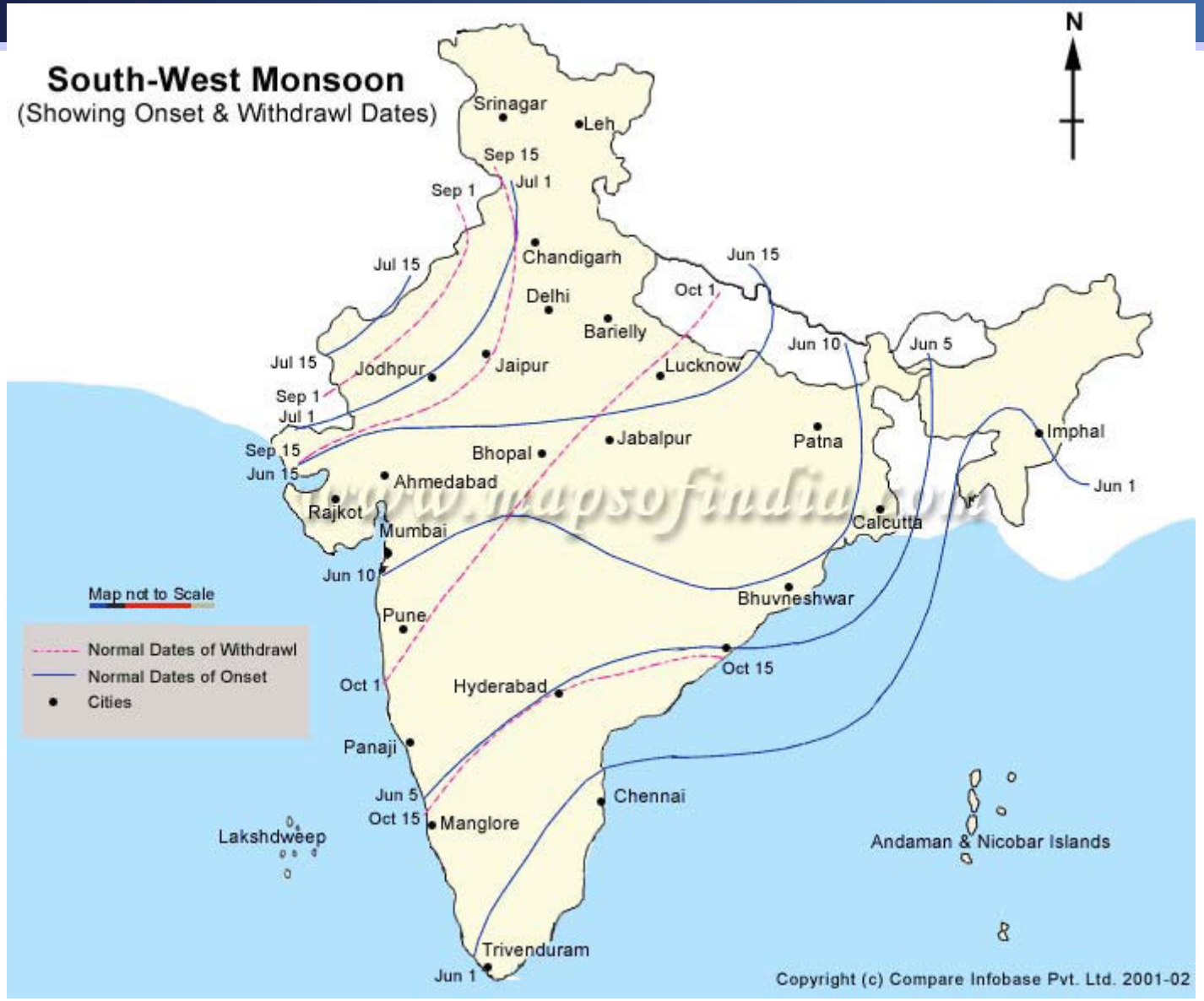
South-West Monsoon
(Showing Onset & Withdrawl Dates)
N
Srinagar
Leh
Sep 15
Jul 1
Sep 1
Chandigarh
Jul 15
Jun 15
Delhi
Oct 1
Bareilly
Jun 10
Jun 5
Jul 15
Jodhpur
Jaipur
Lucknow
Sep 1
Jul 1
Imphal
Sep 15
Jun 15
Bhopal
Jabalpur
Patna
Jun 1
Ahmedabad
Rajkot
Mumbai
Calcutta
Jun 10
Bhuvneshwar
Map not to Scale
Pune
Normal Dates of Withdrawl
Normal Dates of Onset
Cities
Oct 1
Hyderabad
Oct 15
Panaji
Jun 5
Chennai
Oct 15
Manglore
Lakshdweep
Andaman & Nicobar Islands
Trivenduram
Jun 1
Copyright (c) Compare Infobase Pvt. Ltd. 2001-02

Introduction

- The Indian summer monsoon rainfall (ISMR) occurring during June-September plays a crucial role on both the agriculture and economy of the Indian subcontinent.
- Of the many phenomena that excite the ISMR variability [*Krishna Kumar et al.,* 1995, *Slingo,* 1999], the most important large-scale forcing was the El Niño/Southern Oscillation (ENSO) till late 1980s.
- The interannual variations of ISMR have motivated studies of the ENSO since the turn of the twentieth century [*Walker,* 1923, *Barnett,* 1984]. It is widely known that there was a negative correlation between the anomalies of the ISMR and NINO3 SSTA (area-averaged sea surface temperature anomalies over 5°N-5°S, 150W°-90°W).

Introduction (Cont'd)

- However, the relationship between the ISMR and ENSO was found to be weakening (*Krishna Kumar et al.,* 1999).
- IOD discovered (1999).

- *Link?*

Background of IOD

- Dipolelike SST anomalies
- equatorial wind anomalies
- sea level low(high) in the east(west)
- suppressed(enhanced) rain in the east(west)
- ocean dynamics may play a significant role
- strong cross correlation between all the variables mentioned above

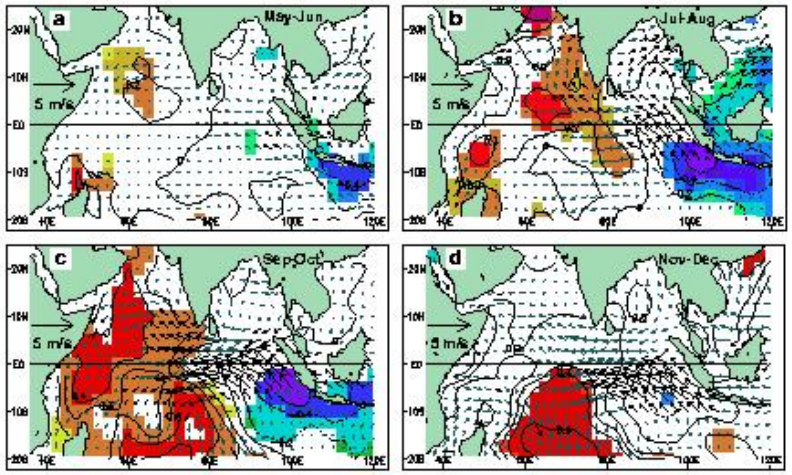

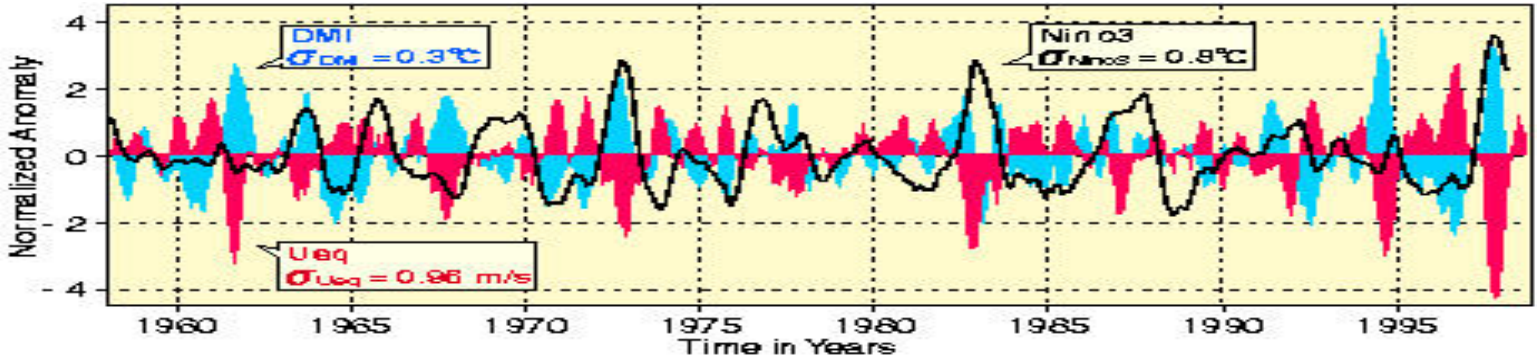

- *Saji et al. (2001)'s IODMI: SSTA(-10°S-10°N, 50°-70°E)-SSTA (10°S-Equator,*
- *90°E-110°E).*

Positive IOD

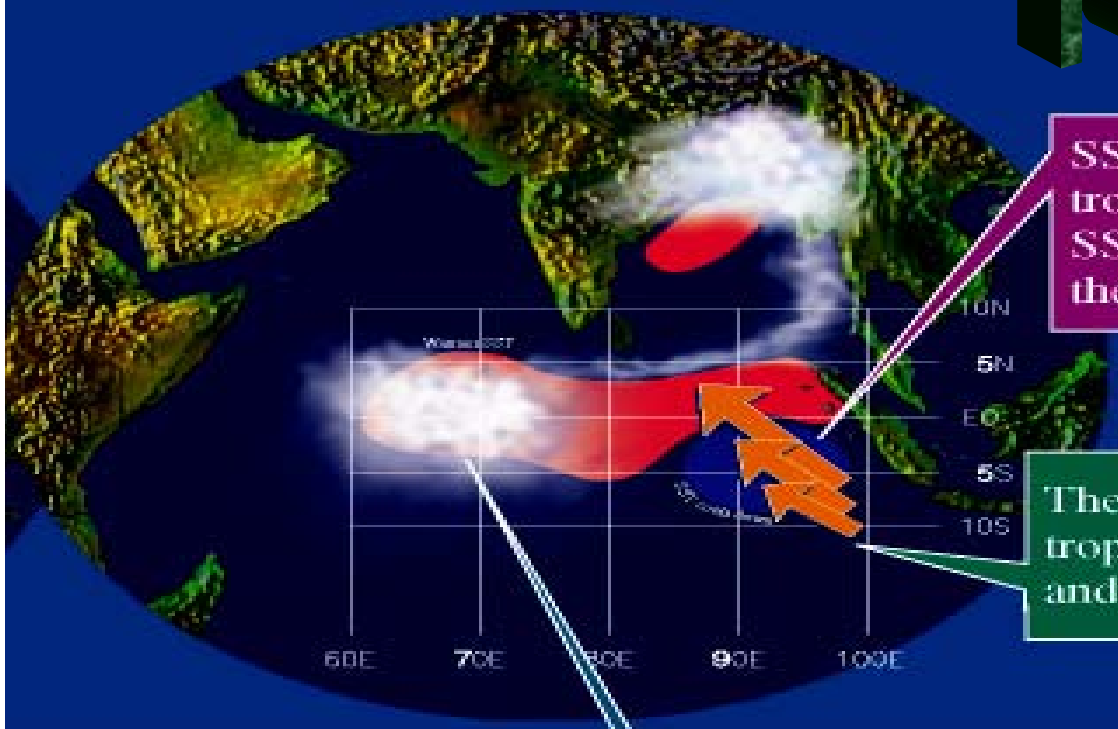

SST cools down in the southeast tropical Indian Ocean, making the SST distribution asymmetric about the equator.

The southeast trades at the southeast tropical Indian Ocean has strengthened and extended across the equator.

The OTCZ has disappeared; convection has strengthened over the tropical western Indian Ocean where the SST is warmer than usual.

Hypotheses on the origins of the variability

- It is a part of ENSO (Baquero-Bernal&Latif 2001, Hendon 2003) : cannot explain independent events

- Triggered by ENSO at times (Xie et al 2001, Annamalai et al 2003), by monsoon variability at others (Wang et al 2003), by ISO's (Li et al 2003) or by Southern Hemisphere variability (annular mode?, Lau and Nath 2003).

Hypotheses on the origins of the variability

- QBO (Meehl et al. 2003)

- Inherent oscillation (Saji et al 1999, Rao et al. 2002, Yamagata et al 2002). Ashok et al (2003a)'s wavelet coherence also demonstrates that IOD events largely due to intra-basin coupled processes.

IOD variability

- The primary significant power at biennial peak (Saji et al, 1999), followed by a quasi-pentadal peak (Ashok et al., 2003a; *from GISST 1871-1998*).
- *Also, significant at 90% confidence level is a peak at 125-months (Ashok et al. 2003a; from GISST 1871-1998*).

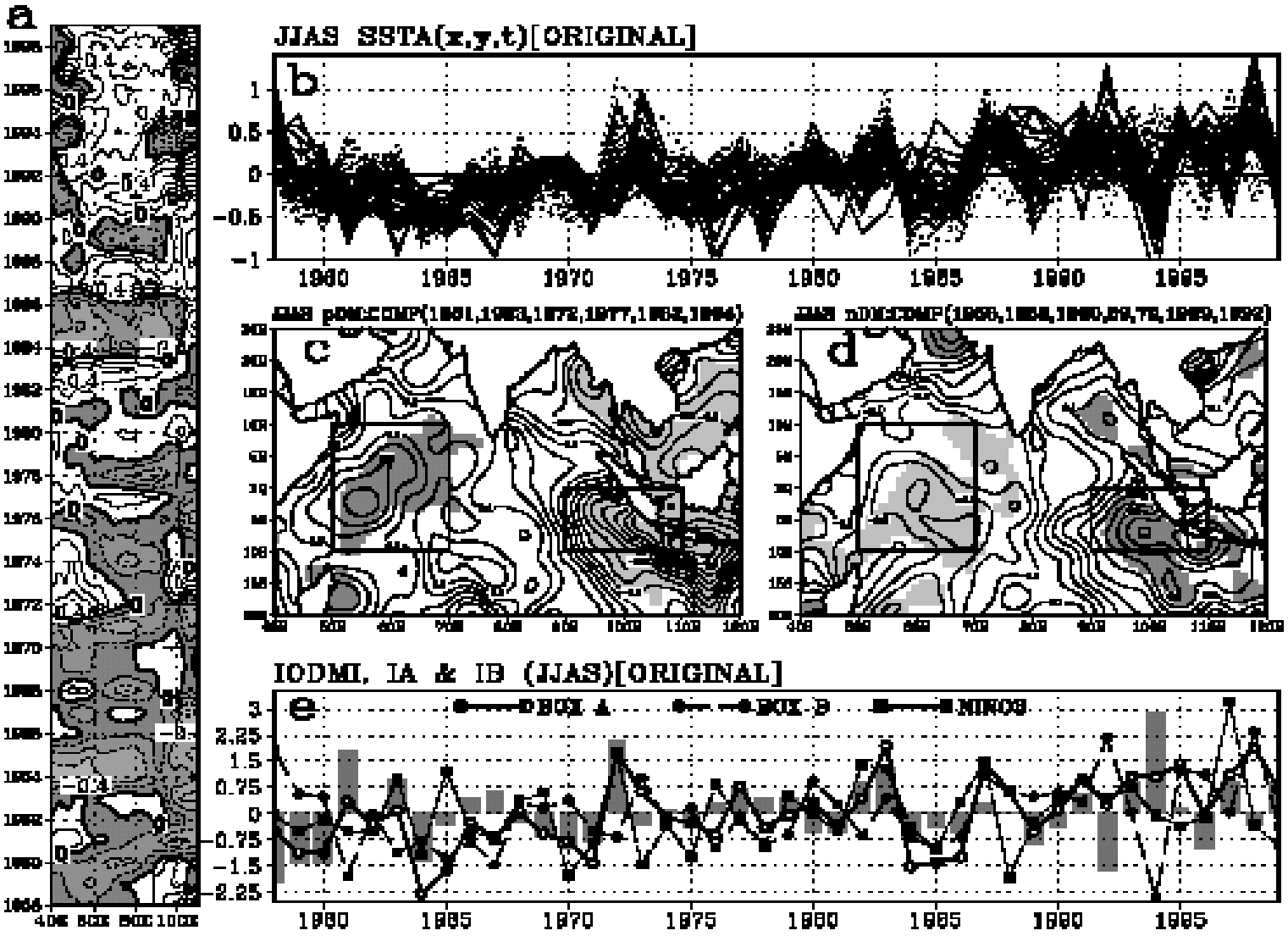
a
JJAS SSTA(x,y,t)[ORIGINAL]
b
1
0.5
0
−0.5
−1
1960
1965
1970
1975
1980
1985
1990
1995
c
d
IODMI, IA & IB (JJAS)[ORIGINAL]
e
BOX A
BOX B
NINO3
3
2.25
1.5
0.75
0
−0.75
−1.5
−2.25

Data (From 1958-1997)

- ISMR data (Parthasarathy et al., 1993) available from http://www.tropmet.res.in
- GISST dataset (Raynet et al., 1996)
- Global rainfall data set (Le Gates and Willmont, 1991)
- NCEP/NCAR wind analysis (Kalnay et al., 1996)

The correlation between the IOD and Indian rainfallas 0.32 (Saji,1999). However, of the 11 intense (anomalies more than one standard deviation) positive IOD events that occurred during 1958–1997, eight events (1961, 1963, 1967, 1977, 1983, 1993, 1994, and 1997; 73% of the positive IOD events during this period) correspond with the positive anomalies of the concurrent ISMR. Similarly, of the three negative IOD events during this 1958–1997, two events (1960 and 1992; 67% of the negative IOD events) correspond with negative anomalies of the ISMR.

This observation, and the frequent occurrence of intense IOD events in the last decade, has prompted us to investigate whether the moving correlation between the IOD–ISMR changes from decade to decade and, in particular, its role in the weakening of the monsoon–ENSO correlation.

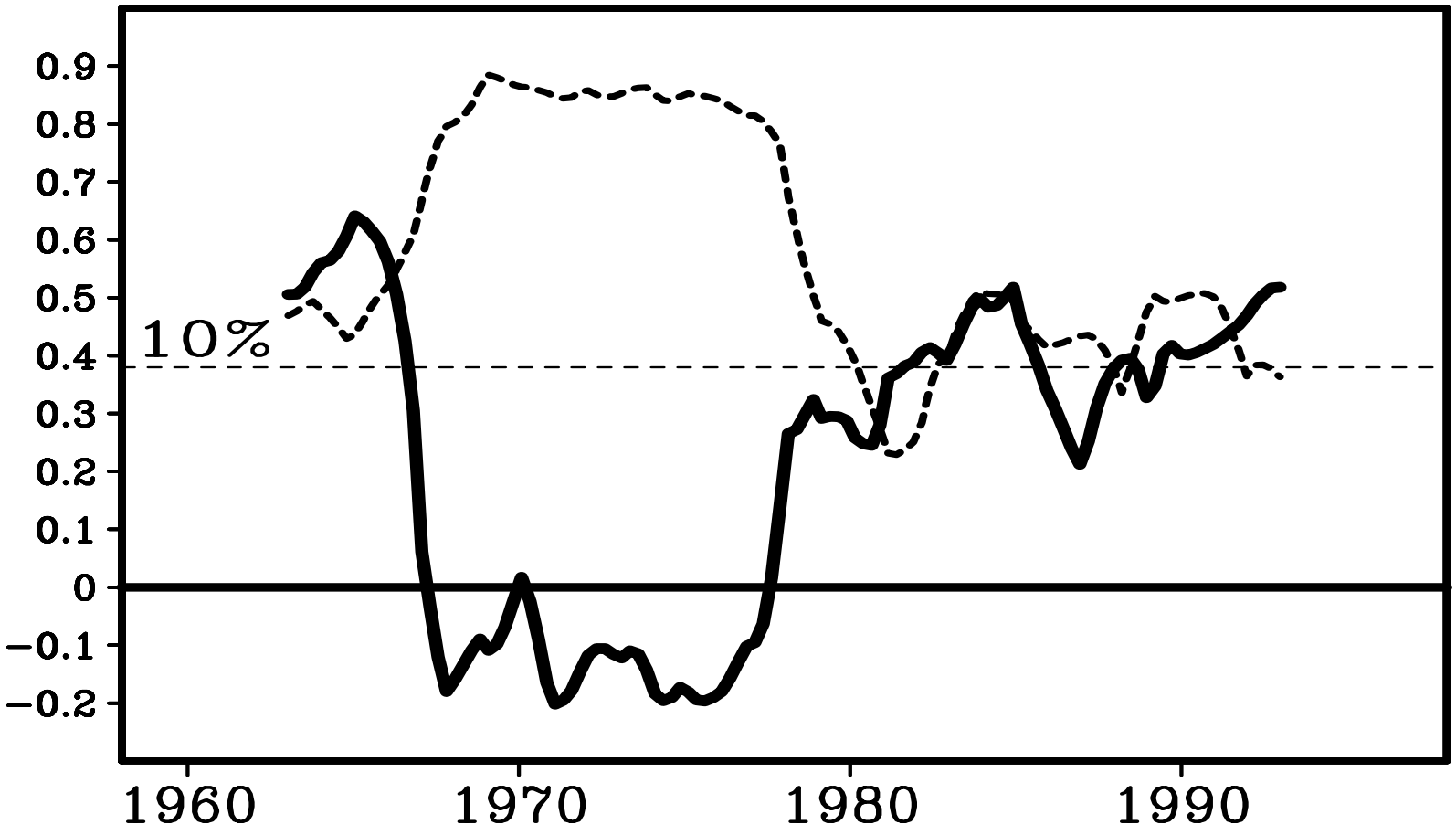

The 41-month sliding correlation coefficients between ISMR and IODMI (solid), and those between monthly ISMR and NINO3 SST (dashed; to be multiplied by −1) during 1958-1997. The significant correlation value at 90% confidence level is 0.38 (verified by 1,000 randomized time series, using the Monte-Carlo simulations)

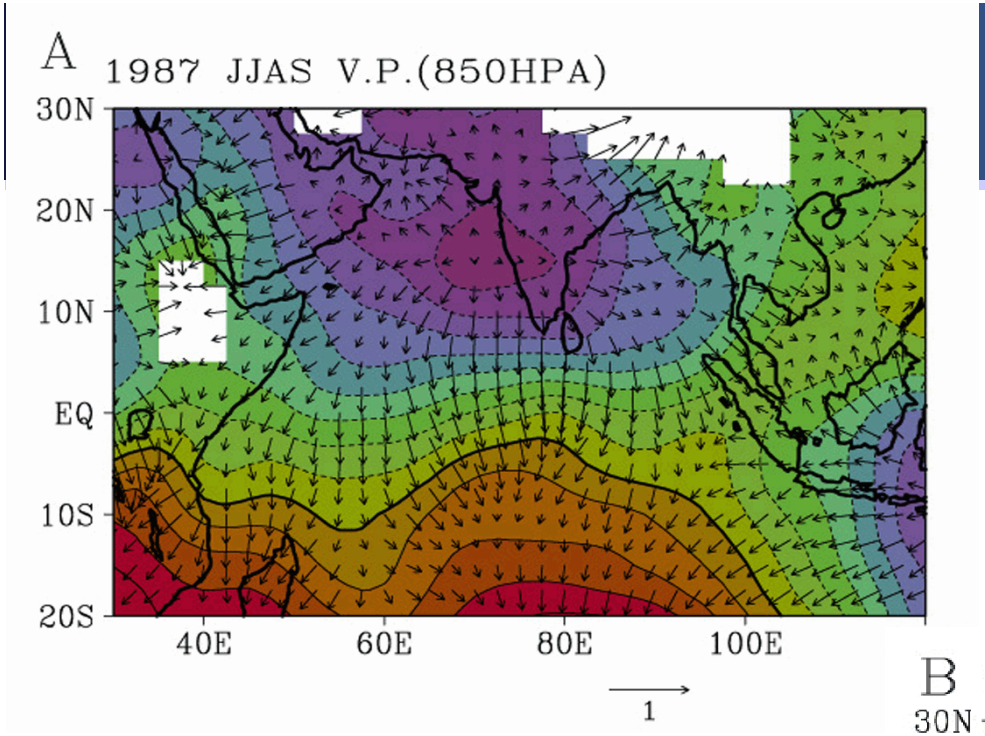
A
1987 JJAS V.P.(850HPA)
30N
20N
10N
EQ
10S
20S
40E
60E
80E
100E
1

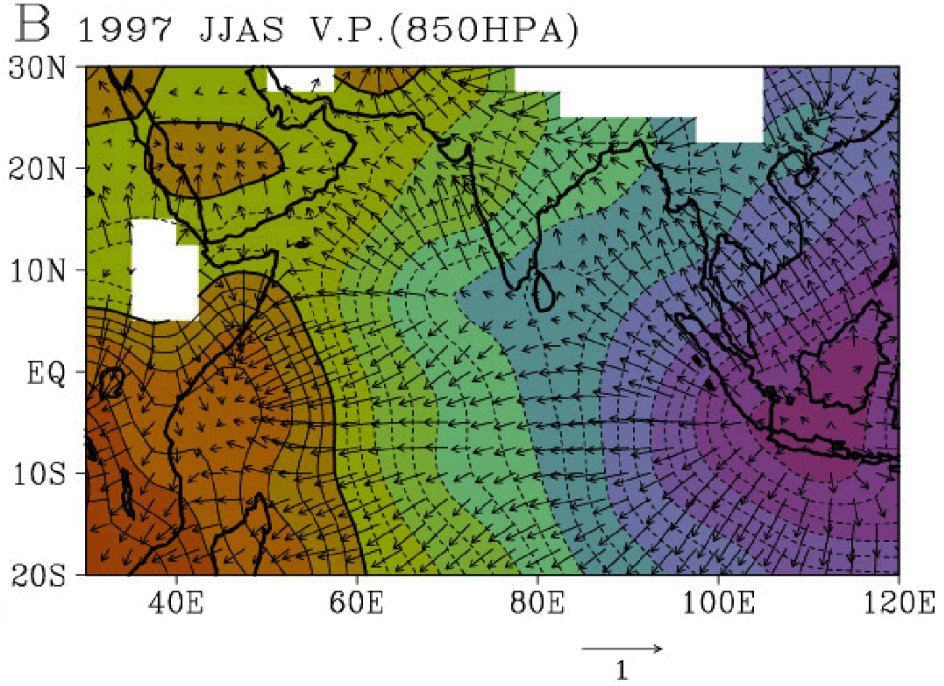
B
1997 JJAS V.P.(850HPA)
30N
20N
10N
EQ
10S
20S
40E
60E
80E
100E
120E
1

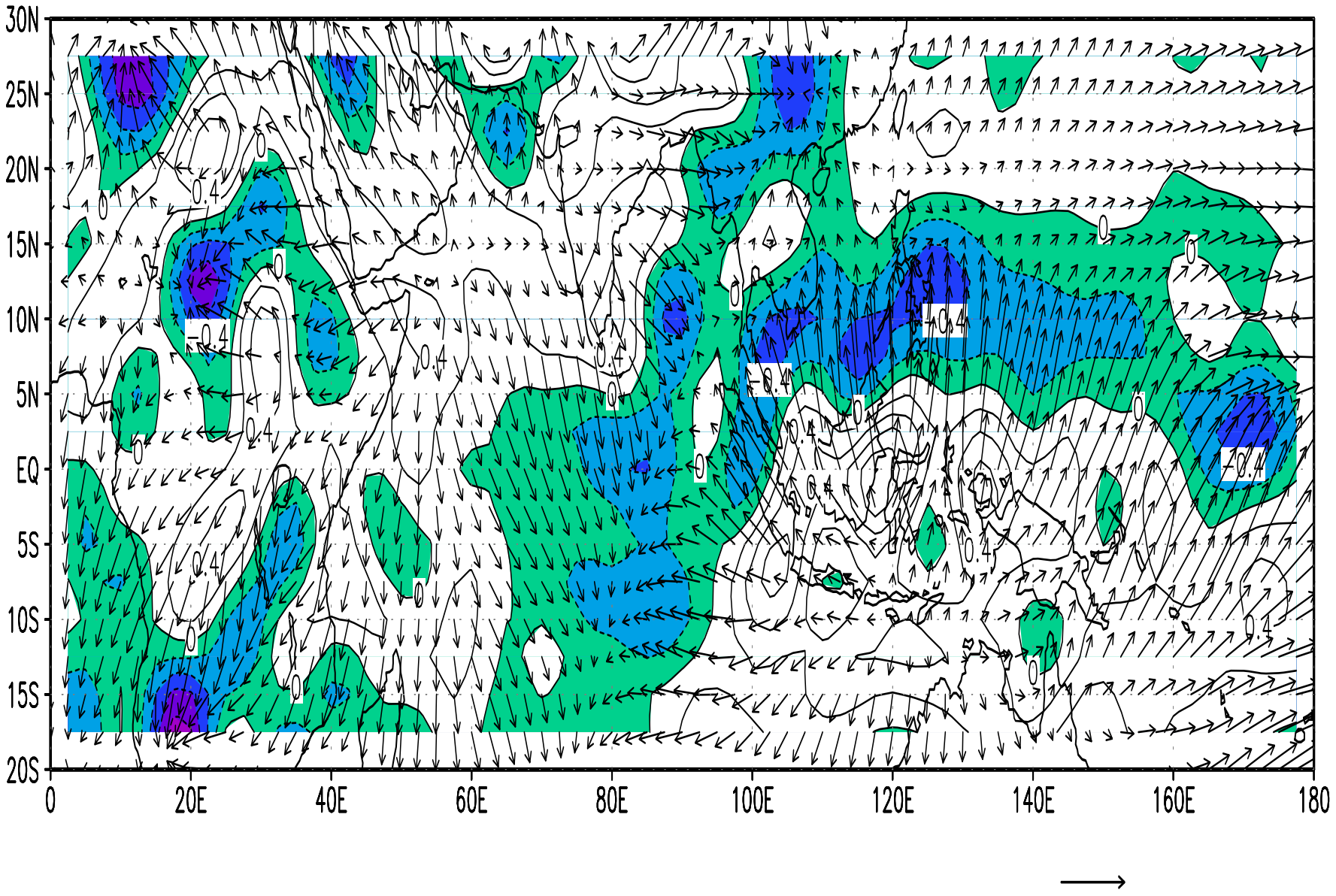
1957,65,72,82,86,87,91 mC V.P. 850hPa
30N
25N
20N
15N
10N
5N
EQ
5S
10S
15S
20S
0
20E
40E
60E
80E
100E
120E
140E
160E
180

1957,65,72,82,86,87,91 mC V.P.A. 200hPa

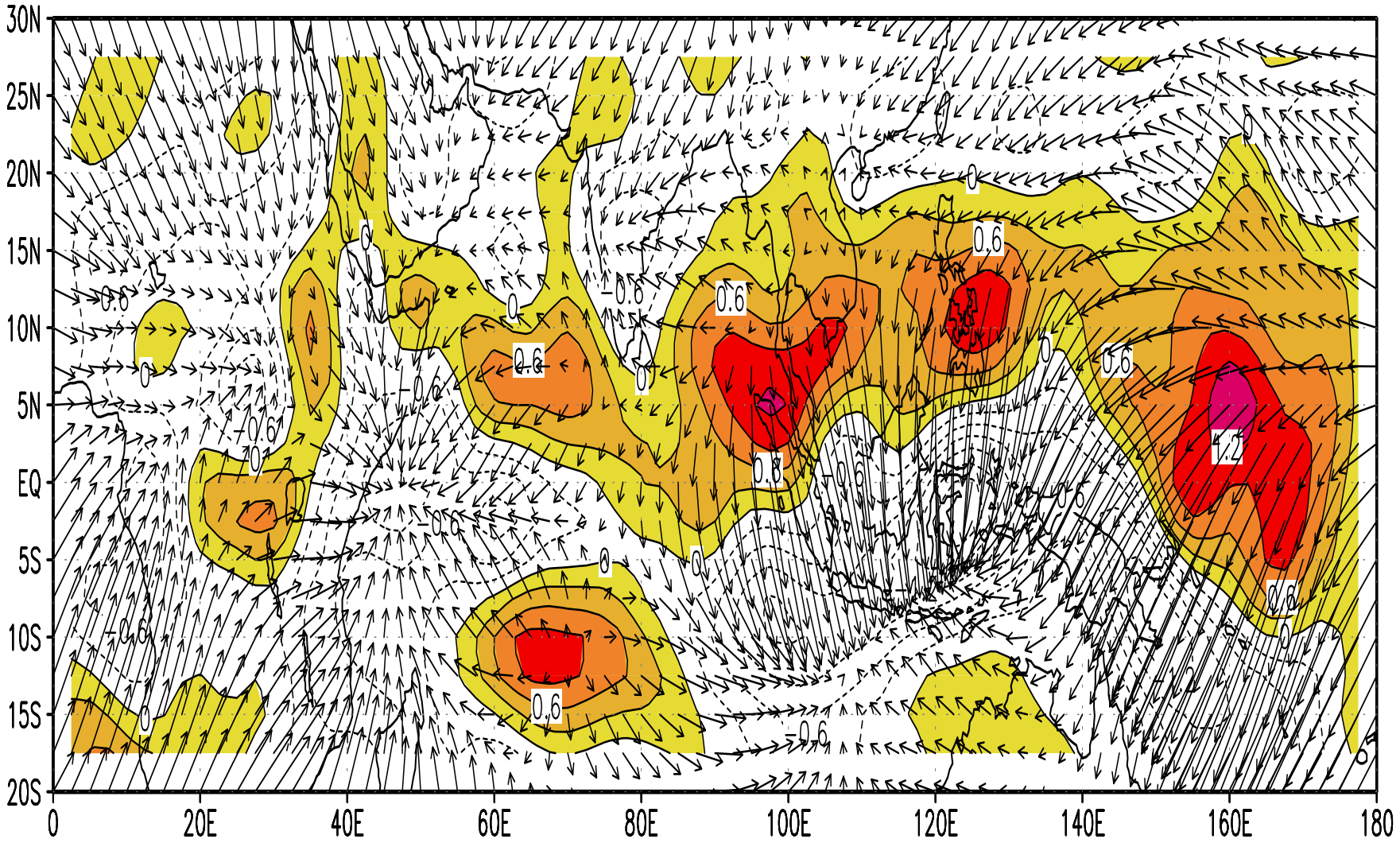

The Frontier Atmospheric General Circulation Model version 1.0 (FrAM1.0)

- ***T42***
- ***Hybrid Vertical Co-Ordinates; 28 layers***
- ***Cumulus convection (Kuo, 1974)***
- ***Long Wave Radiation (Shibata and Aoki, 1989), Shibata (1989)***
- ***Short Wave Radiation (Lacis and Hansen, 1974)***
- ***Vertical Mixing (Miller and Yamada, 1974)***
- ***Land surface Model (Viterbo and Beljaars, 1995)***

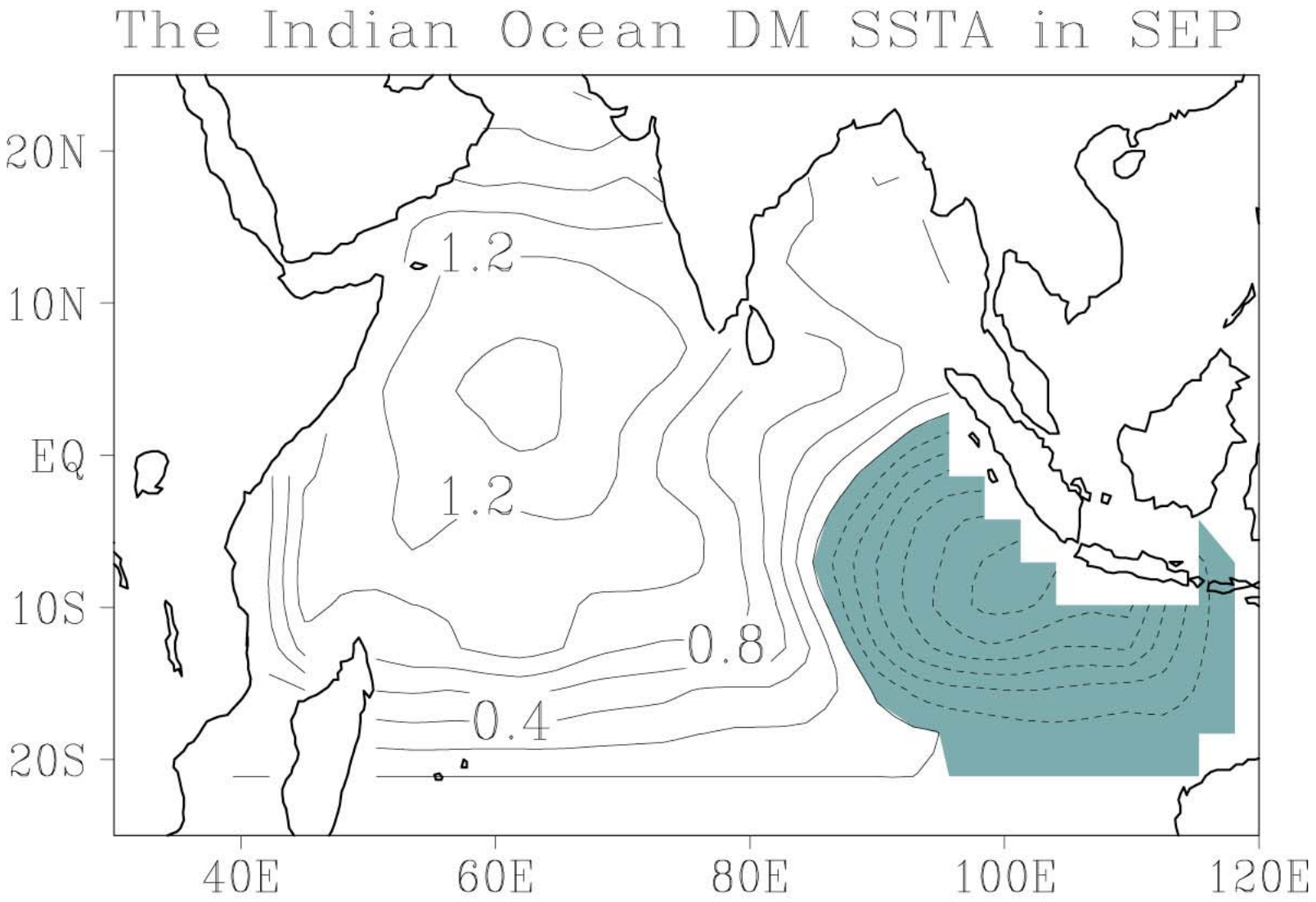

SSTA forcing for Positive Dipole type of AGCM experiments

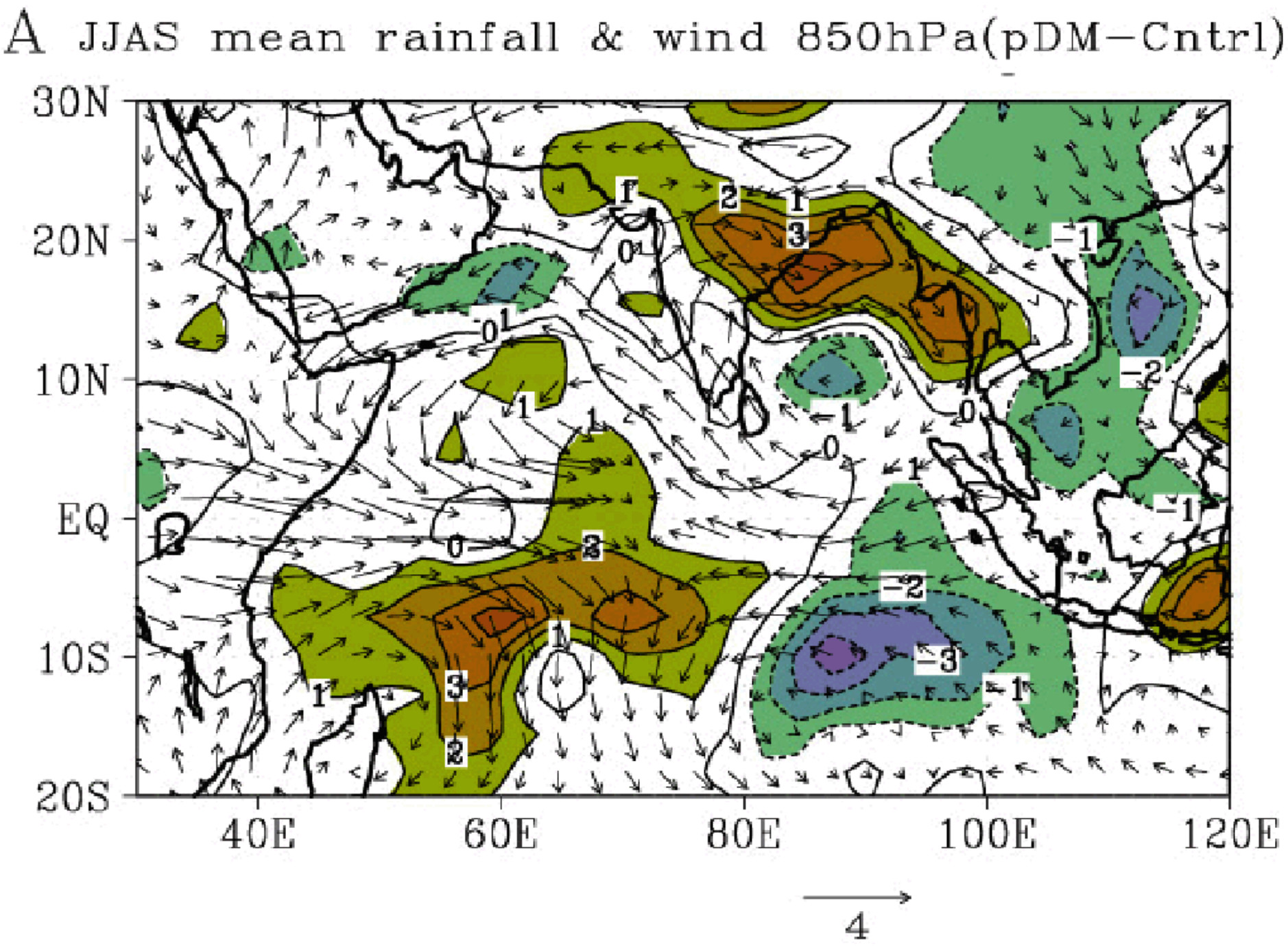
A JJAS mean rainfall & wind 850hPa(pDM−Cntrl)
30N
20N
10N
EQ
10S
20S
40E
60E
80E
100E
120E
4

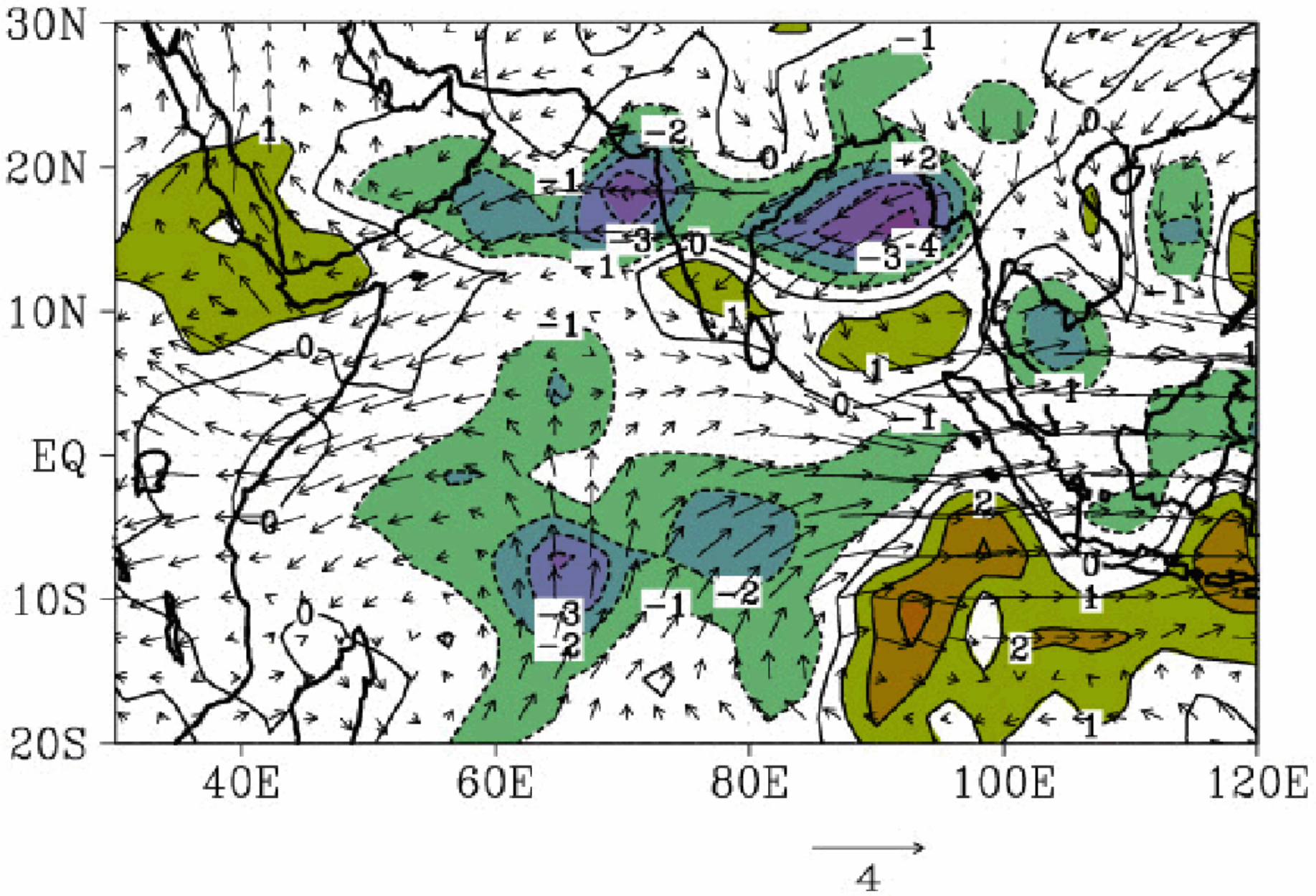
B JJAS mean rainfall & wind 850hPa(nDM−Cntrl)
30N
20N
10N
EQ
10S
20S
40E
60E
80E
100E
120E
4

A JJAS velocity potential 850hPa(pDM−nDM)

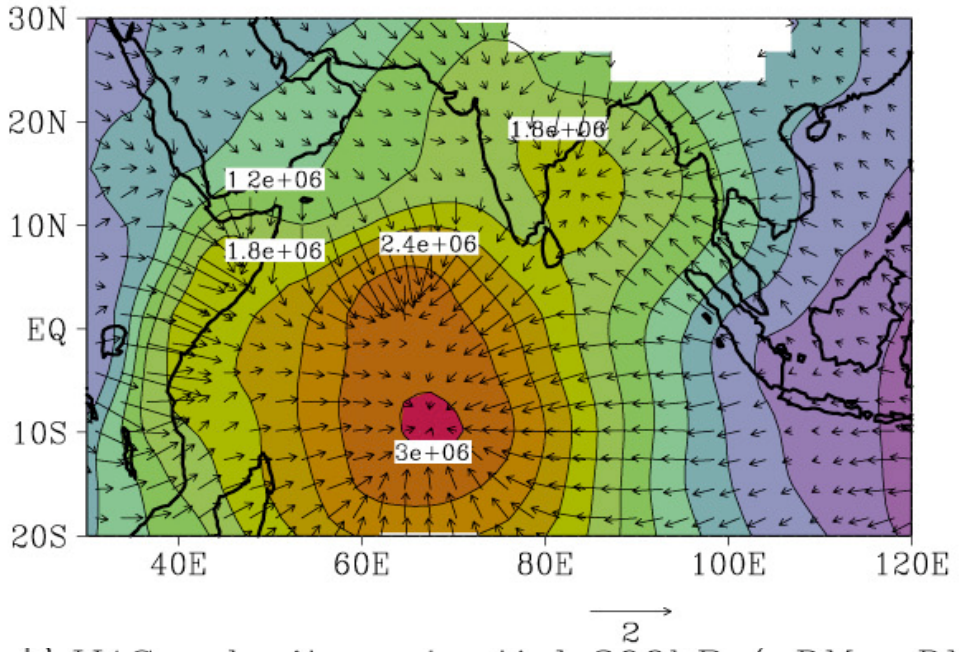

B JJAS velocity potential 200hPa(pDM−nDM)

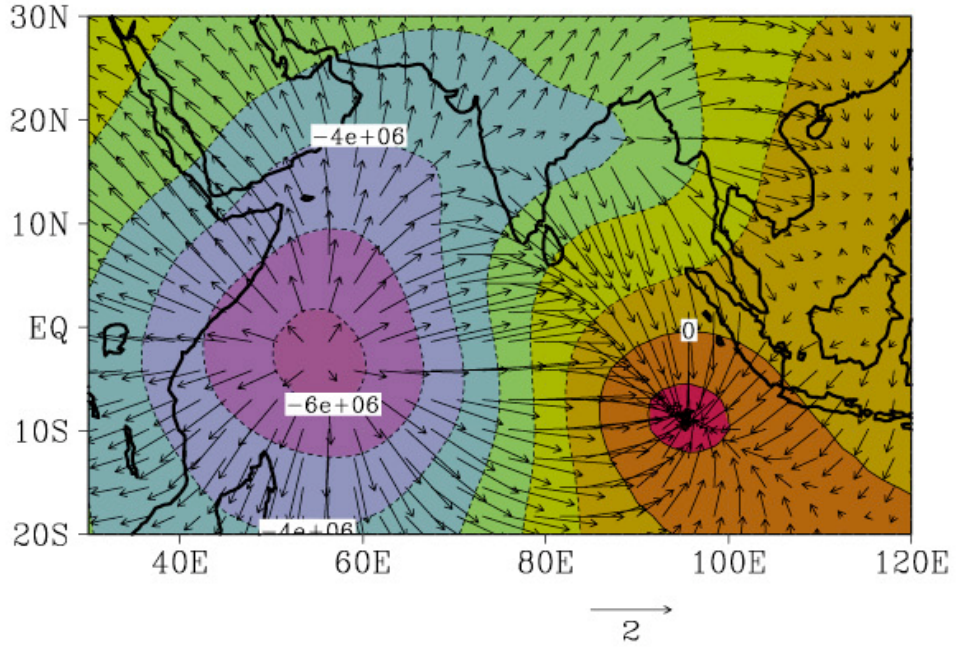

Conclusions

- *For the last four decades (till 1997) the ENSO & the IOD have complementarily influenced the ISMR.*
- *The recent weakening of the ENSO–ISMR relationship is because of the frequent occurrence of the intense IOD events in recent period.*
- *The monsoon may be the bridge to transfer the IOD influence to the mid-latitudes.*

Response of the tropical atmosphere to the Indian Ocean Dipole

- *Indian Ocean Dipole (IOD)*
- *Frontier Atmospheric General Circulation Model (FrAM1.0) Climatology*
- *Some IOD Statistics*
- *Sensitivity Experiments*
- *Summary & Conclusions*

The Frontier Atmospheric General Circulation Model version 1.0 (FrAM 1.0)

- ***T42***
- ***Hybrid Vertical Co-Ordinates; 28 layers***
- ***Cumulus convection (Kuo, 1974)***
- ***Long Wave Radiation (Shibata and Aoki, 1989), Shibata (1989)***
- ***Short Wave Radiation (Lacis and Hansen, 1974)***
- ***Vertical Mixing (Miller and Yamada, 1974)***
- ***Land surface Model (Viterbo and Beljaars, 1995)***

Boundary and initial conditions

GISST dataset is used as the lower boundary SST forcing for the FrAM1.0 in this study. SI GRID compiled at Joint Ice Center (JIC) coop erated by US NAVY and NOAA (Thompson, 19 81) is adopted for sea ice distribution. Ozone density is from the distribution of Klenk et al (1983). The maximum of topography is 4000 m. The model atmosphere is isothermal and a lso at rest at the initial time.

DP Fig.1

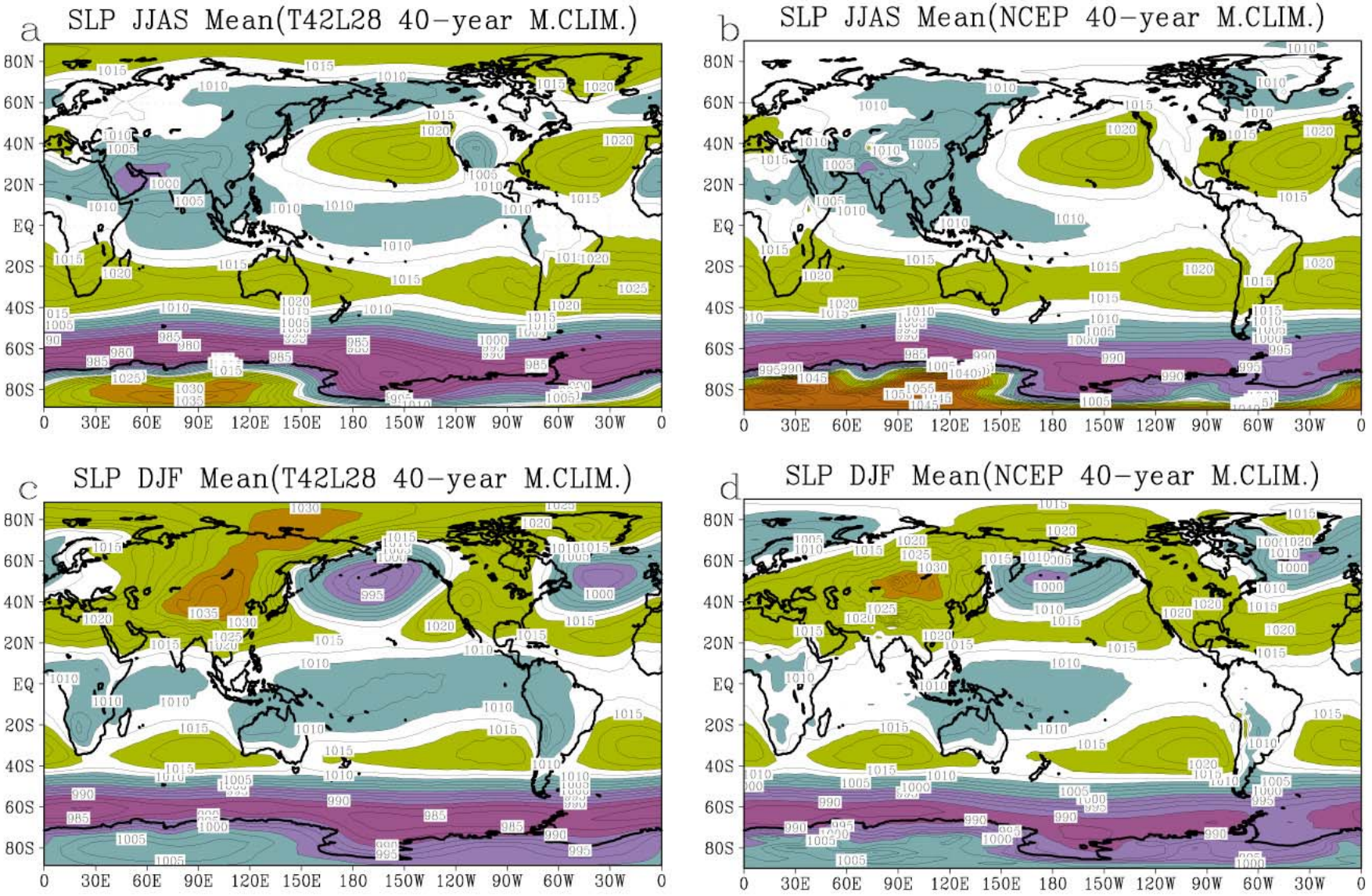
a
SLP JJAS Mean(T42L28 40-year M.CLIM.)
b
SLP JJAS Mean(NCEP 40-year M.CLIM.)
c
SLP DJF Mean(T42L28 40-year M.CLIM.)
d
SLP DJF Mean(NCEP 40-year M.CLIM.)
80N
60N
40N
20N
EQ
20S
40S
60S
80S
0
30E
60E
90E
120E
150E
180
150W
120W
90W
60W
30W
0

DP Fig.2

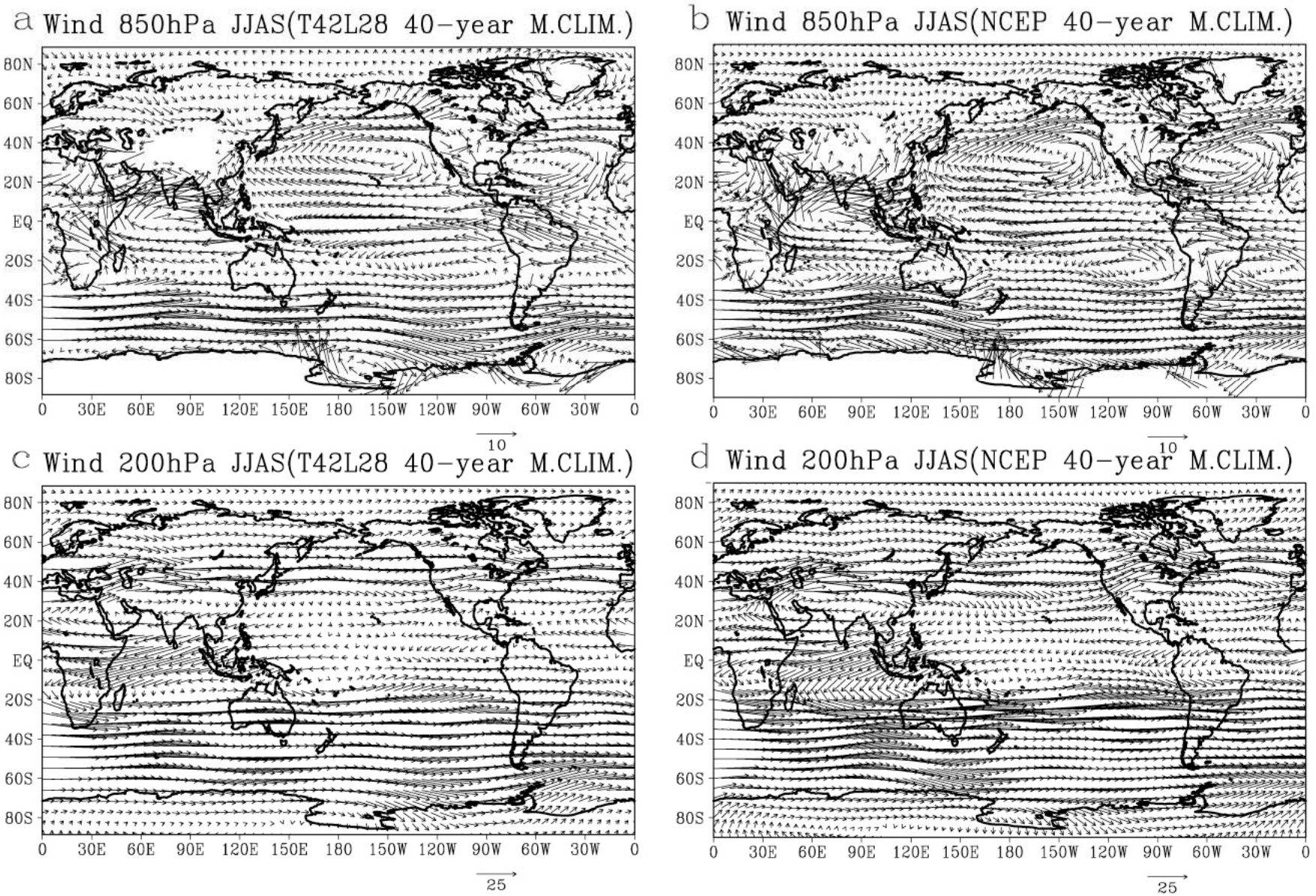
a Wind 850hPa JJAS(T42L28 40-year M.CLIM.)
b Wind 850hPa JJAS(NCEP 40-year M.CLIM.)
c Wind 200hPa JJAS(T42L28 40-year M.CLIM.)
d Wind 200hPa JJAS(NCEP 40-year M.CLIM.)
80N
60N
40N
20N
EQ
20S
40S
60S
80S
0 30E 60E 90E 120E 150E 180 150W 120W 90W 60W 30W 0
10
25

DP Fig.3

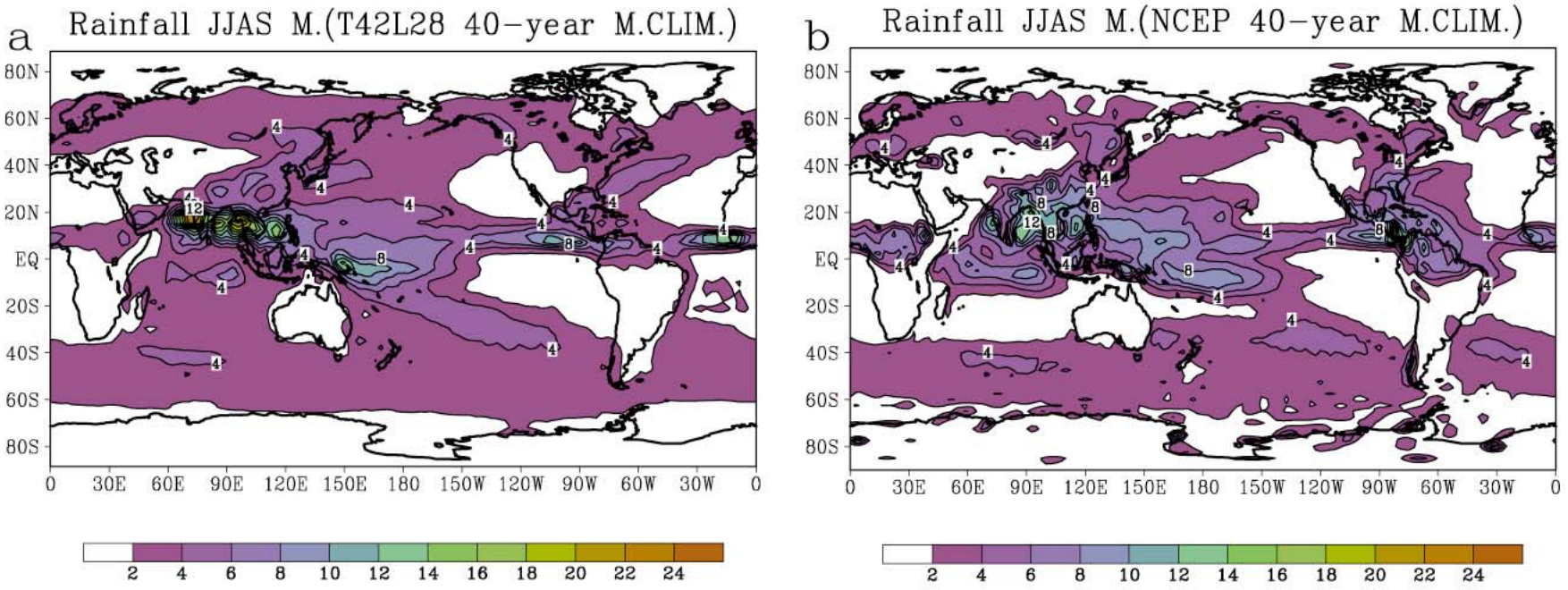
a
Rainfall JJAS M.(T42L28 40-year M.CLIM.)
80N
60N
40N
20N
EQ
20S
40S
60S
80S
0 30E 60E 90E 120E 150E 180 150W 120W 90W 60W 30W 0
2 4 6 8 10 12 14 16 18 20 22 24
b
Rainfall JJAS M.(NCEP 40-year M.CLIM.)
80N
60N
40N
20N
EQ
20S
40S
60S
80S
0 30E 60E 90E 120E 150E 180 150W 120W 90W 60W 30W 0
2 4 6 8 10 12 14 16 18 20 22 24

DP Fig.4

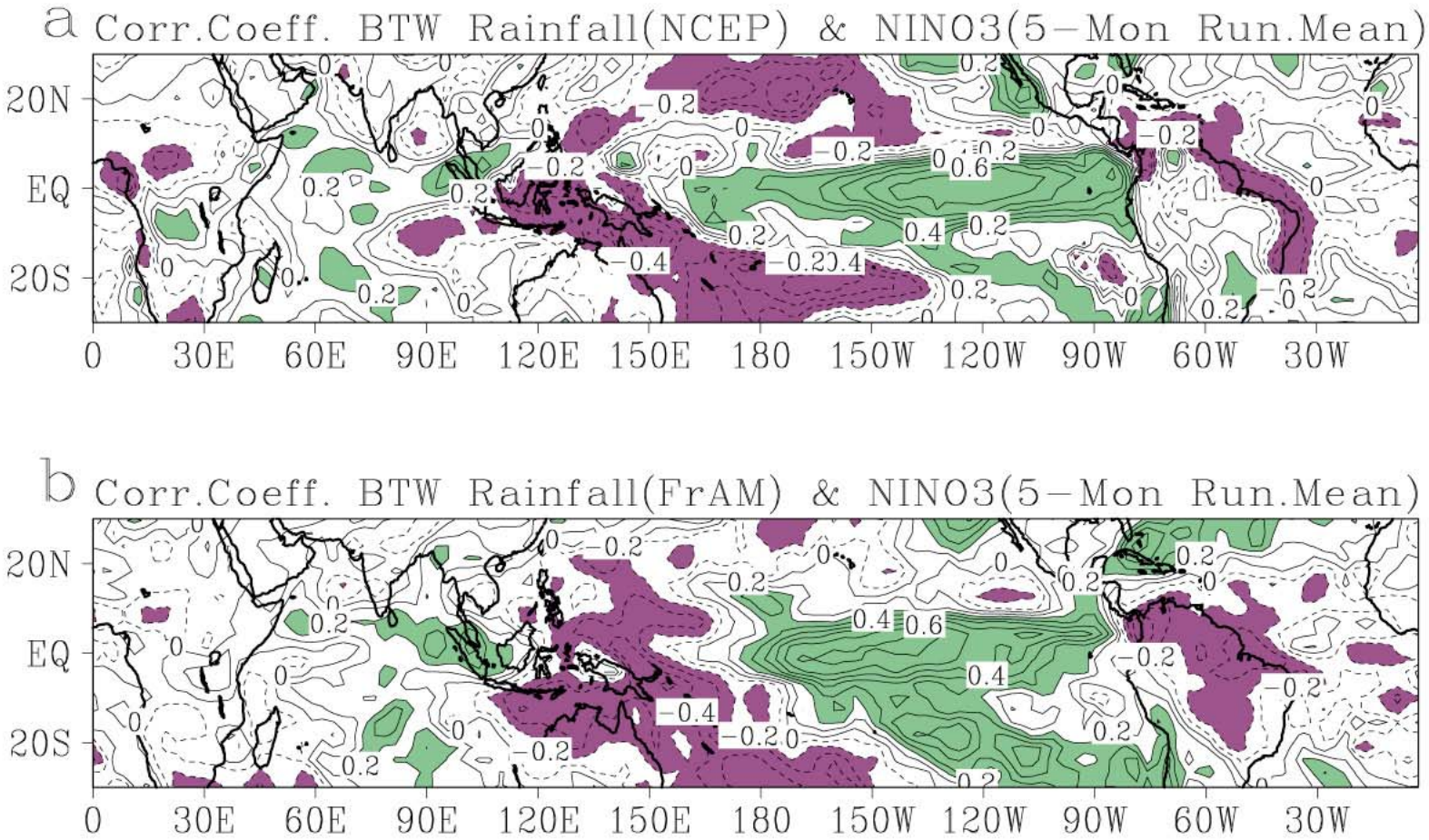
a Corr.Coeff. BTW Rainfall(NCEP) & NINO3(5-Mon Run.Mean)
20N
EQ
20S
0
30E
60E
90E
120E
150E
180
150W
120W
90W
60W
30W
b Corr.Coeff. BTW Rainfall(FrAM) & NINO3(5-Mon Run.Mean)
20N
EQ
20S
0
30E
60E
90E
120E
150E
180
150W
120W
90W
60W
30W

DP Fig.5

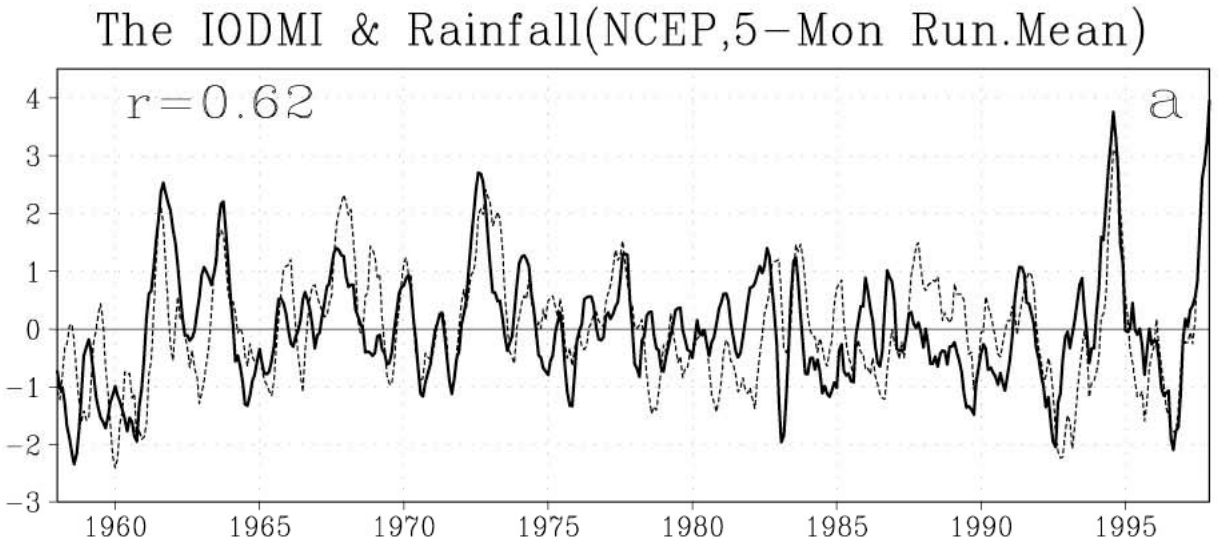

sigma rainfall 1.10mm/d
sigma iodmi 0.29 d.c.

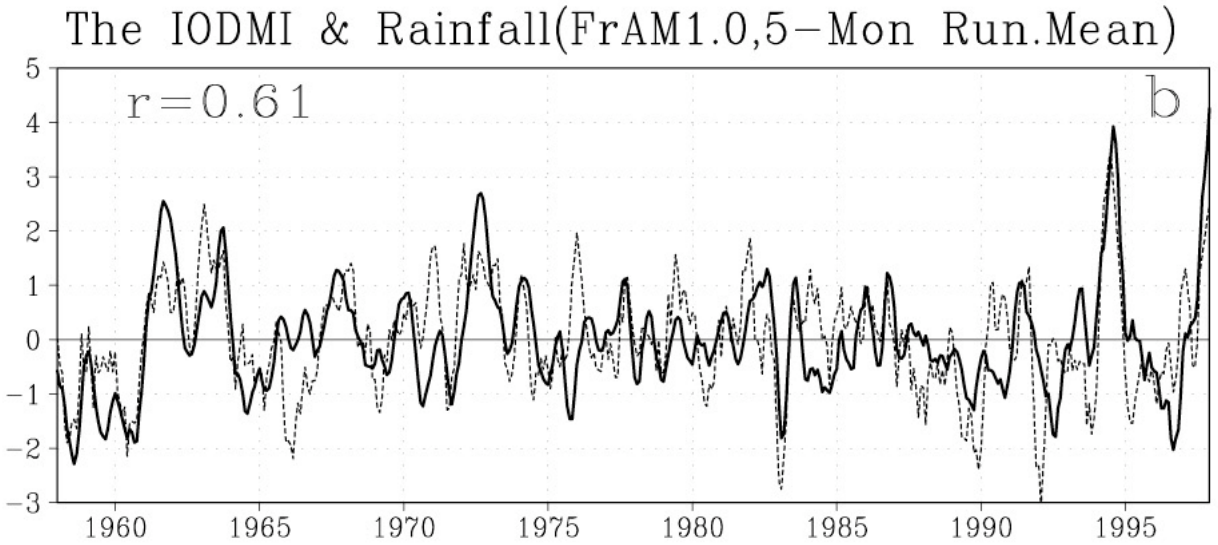

sigma rainfall 1.30 mm/d
sigma iodmi 0.29 d.c.

DP Fig.6ab

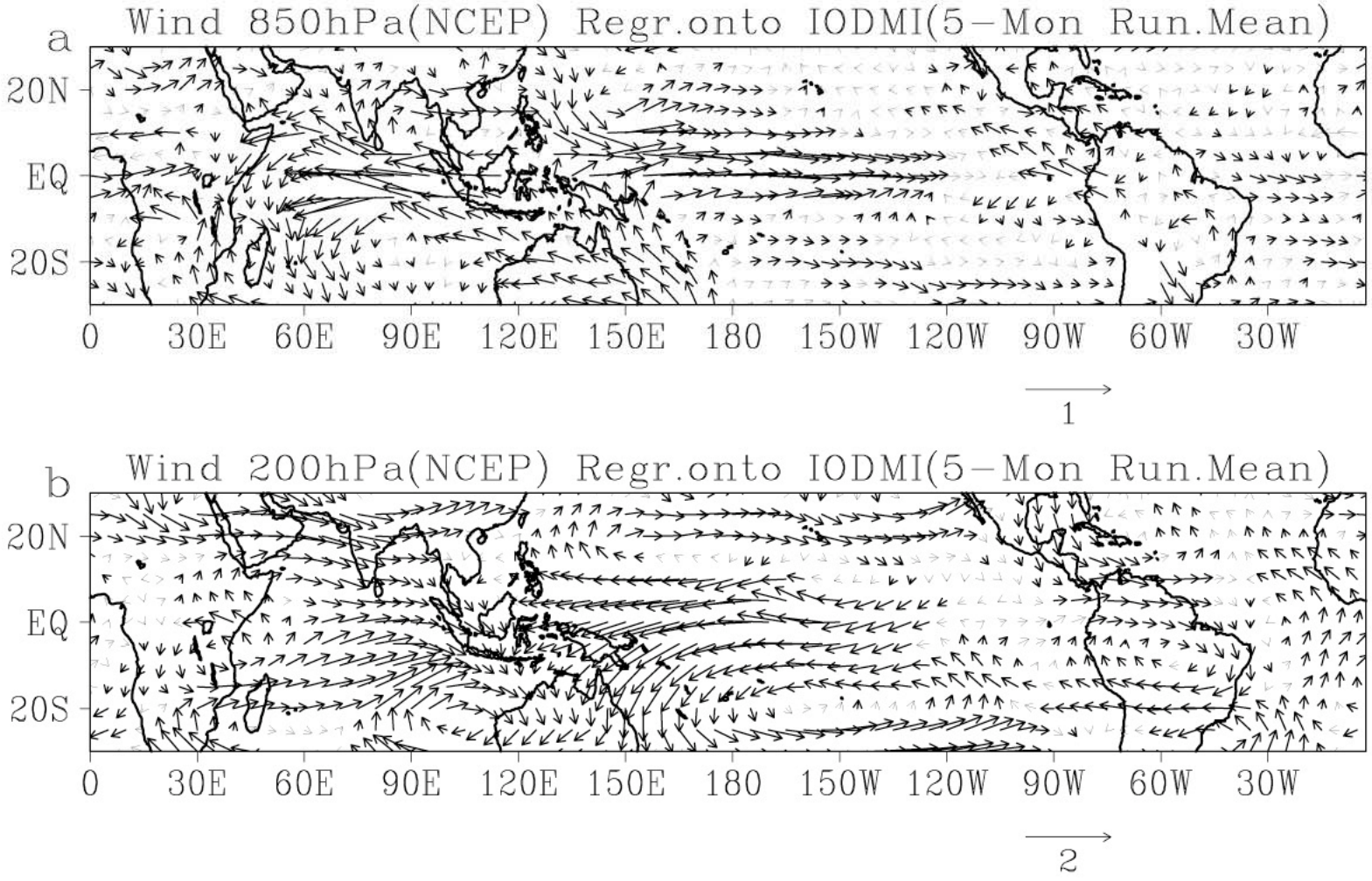
a
Wind 850hPa(NCEP) Regr.onto IODMI(5-Mon Run.Mean)
20N
EQ
20S
0
30E
60E
90E
120E
150E
180
150W
120W
90W
60W
30W
1
b
Wind 200hPa(NCEP) Regr.onto IODMI(5-Mon Run.Mean)
20N
EQ
20S
0
30E
60E
90E
120E
150E
180
150W
120W
90W
60W
30W
2

DP Fig.6cd

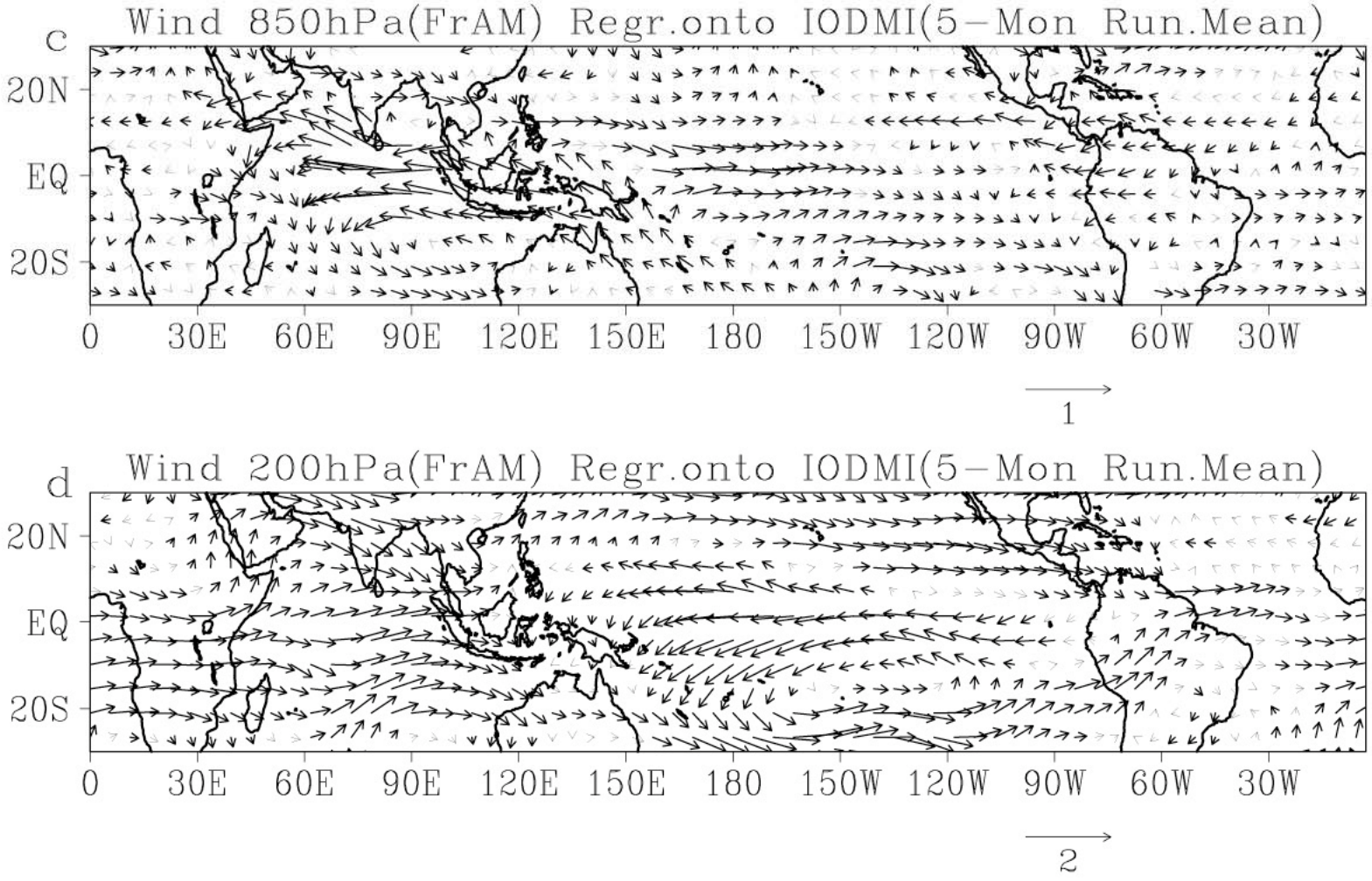
c
Wind 850hPa(FrAM) Regr.onto IODMI(5-Mon Run.Mean)
20N
EQ
20S
0
30E
60E
90E
120E
150E
180
150W
120W
90W
60W
30W
1
d
Wind 200hPa(FrAM) Regr.onto IODMI(5-Mon Run.Mean)
20N
EQ
20S
0
30E
60E
90E
120E
150E
180
150W
120W
90W
60W
30W
2

DP Fig.7

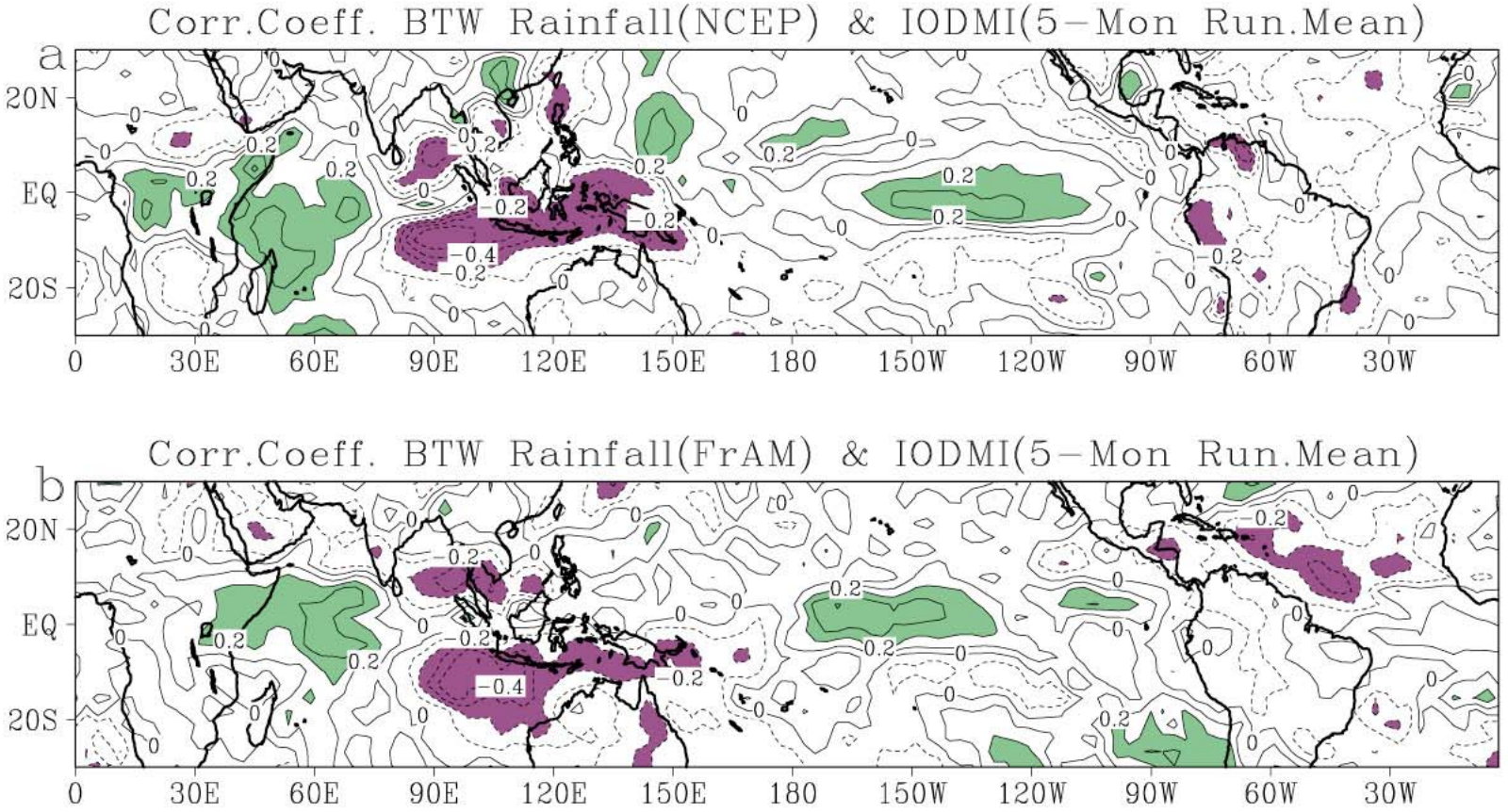
Corr.Coeff. BTW Rainfall(NCEP) & IODMI(5-Mon Run.Mean)
a
20N
EQ
20S
0
30E
60E
90E
120E
150E
180
150W
120W
90W
60W
30W
Corr.Coeff. BTW Rainfall(FrAM) & IODMI(5-Mon Run.Mean)
b
20N
EQ
20S
0
30E
60E
90E
120E
150E
180
150W
120W
90W
60W
30W

DP Fig.8

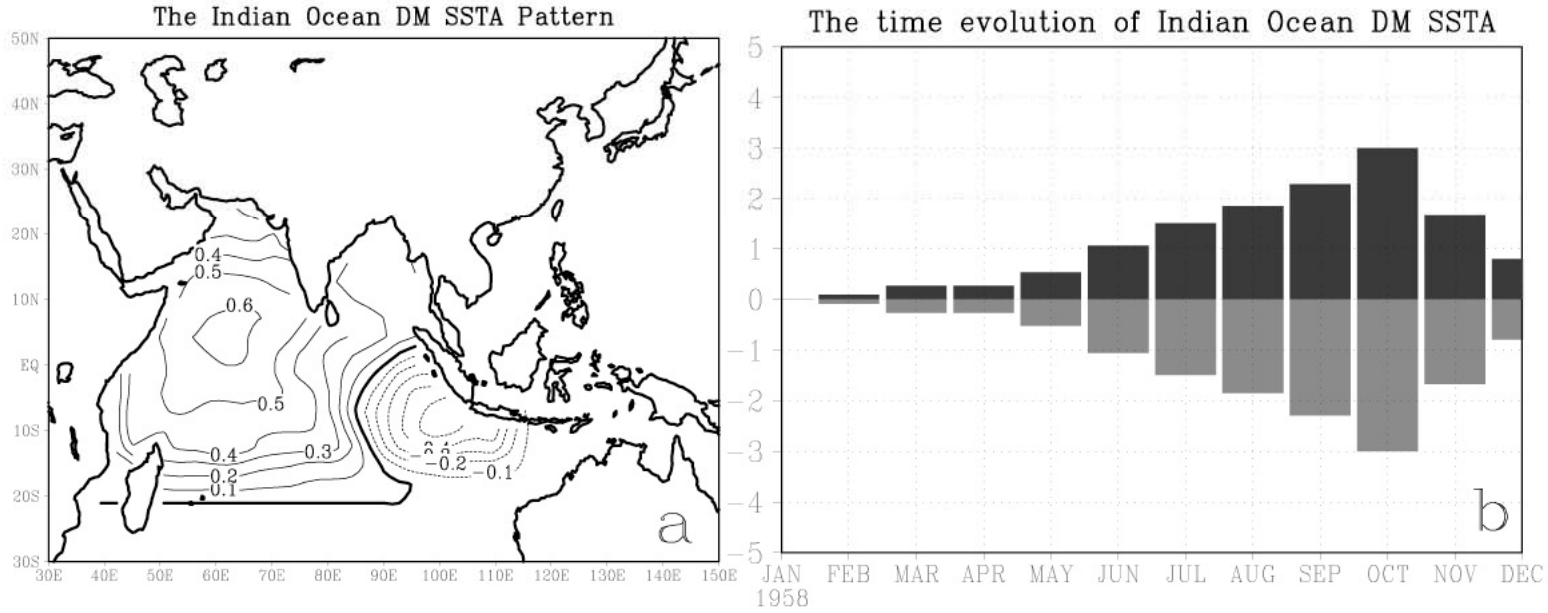
The Indian Ocean DM SSTA Pattern
50N
40N
30N
20N
10N
EQ
10S
20S
30S
30E
40E
50E
60E
70E
80E
90E
100E
110E
120E
130E
140E
150E
0.4
0.5
0.6
0.5
0.4
0.3
0.2
0.1
−0.2
−0.1
a
The time evolution of Indian Ocean DM SSTA
5
4
3
2
1
0
−1
−2
−3
−4
−5
JAN
1958
FEB
MAR
APR
MAY
JUN
JUL
AUG
SEP
OCT
NOV
DEC
b

DP Fig.9ab

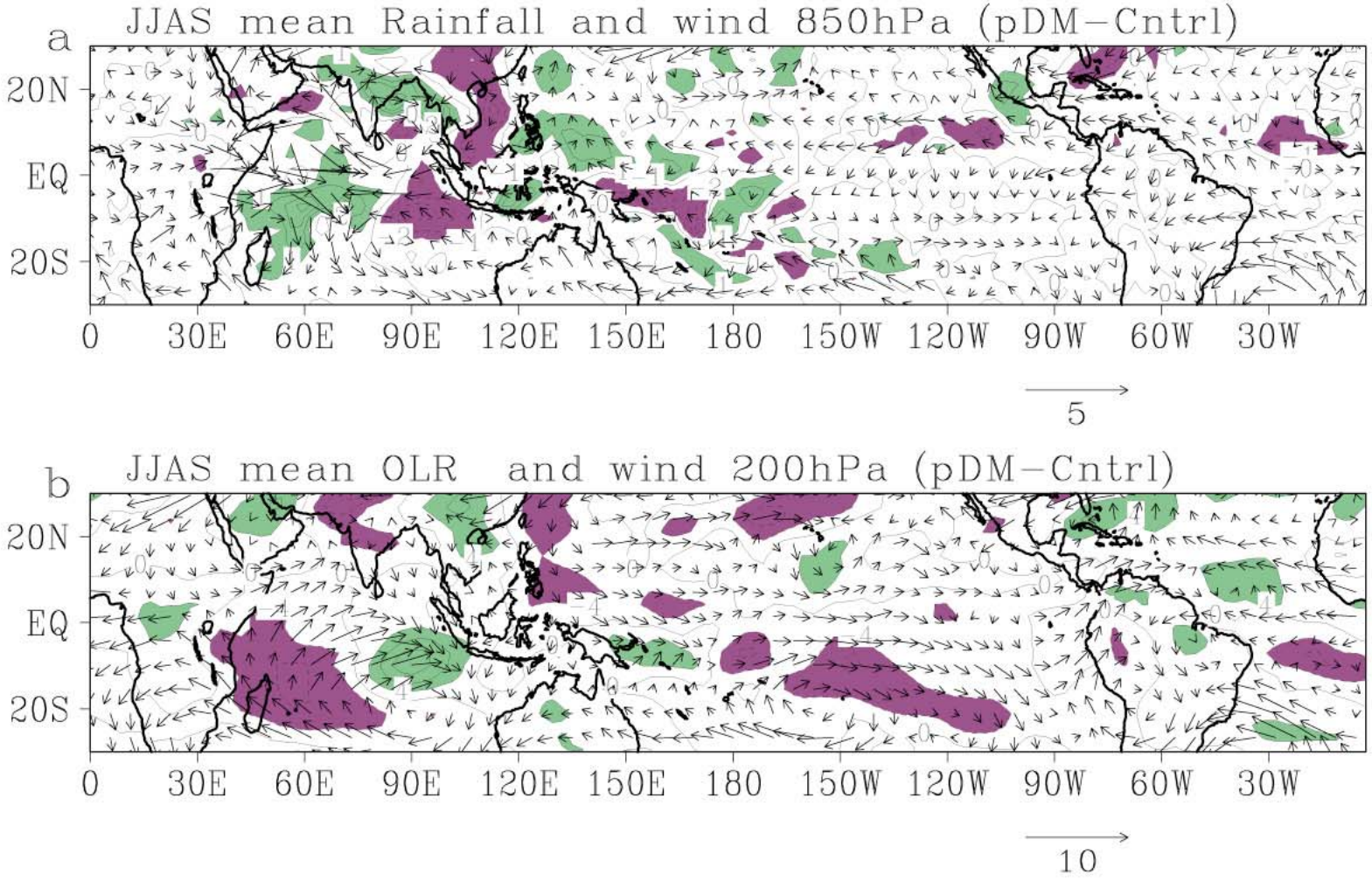
a
JJAS mean Rainfall and wind 850hPa (pDM−Cntrl)
20N
EQ
20S
0
30E
60E
90E
120E
150E
180
150W
120W
90W
60W
30W
5
b
JJAS mean OLR and wind 200hPa (pDM−Cntrl)
20N
EQ
20S
0
30E
60E
90E
120E
150E
180
150W
120W
90W
60W
30W
10

DP Fig.9cd

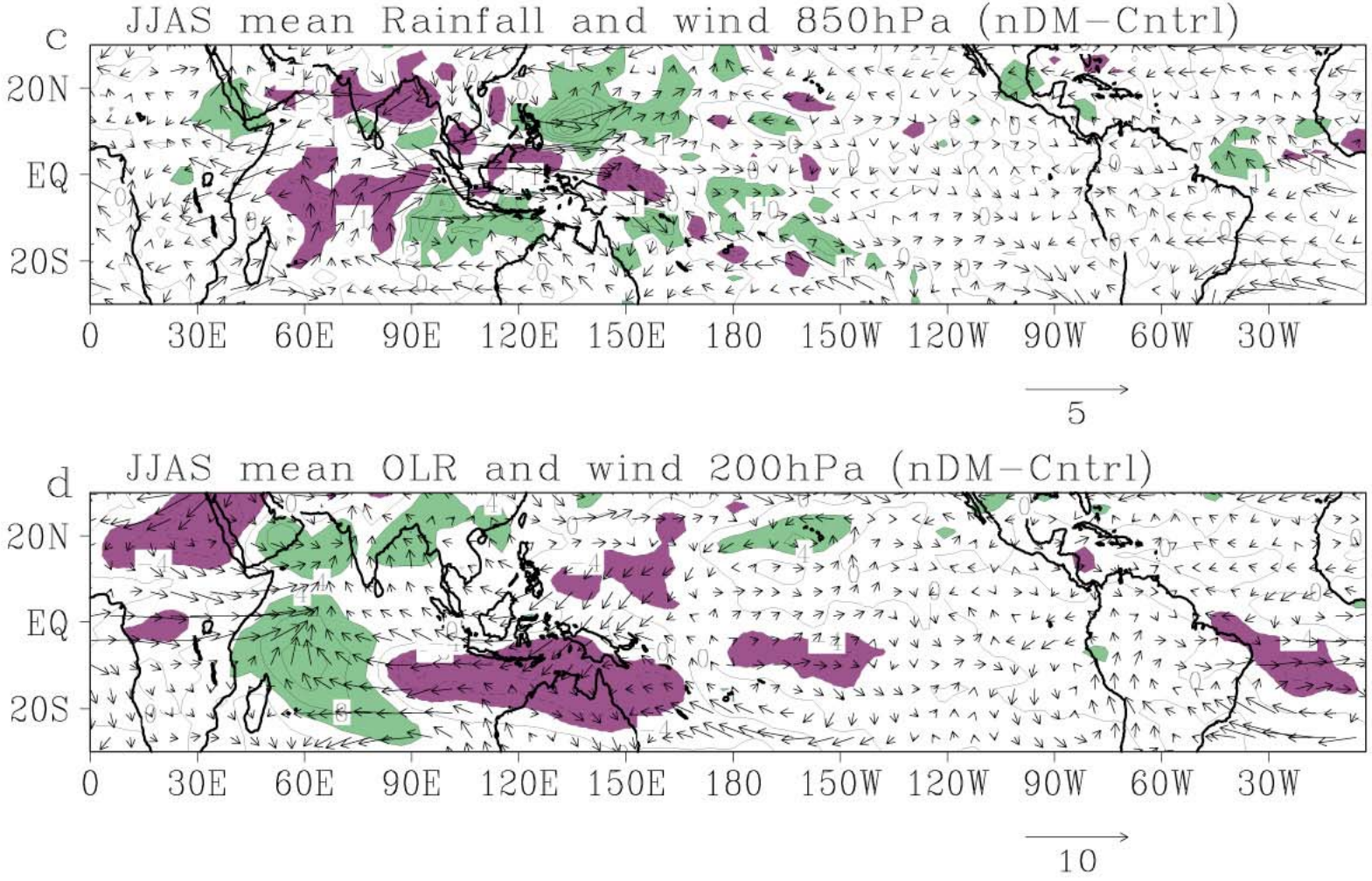
c
JJAS mean Rainfall and wind 850hPa (nDM−Cntrl)
20N
EQ
20S
0
30E
60E
90E
120E
150E
180
150W
120W
90W
60W
30W
5
d
JJAS mean OLR and wind 200hPa (nDM−Cntrl)
20N
EQ
20S
0
30E
60E
90E
120E
150E
180
150W
120W
90W
60W
30W
10

DP Fig.10ab

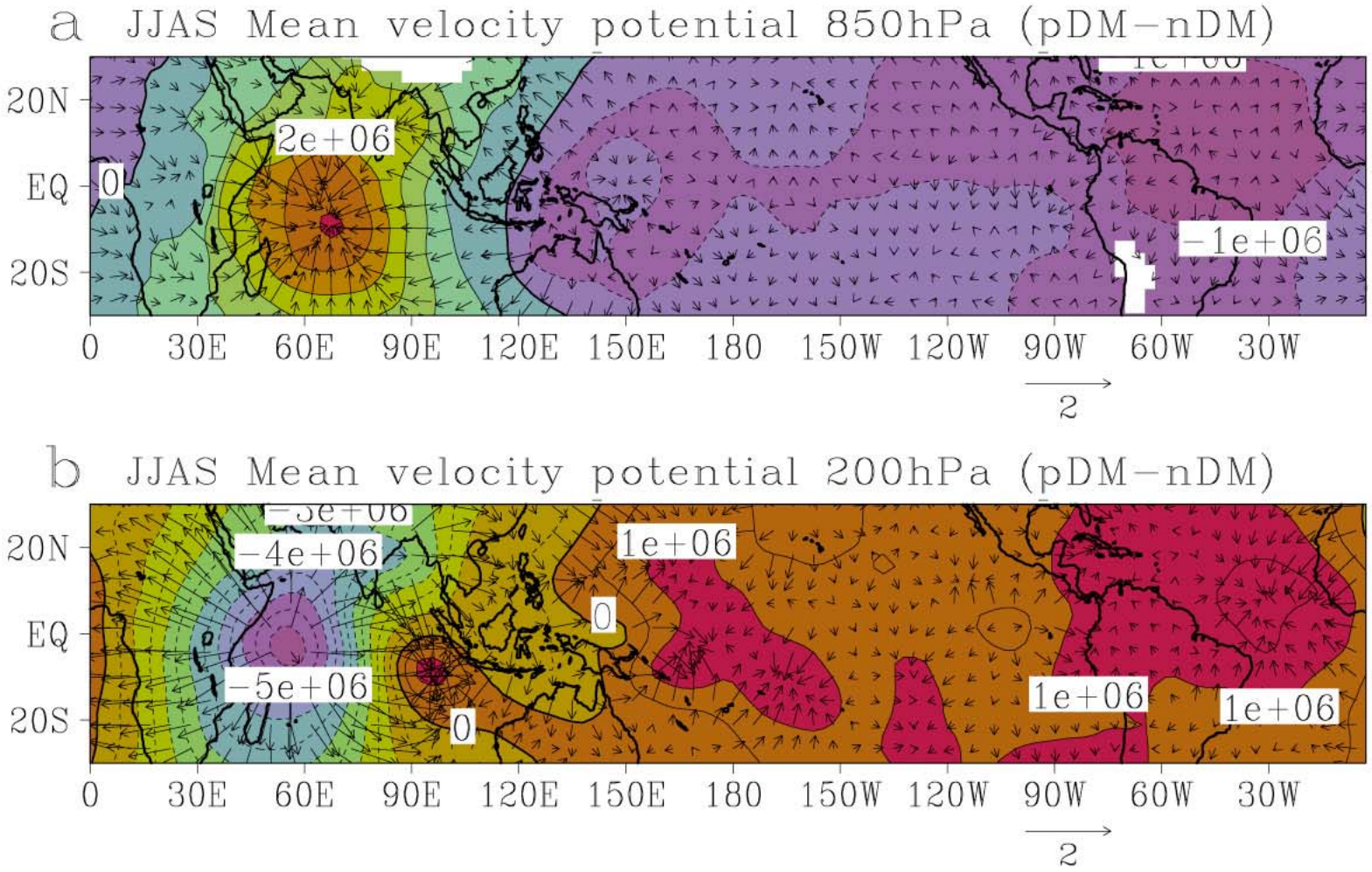
a JJAS Mean velocity potential 850hPa (pDM−nDM)
20N
EQ
20S
2e+06
0
−1e+06
0 30E 60E 90E 120E 150E 180 150W 120W 90W 60W 30W
2
b JJAS Mean velocity potential 200hPa (pDM−nDM)
20N
EQ
20S
−4e+06
1e+06
0
−5e+06
0
1e+06
1e+06
0 30E 60E 90E 120E 150E 180 150W 120W 90W 60W 30W
2

DP Fig.10cd

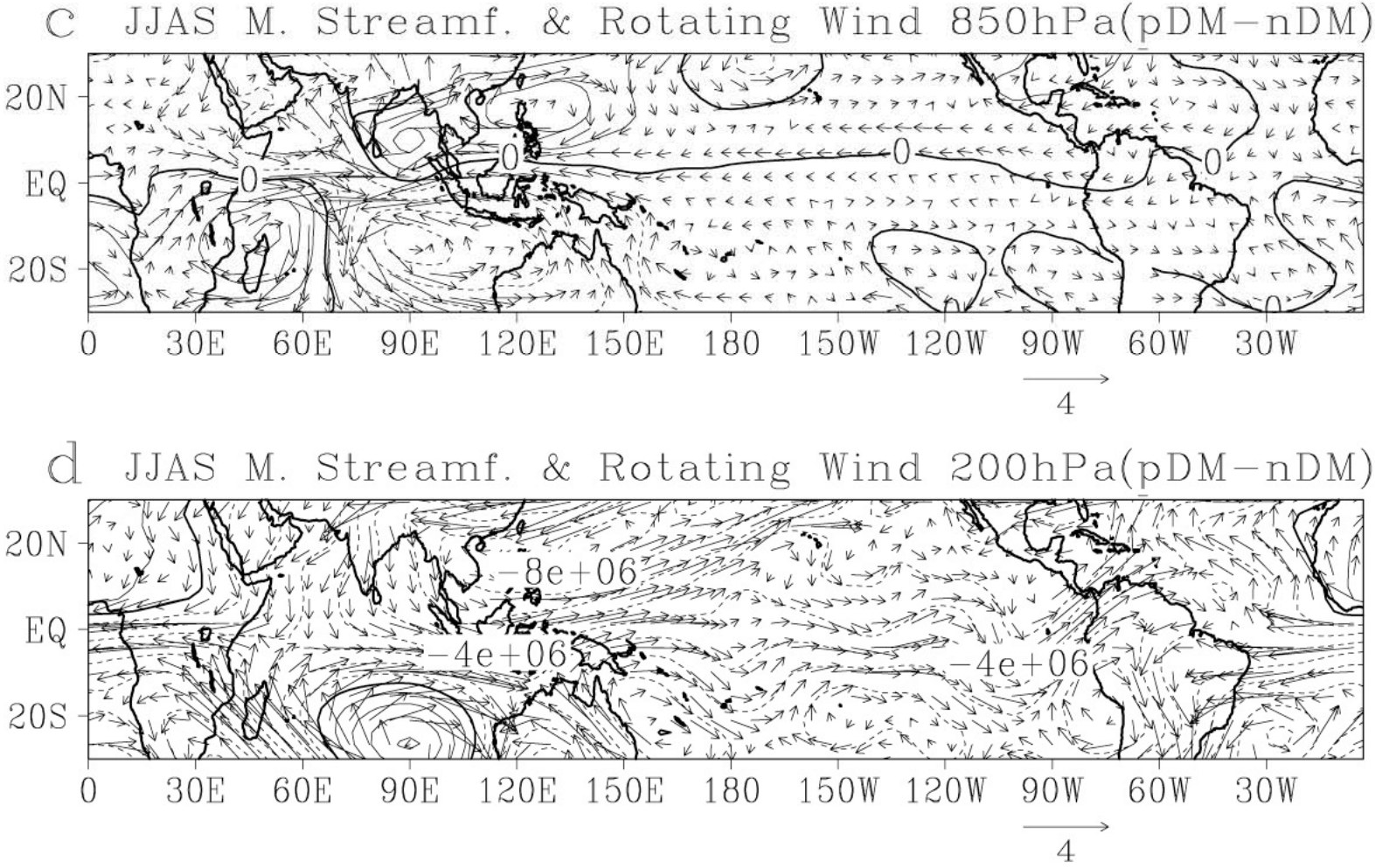
c JJAS M. Streamf. & Rotating Wind 850hPa(pDM−nDM)
20N
EQ
20S
0
0
0
0
0 30E 60E 90E 120E 150E 180 150W 120W 90W 60W 30W
4
d JJAS M. Streamf. & Rotating Wind 200hPa(pDM−nDM)
20N
EQ
20S
−8e+06
−4e+06
−4e+06
0 30E 60E 90E 120E 150E 180 150W 120W 90W 60W 30W
4

DP Fig.11

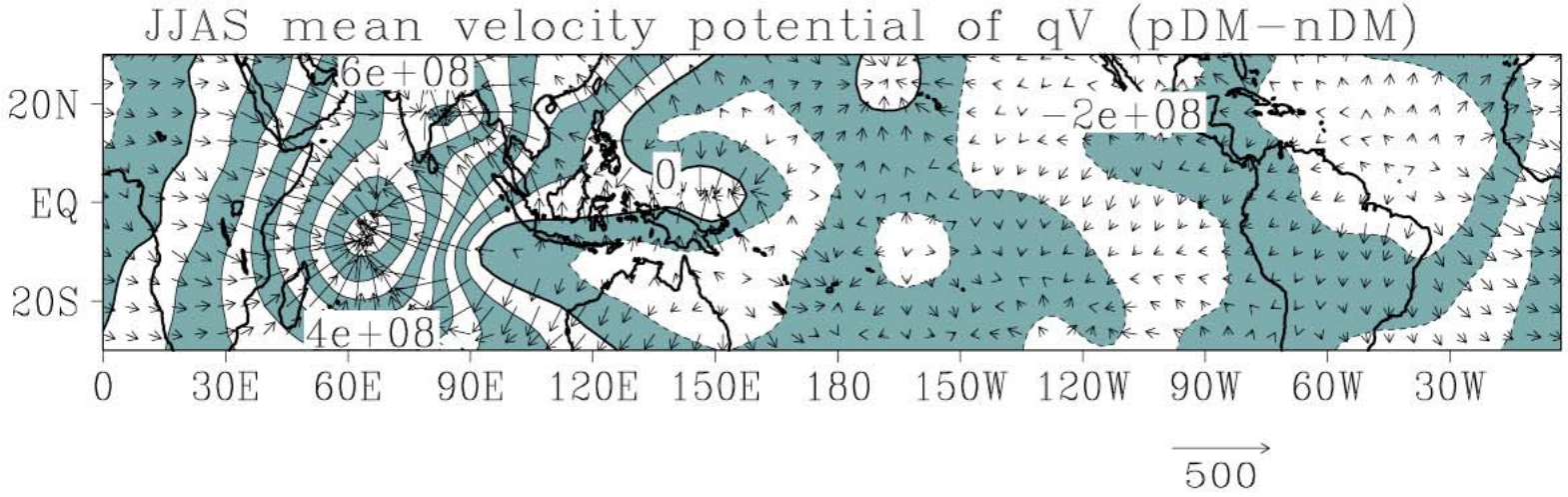
JJAS mean velocity potential of qV (pDM−nDM)
6e+08
−2e+08
0
4e+08
20N
EQ
20S
0
30E
60E
90E
120E
150E
180
150W
120W
90W
60W
30W
500

DP Fig.12

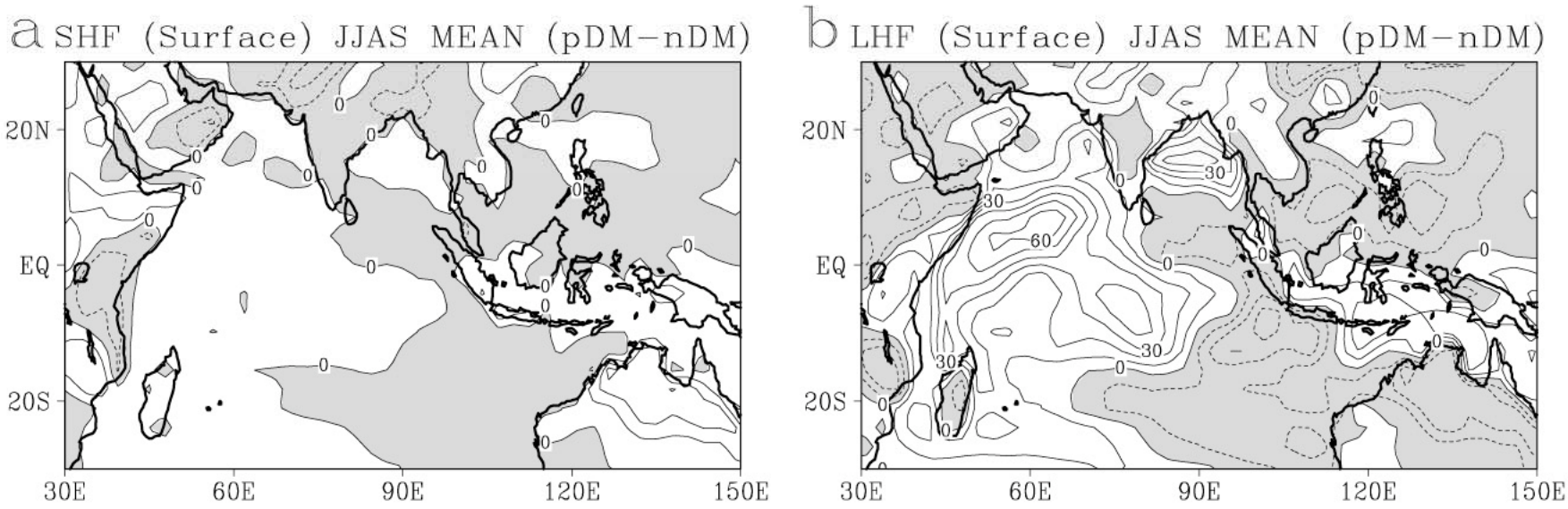
a SHF (Surface) JJAS MEAN (pDM−nDM)
b LHF (Surface) JJAS MEAN (pDM−nDM)
20N
EQ
20S
30E
60E
90E
120E
150E
0
30
60

DP Fig.13

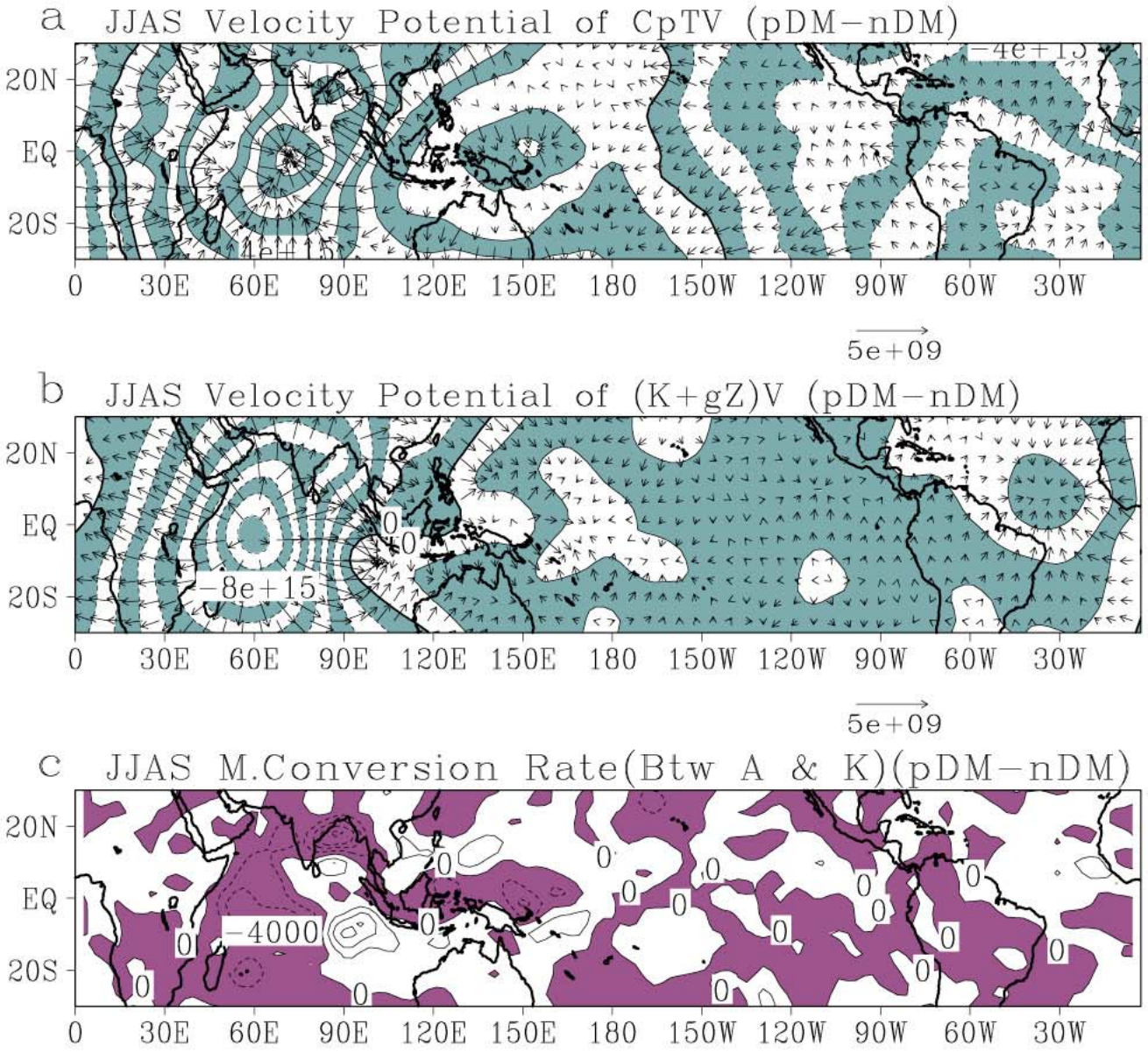
a JJAS Velocity Potential of CpTV (pDM−nDM)
20N
EQ
20S
0 30E 60E 90E 120E 150E 180 150W 120W 90W 60W 30W
5e+09
b JJAS Velocity Potential of (K+gZ)V (pDM−nDM)
−8e+15
5e+09
c JJAS M.Conversion Rate(Btw A & K)(pDM−nDM)
−4000

Summary

- The FrAM1.0 Simulates the mean climatology and variability of the atmosphere reasonably.
- The atmospheric response to the IOD SSTA has a Dipole structure
- During the positive IOD event, the anomolous SSTA forcing induces anomolous fluxes of the sensible & latent heat with a dipole structure at the surface and causes a net surplus heating over the warmer pole and loss of heating over the colder pole.

• **Our energy budget studies indicate that there is net surplus of vertically integrated anomalous convergence of moisture and that of the enthalpy over the warm pole region of the atmosphere. This facilitates the availability of excess latent heat and enthalpy for conversion in to the kinetic energy and thus causes the anomalous divergence of the mechanical energy. This anomalous divergence of mechanical energy leads to the propagation of the disturbances to the surrounding regions around the IOD and maintains the anomalies of the circulation and energy distribution.**

• From our budget studies we find that during the boreal summer time, the contribution from the transient disturbances to the maintenance of the anomalous response of the mean circulation of the dipole year. This indicates that the influence of the intraseasonal oscillations such as the Madden-Julian Oscillation (MJO) may not strongly influence the atmospheric response to the IOD.
The IOD-MJO relationship needs further investigation.

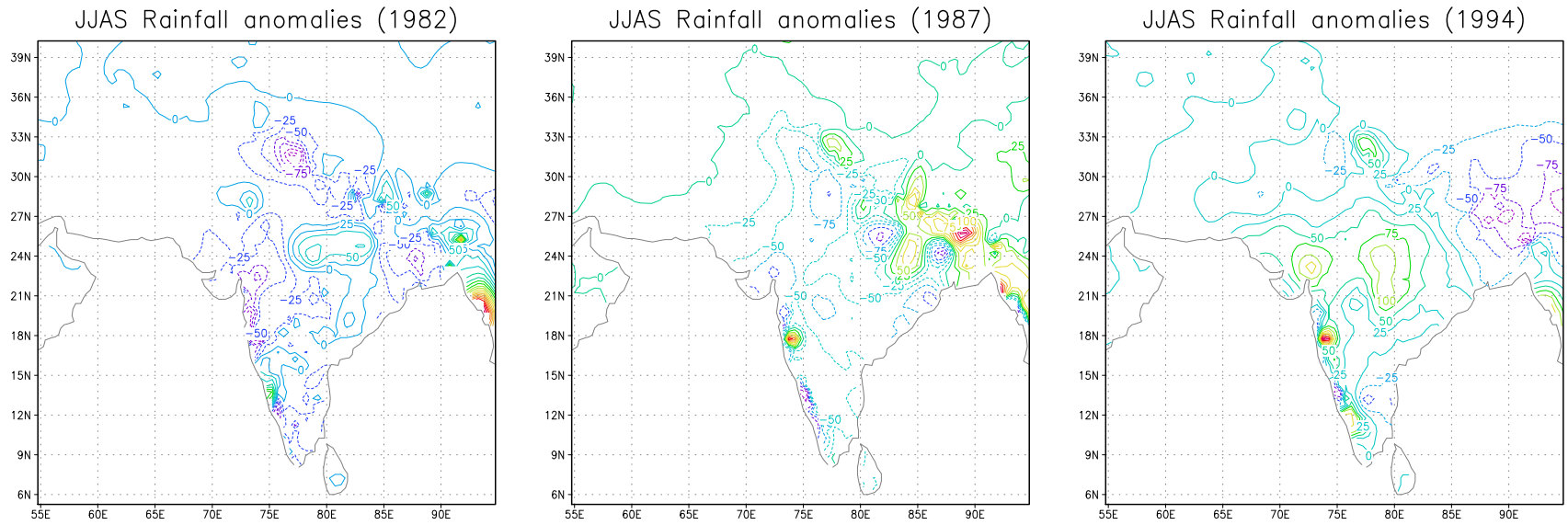
JJAS Rainfall anomalies (1982)
JJAS Rainfall anomalies (1987)
JJAS Rainfall anomalies (1994)
GrADS: COLA/IGES
JJAS Rainfall anomalies (1983)
JJAS Rainfall anomalies (1988)
JJAS Rainfall anomalies (1997)

fig.2

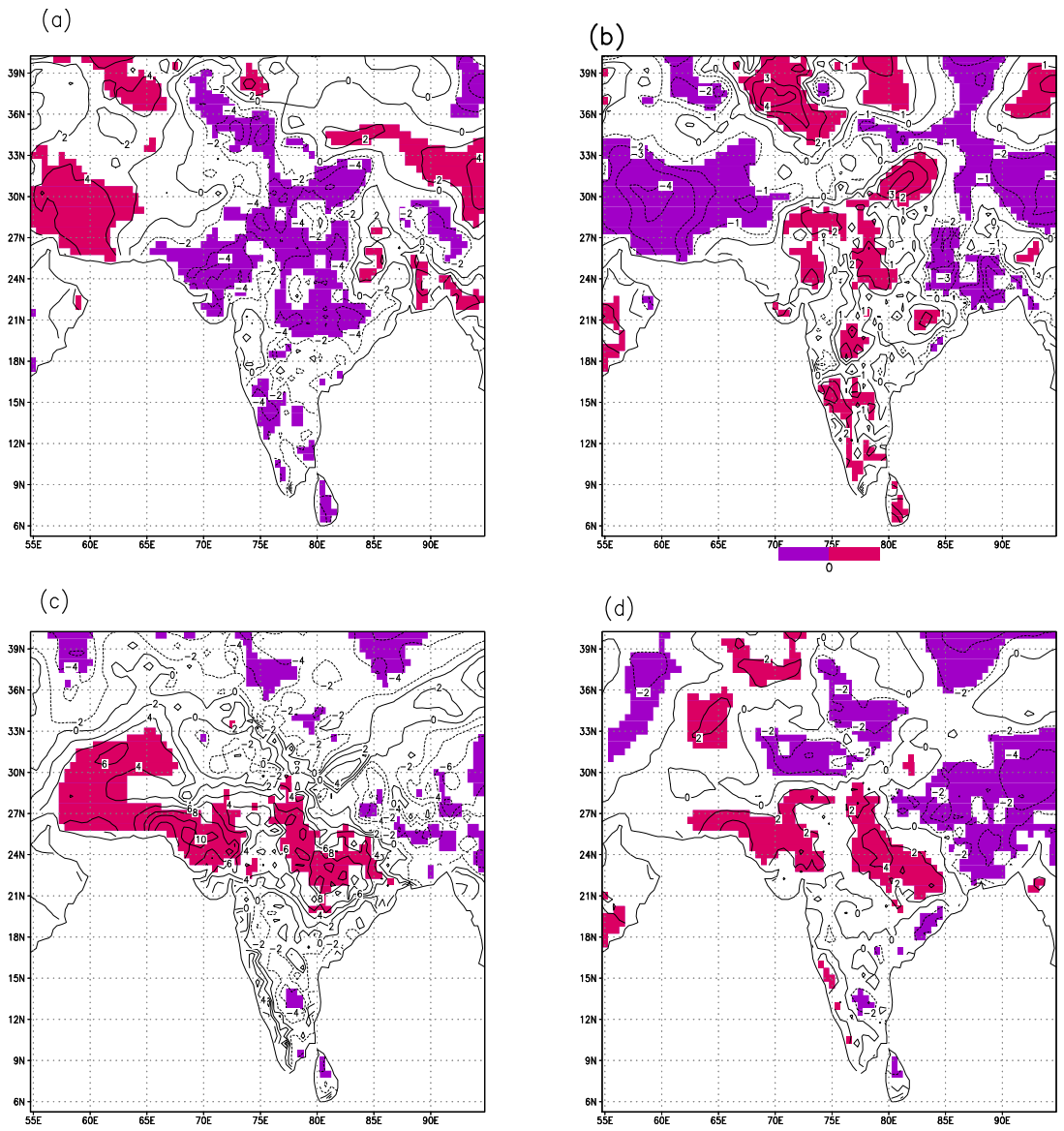

Normalized mean JJAS rainfall anomalies for (a)pure El Nino events
(b) El Ninos with PIOD events minus pure El Ninos
(c) pure pIODevents (d)all pIODevents; significant values
at 90% conf. interval from 2-tailed t-test are shaded;

- Pure ENSO years- 1965, 1969, 1976, 1986, 1987, and 1991)
- all El Niño years (including those events that co-occurred with positive IOD events) between 1958 and 1997- 1963, 1965, 1969, 1972, 1976, 1982, 1983, 1986, 1987, 1991, and 1997
- pure positive IOD years- 1961, 1967, 1977, and 1994
- All positive IOD events - 1961, 1963, 1967, 1972, 1977, 1982, 1983, 1994, and 1997

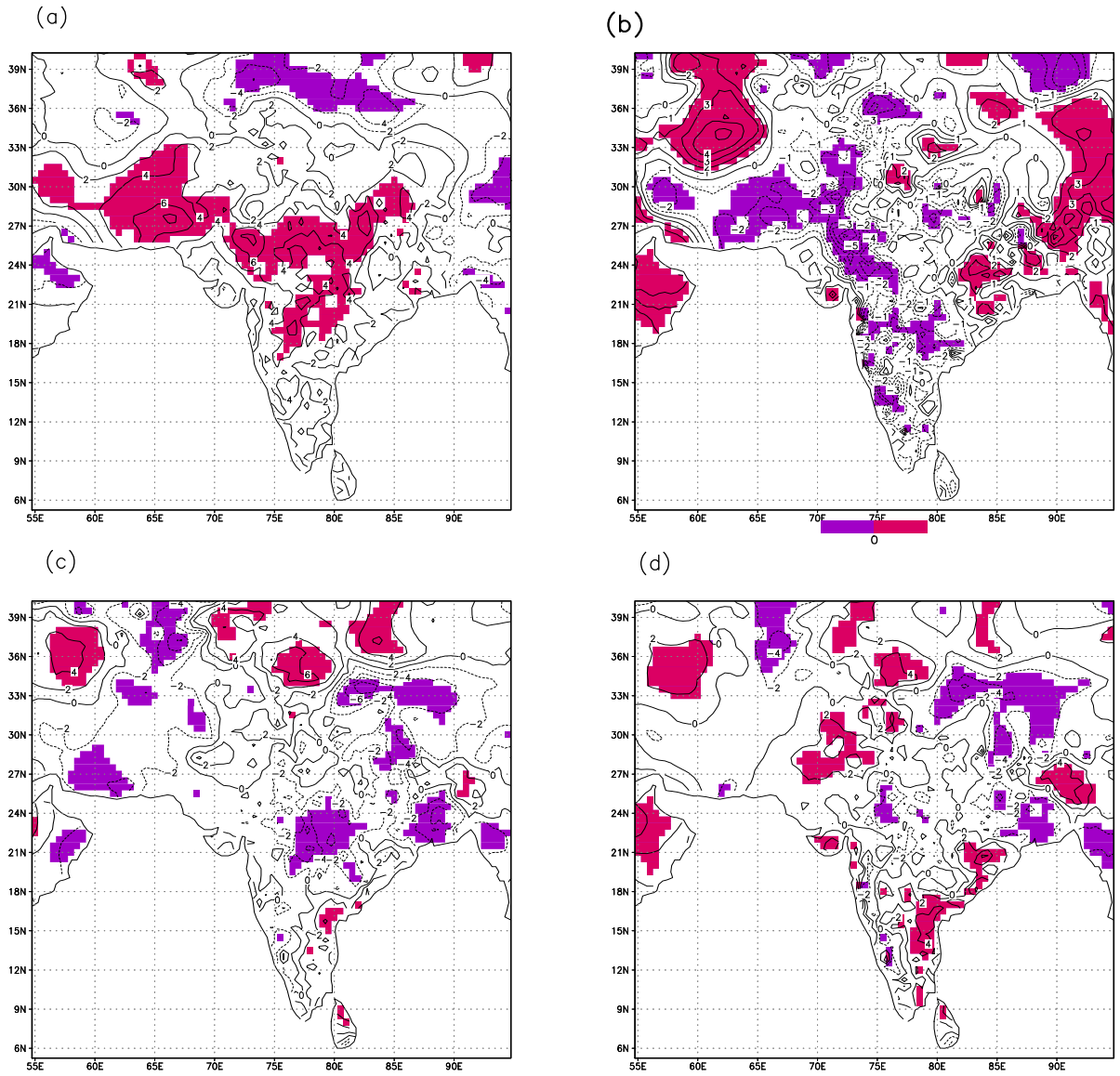

Normalized mean JJAS rainfall anomalies for (a)pure La Nina events (b) La Ninas with nIOD events minus pure La Ninas (c) pure nIODevents (d)all nIODevents; significant values at 90% conf. interval from 2−tailed t−test are shaded;

- pure La Niña years (1967, 1973, 1975, 1988, and 1999).
- all La Niña years (1964, 1967, 1970,1971, 1973, 1975,1985, 1988, and 1999).
- pure negative IOD events (1958, 1960, 1989, 1992, and 1996)
- (1958, 1960, 1964, 1970, 1989, 1992, and 1996)

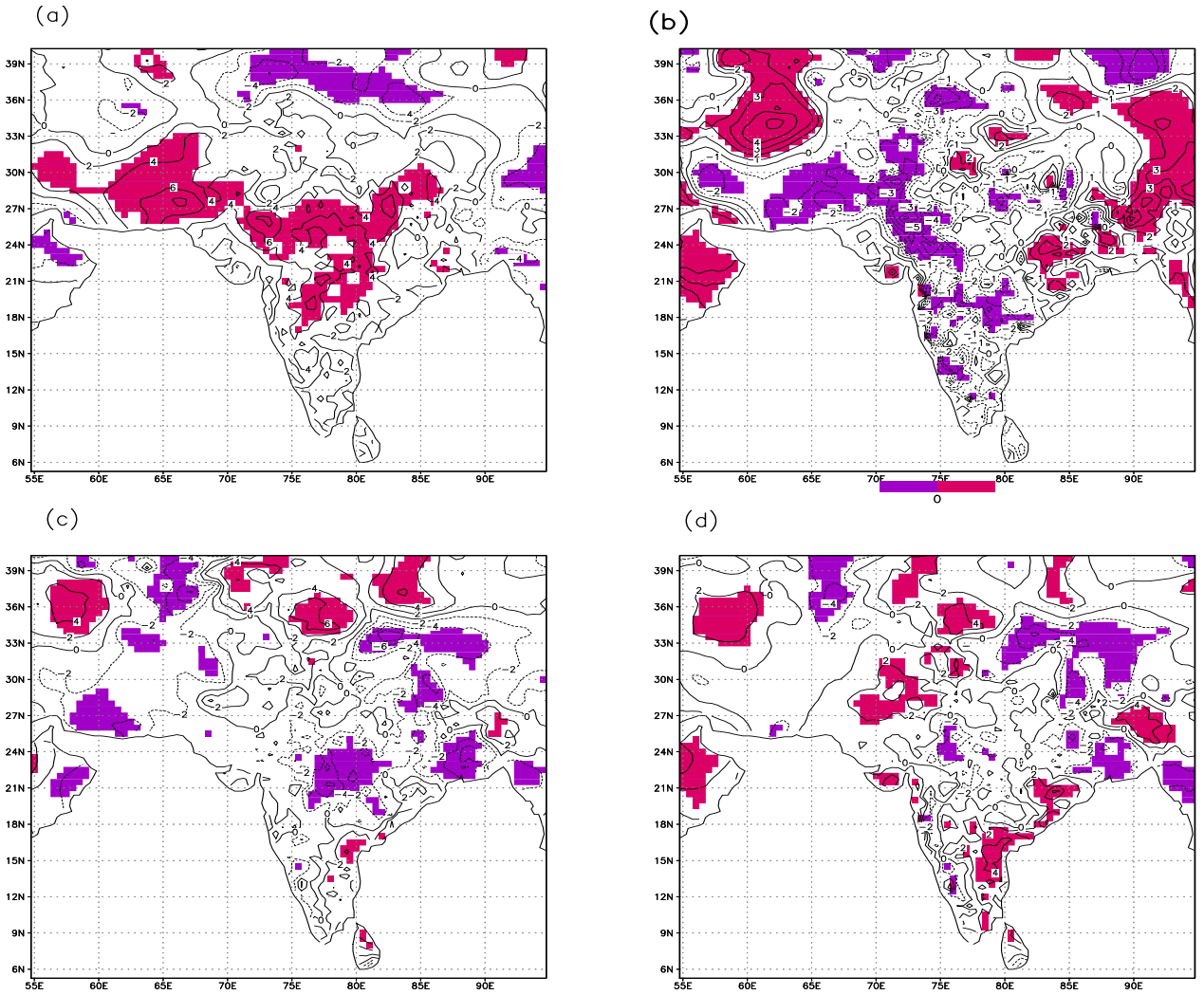

Normalized mean JJAS rainfall anomalies for (a)pure La Nina events
(b) La Ninas with nIOD events minus pure La Ninas
(c) pure nIODevents (d)all nIODevents; significant values
at 90% conf. interval from 2−tailed t−test are shaded;
postive in pink & negative in purple

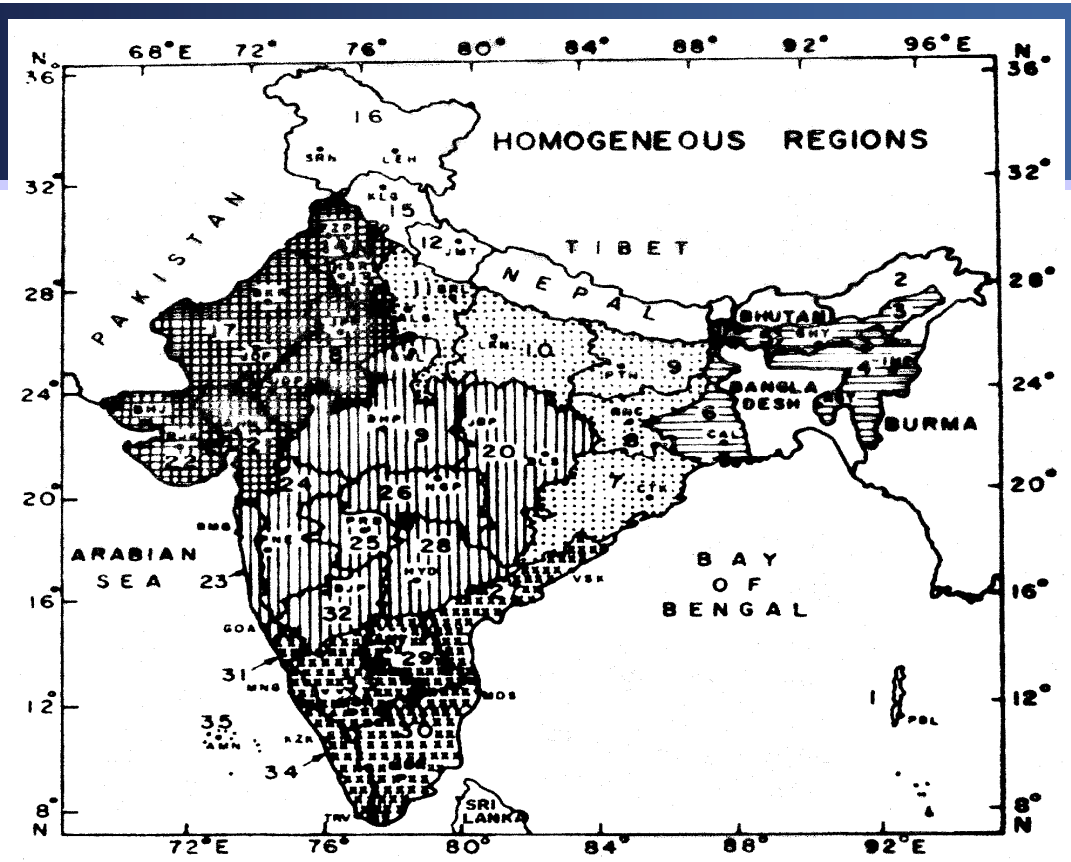

REGIONS	SUB-DIVISION NUMBERS	
NORTHWEST INDIA	13, 14, 17, 18, 21, 22	= 6
WEST CENTRAL INDIA	19, 20, 23, 24, 25, 26, 28, 32	= 8
CENTRAL NORTHEAST INDIA	07, 08, 09, 10, 11	= 5
NORTHEAST INDIA	03, 04, 05, 06	= 4
PENINSULAR INDIA	27, 29, 30, 31, 33, 34	= 6
NOT CONSIDERED	1, 2, 12, 15, 16, 35	= 6

Homogeneous region	Correlations with the IODMI	Correlations with the NINO3 SSTA
All India	**0.40 (0.34)**	**-0.64 (-0.61)**
Homogeneous India	**0.44 (0.38)**	**-0.62 (-0.60)**
Core Monsoon	**0.38 (0.31)**	**-0.56 (-0.55)**
North West India	**0.31** (0.24)	**-0.58 (-0.51)**
West Central India	**0.47 (0.42)**	**-0.60 (-0.60)**
Central North East India	0.24 (0.20)	**-0.33 (-0.38)**
North East India	-0.22 (-0.21)	-0.08 (0.8)
Peninsular India	0.17 (0.12)	-0.53 (-0.47)

SSTA (C) imposed in the ENSO experiment during September

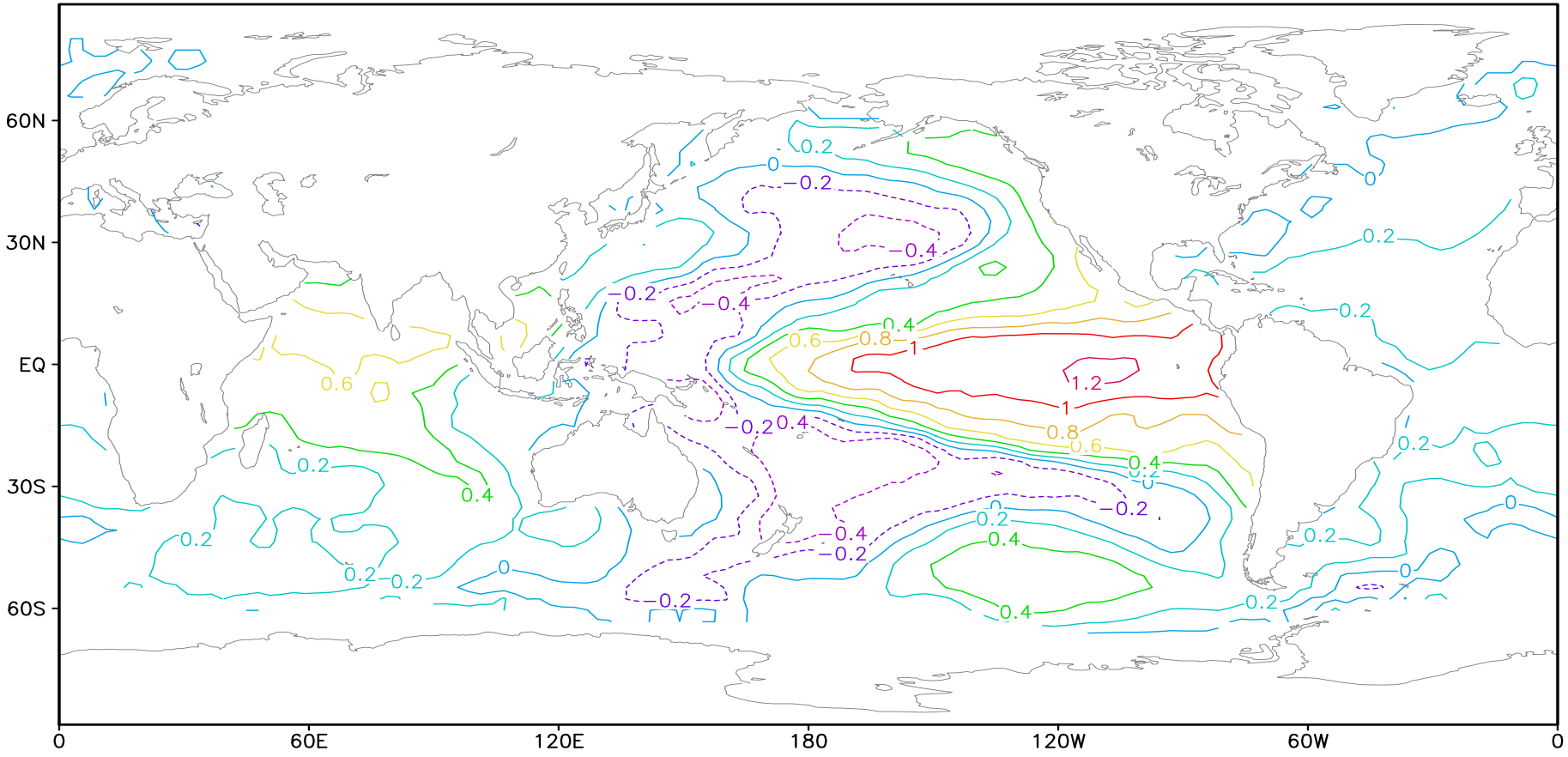

fig. 3a

SSTA (C) imposed in the IOD experiment during September

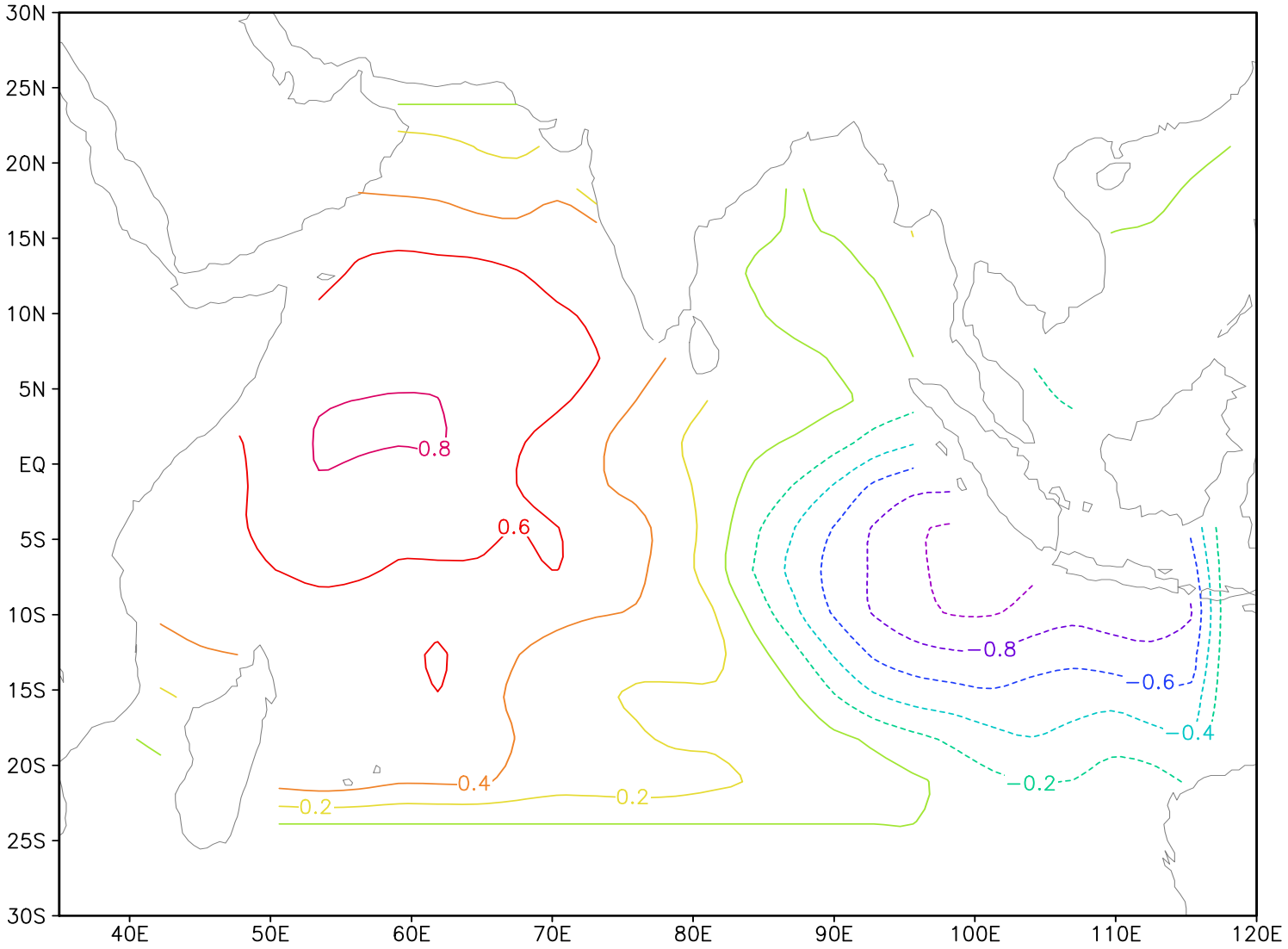

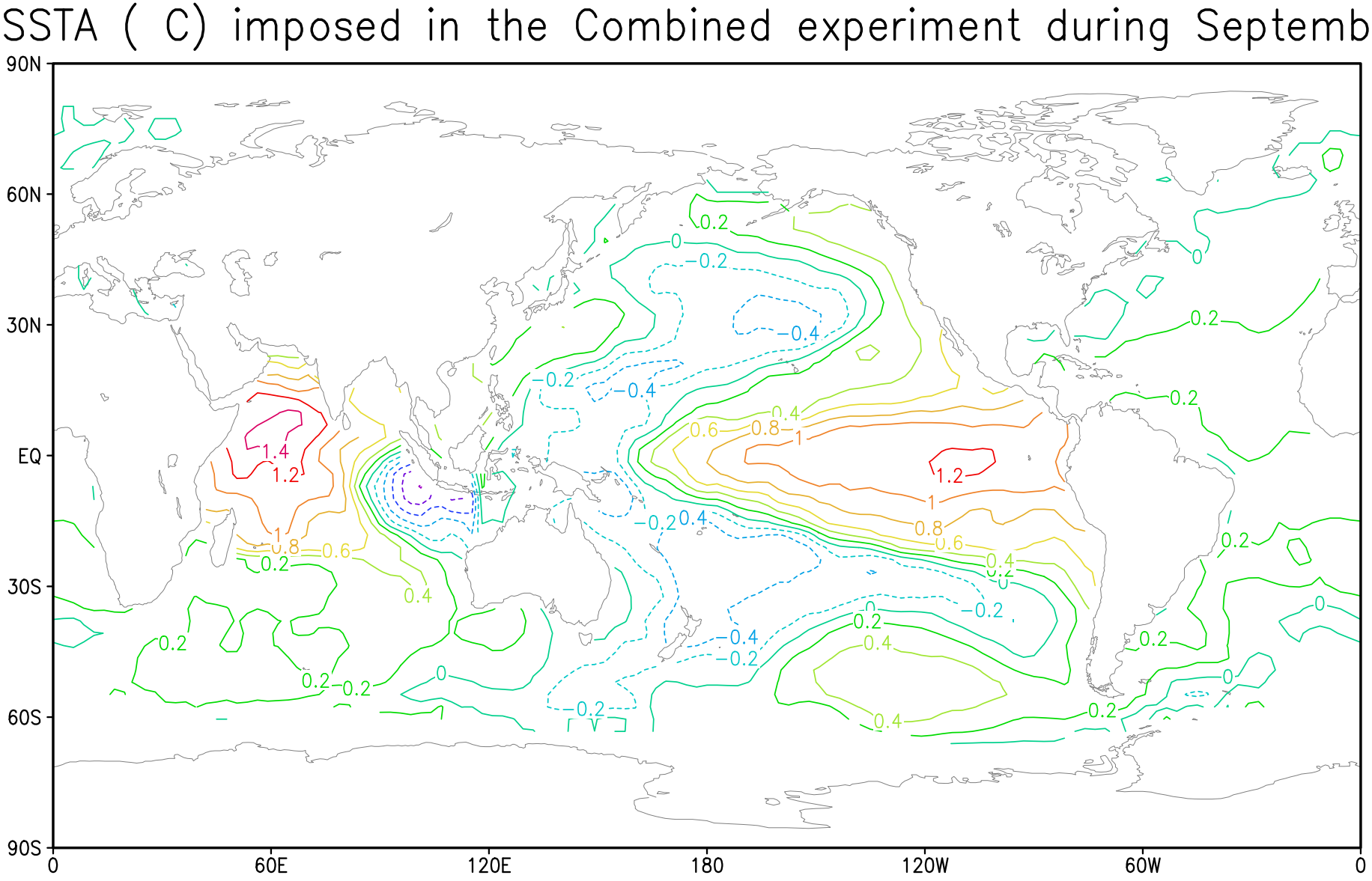
SSTA (C) imposed in the Combined experiment during September
90N
60N
30N
EQ
30S
60S
90S
0
60E
120E
180
120W
60W
0
1.4
1.2
1
0.8
0.6
0.4
0.2
0
-0.2
-0.4

fig. 3c

Model Climatology for JJAS: Rainfall (mm/day) & Wind at 850 hPa

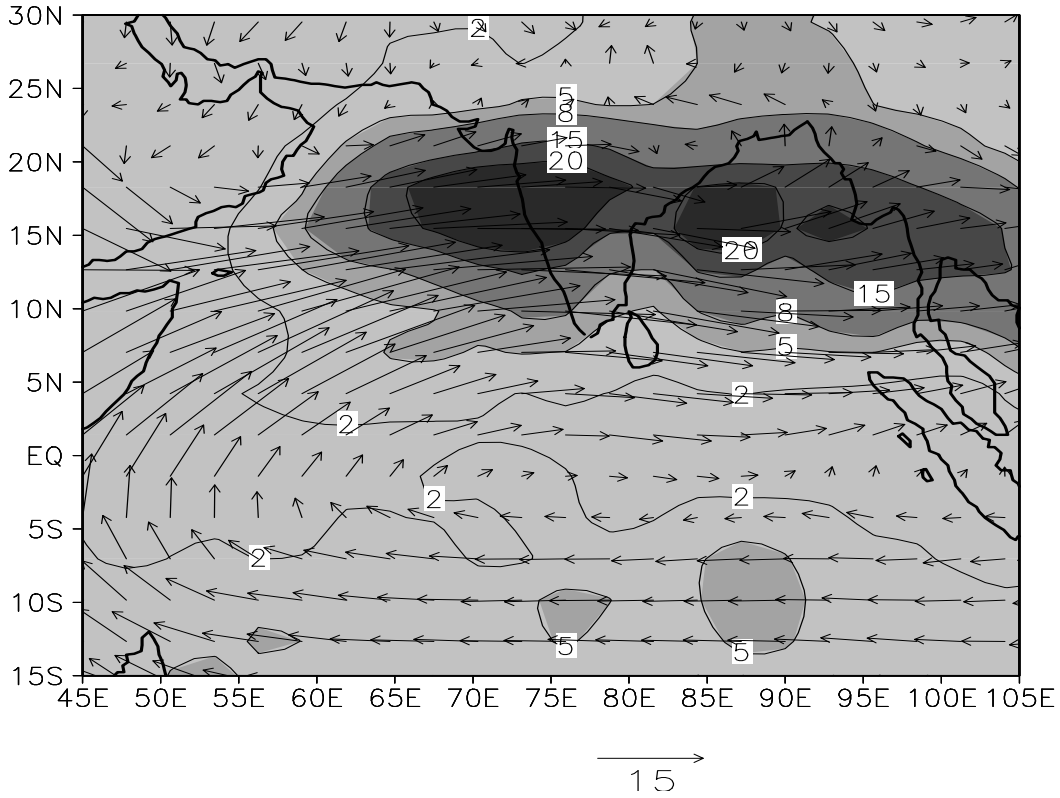

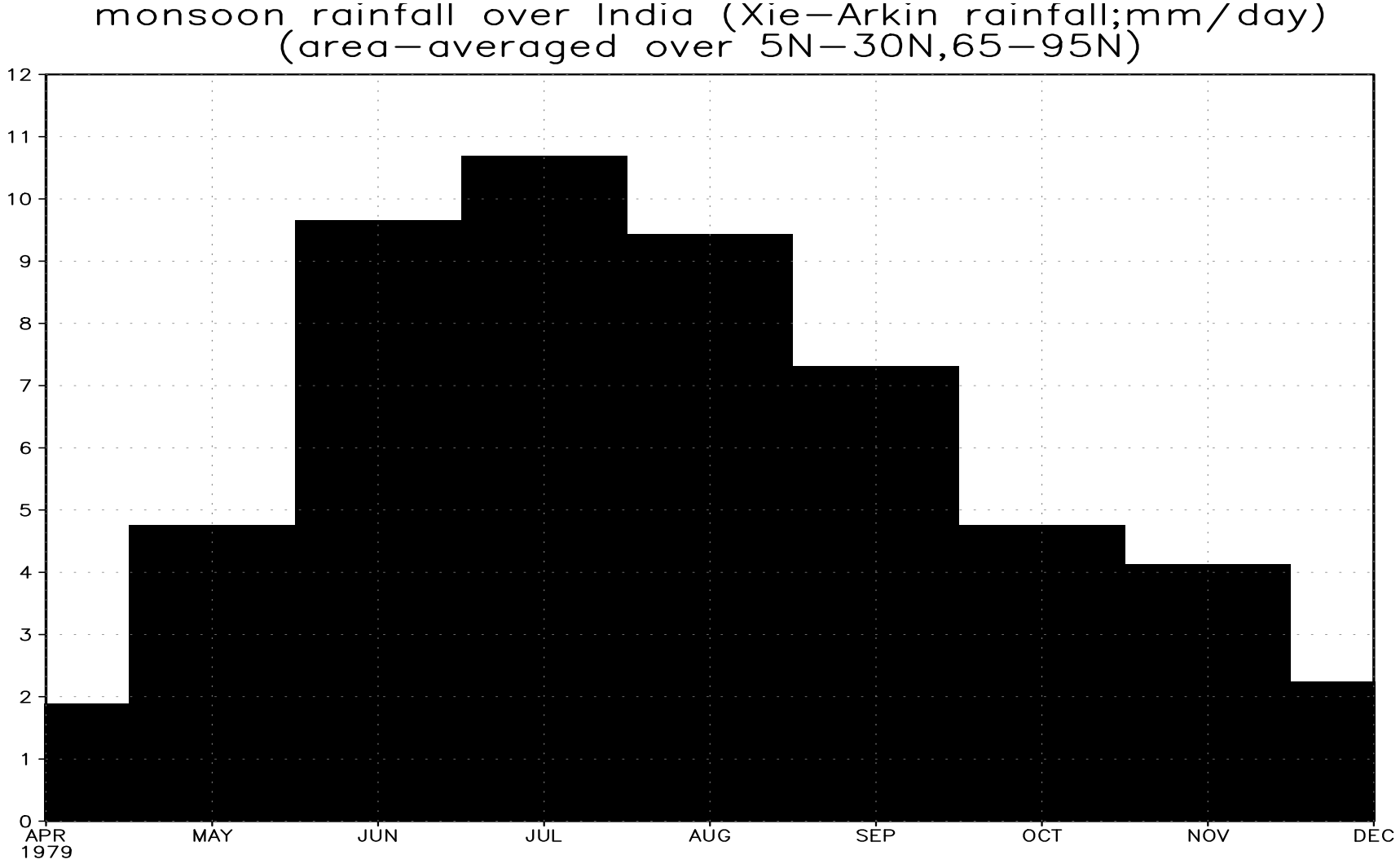
monsoon rainfall over India (Xie-Arkin rainfall;mm/day)
(area-averaged over 5N-30N,65-95N)
12
11
10
9
8
7
6
5
4
3
2
1
0
APR
1979
MAY
JUN
JUL
AUG
SEP
OCT
NOV
DEC

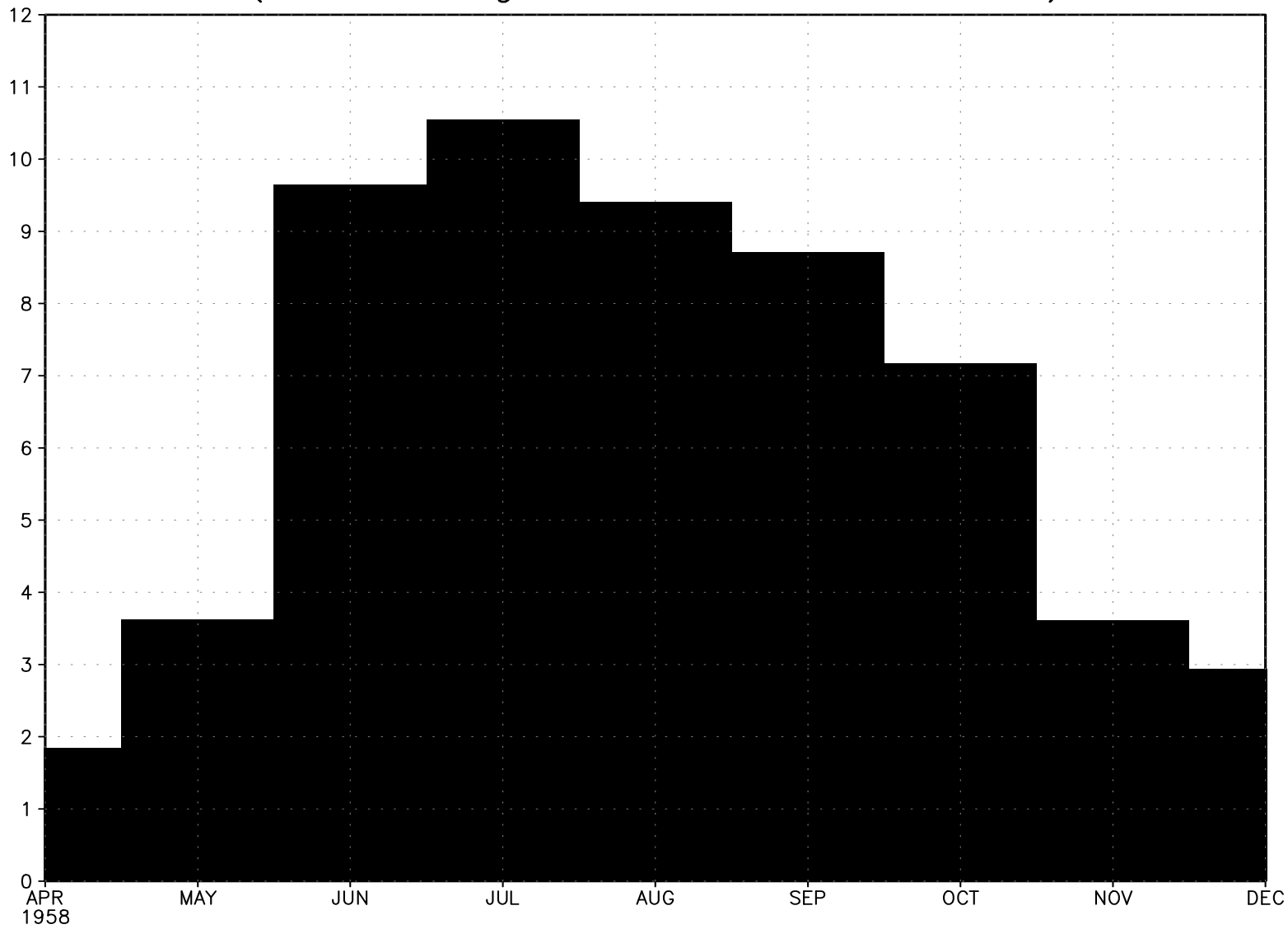
FrAM1.0-simulated mean Indian rainfall (mm/day)
(area-averaged over 5N-30N,65E-95E)
12
11
10
9
8
7
6
5
4
3
2
1
0
APR
1958
MAY
JUN
JUL
AUG
SEP
OCT
NOV
DEC

JJAS anoms. of rainfall (mm/day) and wind (m/s) at 850 hPa:ENSO expt.−Control Expt.

(a)

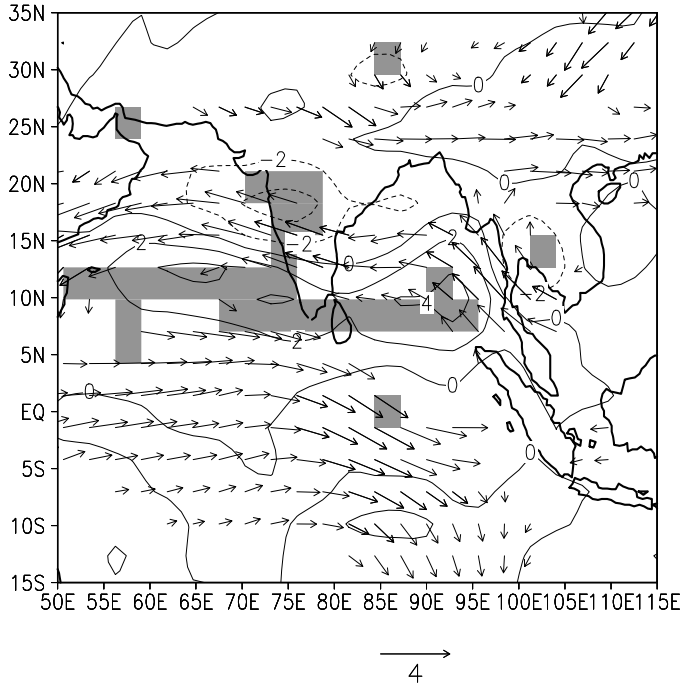

JJAS anoms. of rainfall (mm/day) and wind (m/s) at 850 hPa:Comb. expt.−Climate Expt.

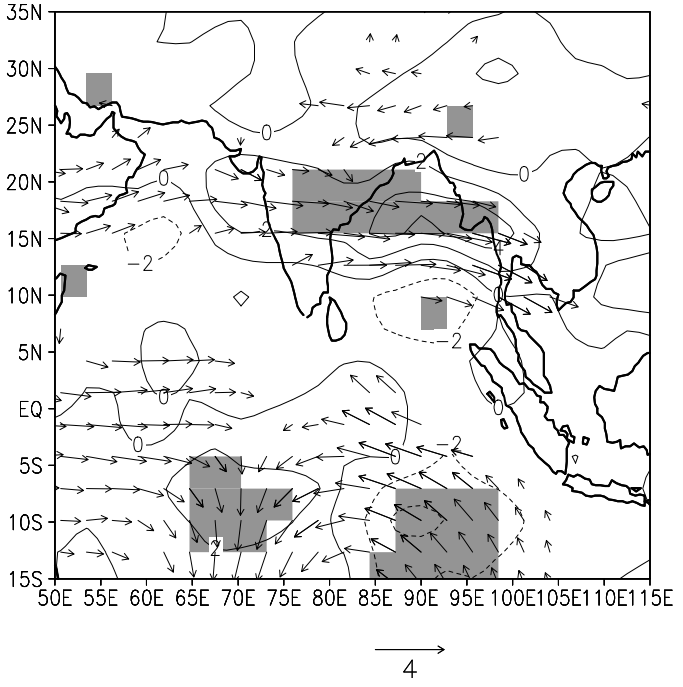

JJAS Velocity potential and wind at 850 hPa (m/s)
ENSO. expt.−Climate Expt

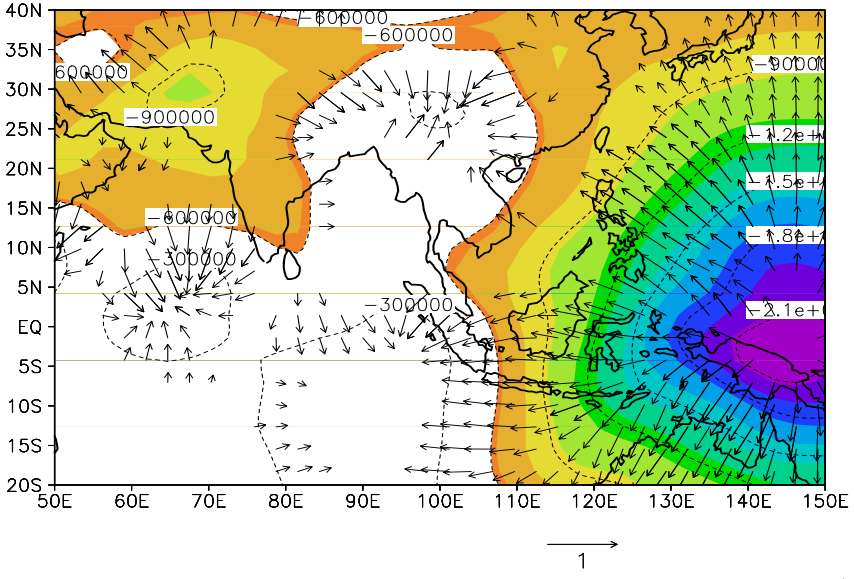

JJAS Velocity potential and wind at 850 hPa (m/s)
Comb. expt.−ENSO Expt

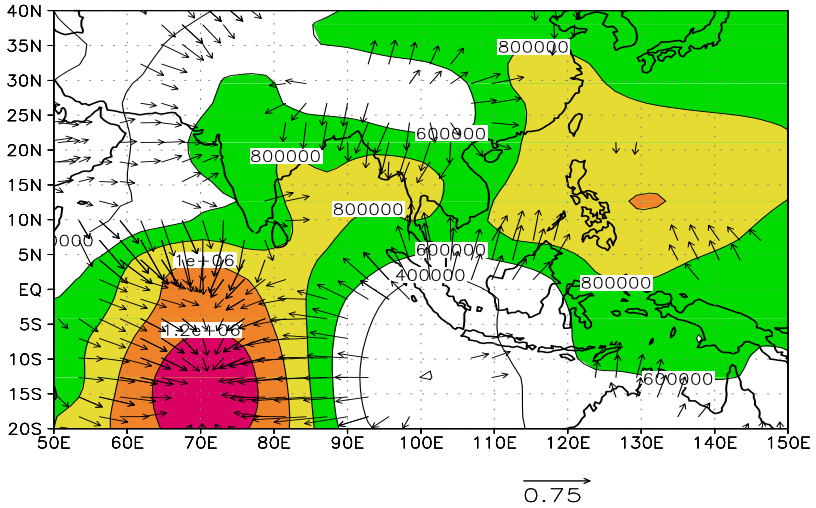

JJAS Velocity potential and wind at 200 hPa (m/s)

(a)

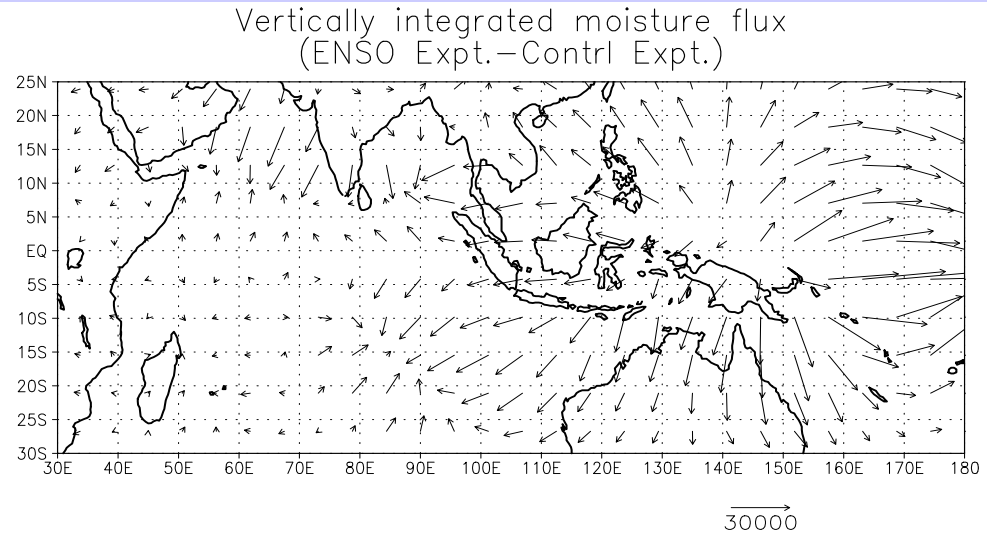
Vertically integrated moisture flux
(ENSO Expt.−Contrl Expt.)
25N
20N
15N
10N
5N
EQ
5S
10S
15S
20S
25S
30S
30E
40E
50E
60E
70E
80E
90E
100E
110E
120E
130E
140E
150E
160E
170E
180
30000

(b)

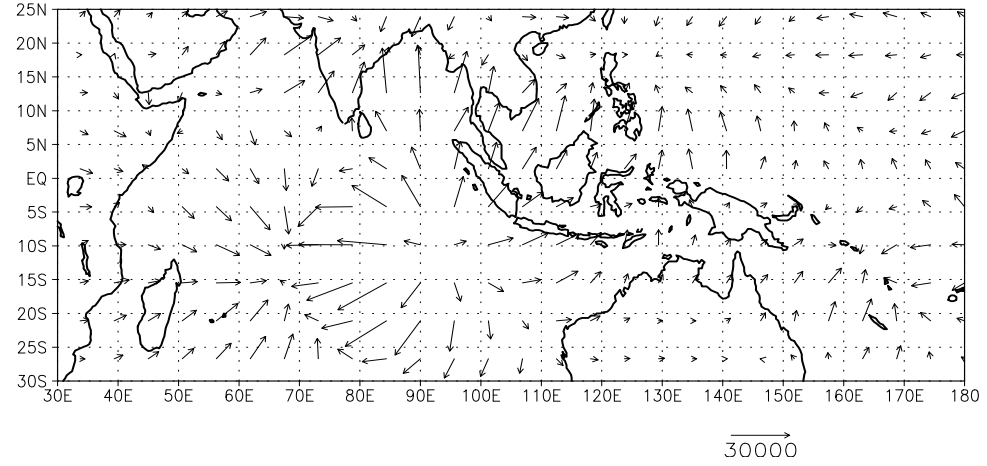
Vertically integrated moisture flux
(Combnation Expt.−ENSO Expt.)
25N
20N
15N
10N
5N
EQ
5S
10S
15S
20S
25S
30S
30E
40E
50E
60E
70E
80E
90E
100E
110E
120E
130E
140E
150E
160E
170E
180
30000

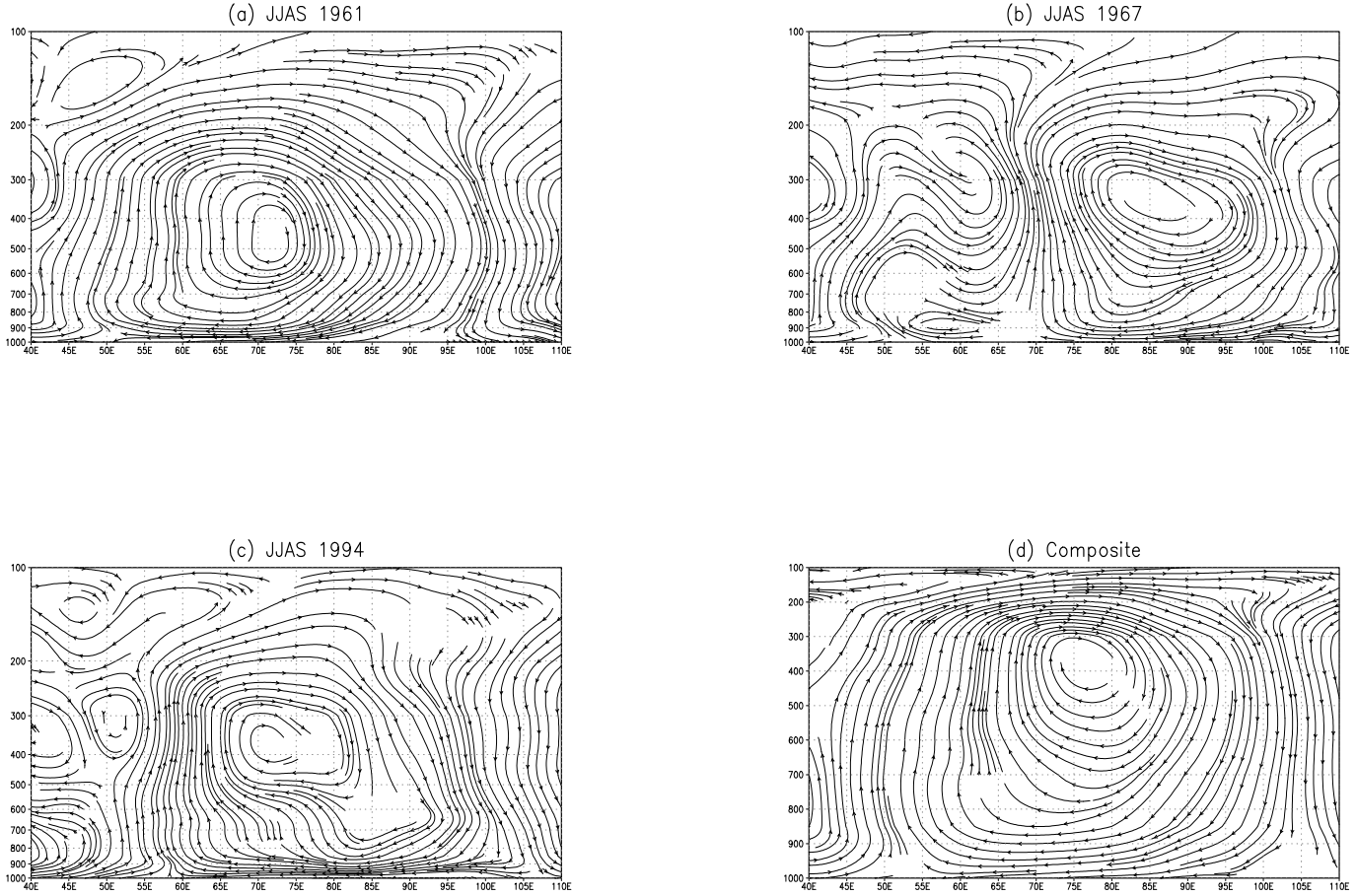

Fig. 10: The anomalous equatorial Walker circulation streamlines during JJAS (averaged over 10ºS-5ºN), derived from the NCEP non-rotating zonal component of the velocity and the vertical velocity, during the years (a) 1961 (b) 1967 (c) 1994 (d) composite of a-c.

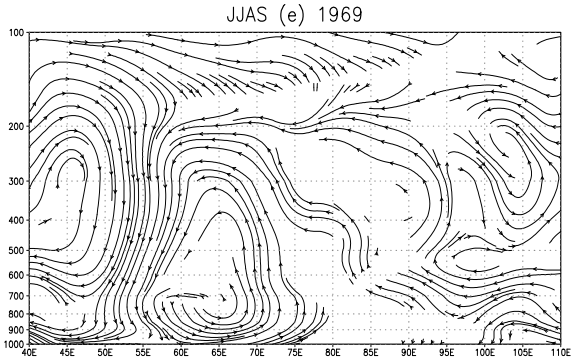

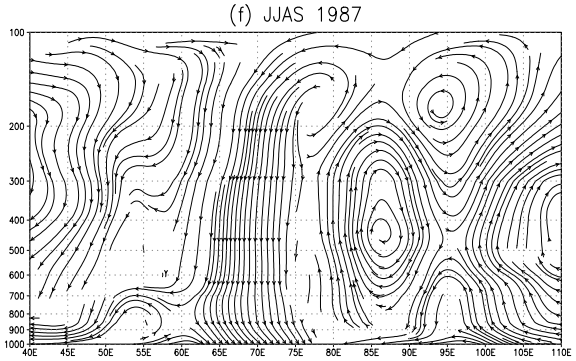

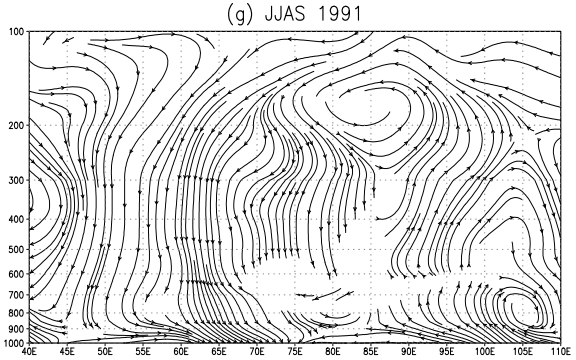

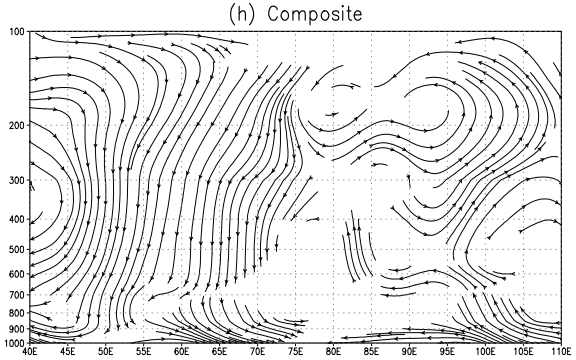

Fig. 10: (a-i) The anomalous equatorial Walker circulation streamlines during JJAS (averaged over 10ºS-5ºN), derived from the NCEP non-rotating zonal component of the velocity and the vertical velocity, during the years (e) 1969 (f)1987 (g) 1991 (h) composite of e-g.; (i) 1997.

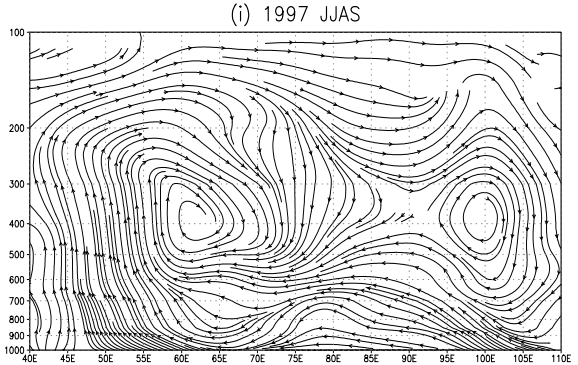

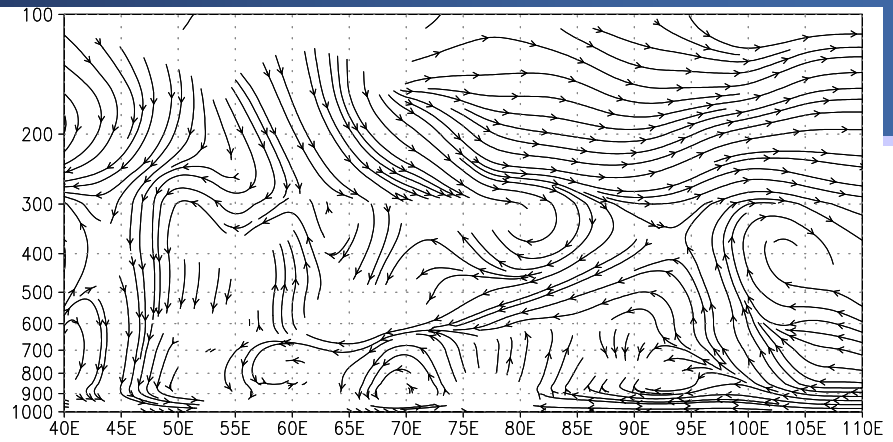

a

JJAS Walker circulation (averaged over 10S–5N);
(ENSO Expt.–Cntrl. Expt.)

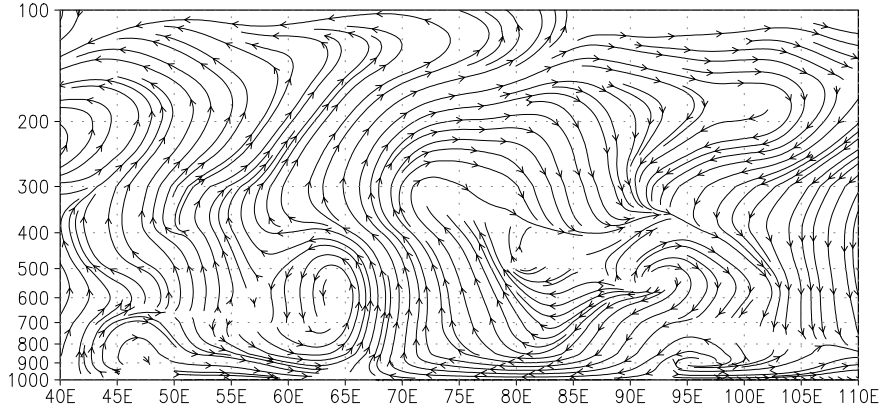

b

JJAS Walker circulation (averaged over 10S–5N);
(Combination Expt.–ENSO Expt.)

a

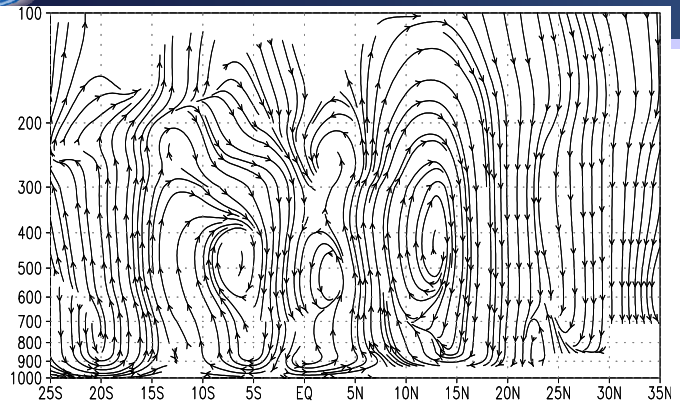

JJAS Hadley circulation averaged over 70–85 E
(ENSO Expt.–Cntrl. Expt.)

b

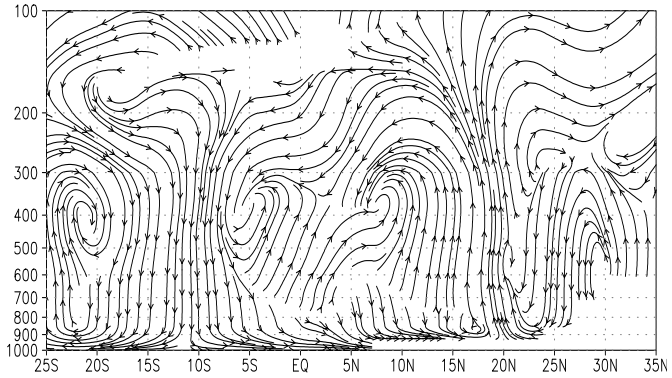

JJAS Hadley circulation averaged over 80–95 E
(Combination Expt.–ENSO Expt.)

c

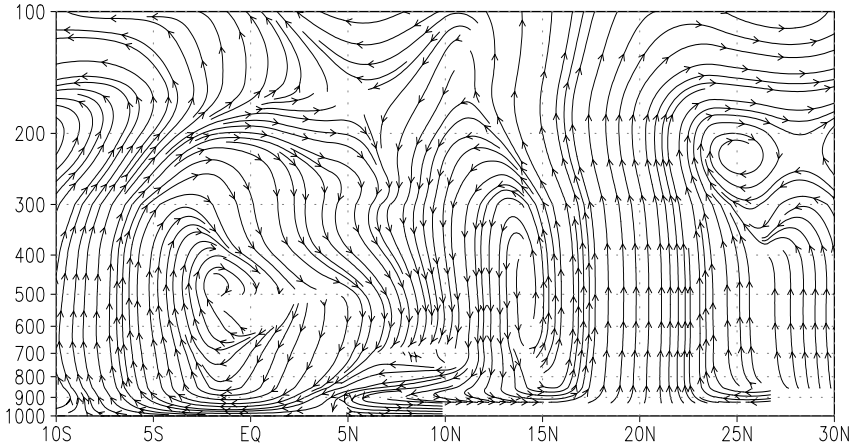

JJAS Hadley circulation averaged over 65–75 E
(Combination Expt.–ENSO Expt.)

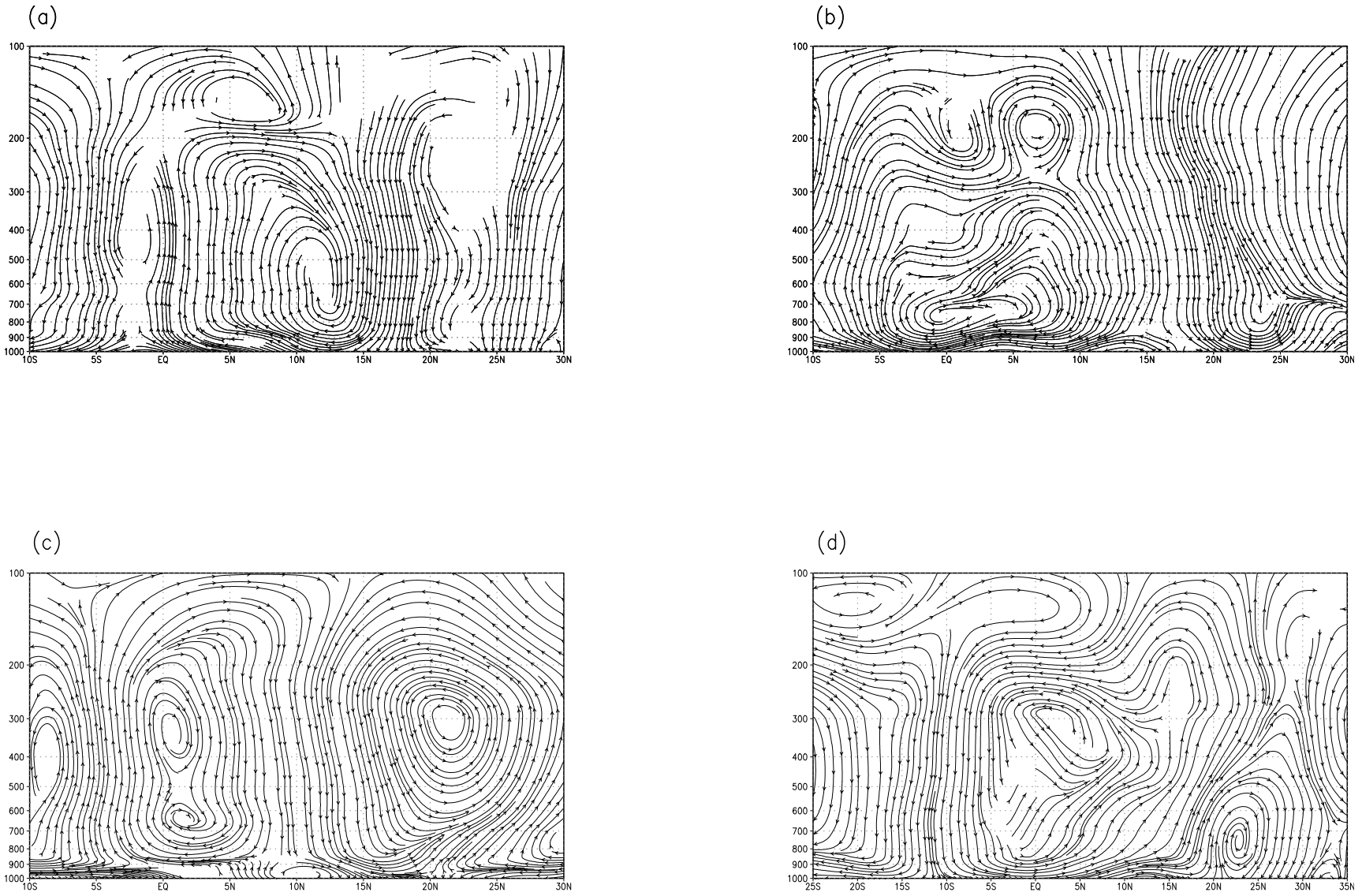

NCEP anomalous JJAS Hadley circulation streamlines (a) zonally averaged over 70ºE-85ºE during 1969 (b) zonally averaged over 70ºE-85ºE during 1987 (c) zonally averaged over 65ºE-75ºE during 1994 (d) zonally averaged over 80ºE-95ºE during 1994.

Correlation with land rain,temperature

From Saji & Yamagata, 2003

- Floods to the west, droughts to the east.
- Floods over the monsoon trough
- warmer temperatures and droughts over extratropics

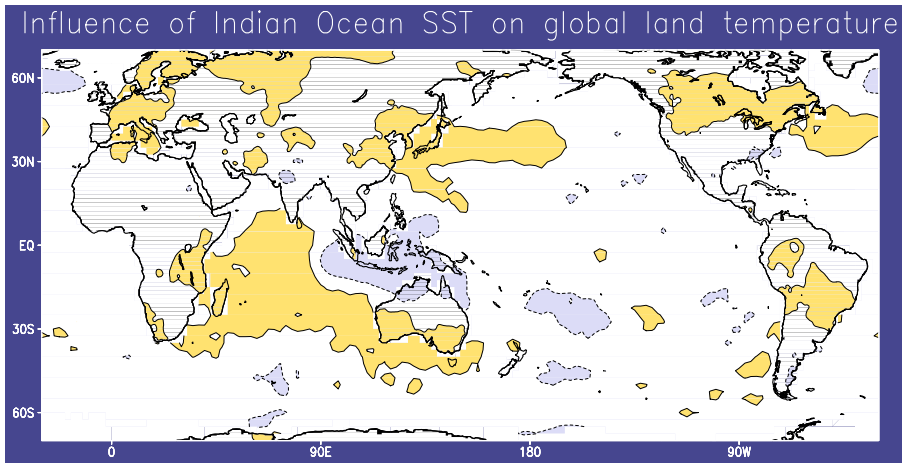

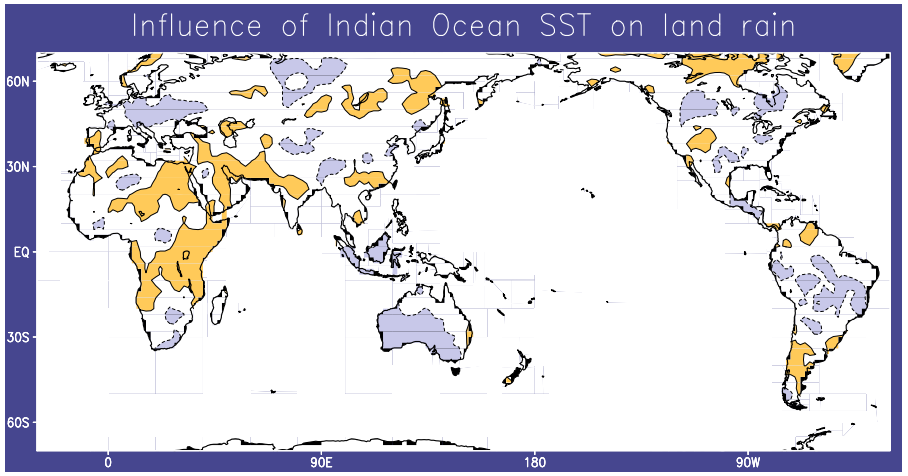

Relative impacts of IOD and ENSO on global temperature (Saji and Yamagata, 2003)

Table 2. Association of land temperature over selected regions with DMI and Nino3. p_d (p_n) is the correlation of temperature on DMI (Nino3), partialling the effects of Nino3(DMI); values in parenthesis are correlations using unfiltered data. Season: the season of largest association with DMI. Eq: equator

Region	Season	p_d	p_n
South Africa (15–25° E, 35–20° S)	SON	+0.49 (+0.43)	−0.04 (−0.09)
E Africa (25–45° E, 10° S–Eq.)	JJA	+0.49 (+0.39)	−0.28 (−0.14)
SE Europe (0–15° E, 30–40° N)	JJA	+0.45 (+0.36)	−0.22 (−0.14)
S Iran (55–65° E, 25–35° N)	SON	+0.45 (+0.30)	−0.21 (−0.05)
NE Asia (115–150° E, 39–45° N)	JJA	+0.55 (+0.51)	−0.40 (−0.31)
Papua New Guinea (135–150° E, 10–Eq.)	SON	−0.53 (−0.38)	−0.13 (−0.07)
N Australia (122–136° E, 21–15° S)	JJA	−0.51 (−0.39)	+0.00 (+0.03)
SW Australia (115–150° E, 40–25° S)	SON	+0.58 (+0.51)	−0.19 (−0.08)
North America (72–54° W, 42–53° N)	JAS	+0.57 (+0.34)	−0.71 (−0.54)
South America (70–40° W, 30–10° S)	ASO	+0.73 (+0.67)	−0.26 (−0.22)

$$pr_1 = \frac{r_{Y1} - r_{Y2}r_{12}}{\sqrt{(1 - r_{12}^2)(1 - r_{Y2}^2)}} \qquad (1)$$

n global

Table 3. Association of land rain over selected regions with DMI and Nino3. p_d (p_n) is the correlation of temperature on DMI (Nino3), partialling the effects of Nino3 (DMI); values in parentheses are correlations using unfiltered data. Season: the season of largest association with DMI

Region	Season	p_d	p_n
South Africa (20–30° E, 35–32° S)	SON	−0.50 (−0.30)	+0.30 (+0.20)
Angola (10–20° E, 20° S–10° N)	OND	+0.49 (+0.33)	−0.32 (−0.27)
Gabon (9–12° E, 6° S–2° N)	OND	+0.50 (−0.36)	−0.45 (+0.39)
Djibouti (41–44° E, 11–13° N)	SON	+0.52 (+0.44)	−0.10 (−0.06)
Ethiopia (32–46° E, 3–7° N)	SON	+0.60 (+0.51)	−0.17 (−0.10)
Somalia (41–46° E, 0–5° N)	SON	+0.60 (+0.56)	+0.11 (+0.11)
Uganda (29–35° E, 1° S–4° N)	SON	+0.53 (+0.50)	−0.32 (−0.30)
Democratic Republic of Congo (24–30° E, 10–2° S)	SON	+0.57 (+0.50)	−0.20 (−0.16)
Tanzania (30–40° E, 10–2° S)	SON	+0.67 (+0.64)	−0.02 (+0.03)
N Mozambique (35–40° E, 14–10° S)	SON	+0.42 (+0.31)	−0.02 (+0.04)
S Germany (8–15° E, 46–51° N)	ASO	−0.52 (−0.46)	+0.05 (+0.09)
Hungary (17–23° E, 44–48° N)	SON	−0.44 (−0.38)	+0.13 (+0.16)
Ukraine (24–34° E, 46–52° N)	SON	−0.53 (0.51)	+0.26 (+0.26)
Egypt (29–34° E, 26–31° N)	SON	+0.51 (+0.50)	+0.15 (+0.13)
S Pakistan (65–69° E, 24–27° N)	JAS	+0.46 (+0.40)	−0.46 (−0.43)
NW India (75–80° E, 20–26° N)	OND	+0.53 (+0.33)	−0.12 (+0.02)
Bhutan (89–92° E, 27–28° N)	JJA	−0.53 (−0.32)	+0.09 (−0.09)
Lhasa (89–94° E, 28–30° N)	JJA	−0.47 (−0.33)	+0.05 (+0.03)
S China (105–112° E, 25–29° N)	SON	+0.58 (+0.51)	+0.22 (+0.18)
Sri Lanka (80–82° E, 6–8° N)	SON	+0.49 (+0.48)	+0.14 (+0.16)
S Sumatra (100–106° E, 6° S–Eq.)	JAS	−0.80 (−0.75)	−0.19 (−0.12)
Java (106–115° E, 8.5–6° S)	SON	−0.65 (−0.56)	−0.33 (−0.27)
Kalimantan (110–118° E, 4° S–5° N)	SON	−0.55 (−0.48)	−0.50 (−0.43)
Sulawesi (119–123° E, 6–1° S)	ASO	−0.52 (−0.40)	−0.62 (−0.51)
New Guinea (134–14&1° E, 10–2° S)	JAS	+0.10 (+0.15)	−0.71 (−0.71)
SW Australia (115–130° E, 34–20° S)	JJA	−0.58 (−0.58)	+0.24 (+0.25)
Central America (97–87° W, 14–19° N)	OND	−0.39 (−0.35)	+0.12 (+0.10)
W USA (112–106° W, 35–39° N)	ASO	+0.46 (+0.39)	−0.16 (−0.13)
Quebec (80–74° W, 49–53° N)	JJA	−0.54 (−0.40)	+0.33 (+0.07)
Venezuela (66–63° W, 5–10° N)	ASO	+0.65 (+0.61)	−0.72 (−0.68)
S Brazil (70–50° W, 25–15° S)	ASO	−0.57 (−0.61)	+0.52 (0.55)
Uruguay (57–52° W, 34–31° S)	JJA	+0.55 (0.42)	−0.23 (−0.16)
S Chile (72–70° W, 36–33° S)	ASO	+0.52 (+0.41)	+0.37 (+0.33)
S Argentina (70–66° W, 45–41° S)	JJA	+0.46 (+0.42)	+0.08 (+0.11)

Extratropical teleconnections of the IOD

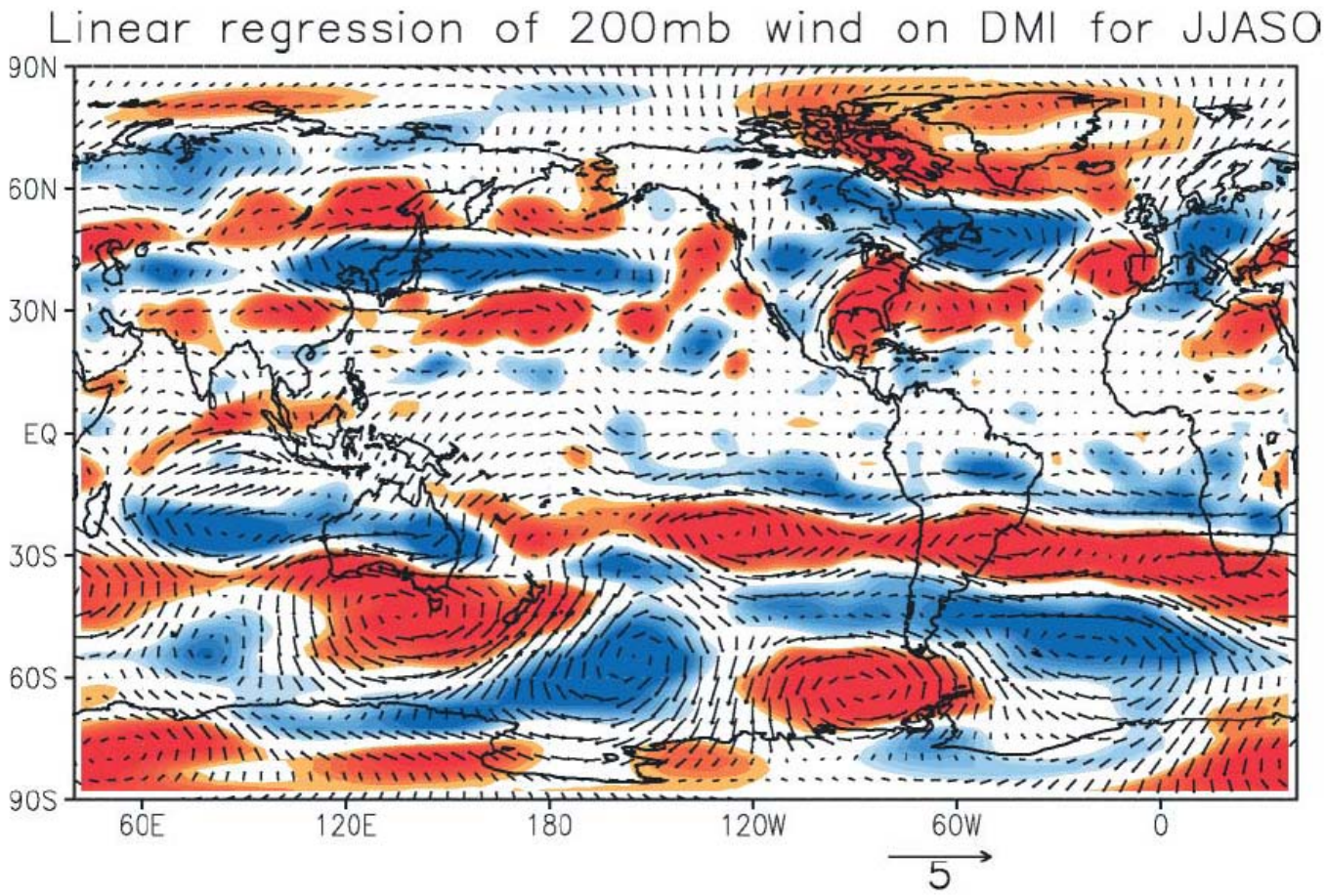

Fig. 20. Partial regression of 200 mb wind anomaly on DMI independent of Nino3 (vectors). Blue (red) shading: negative (positive) curl associated with this wind field

Saji and Yamagata, 2003

Extratropical teleconnections of the IOD

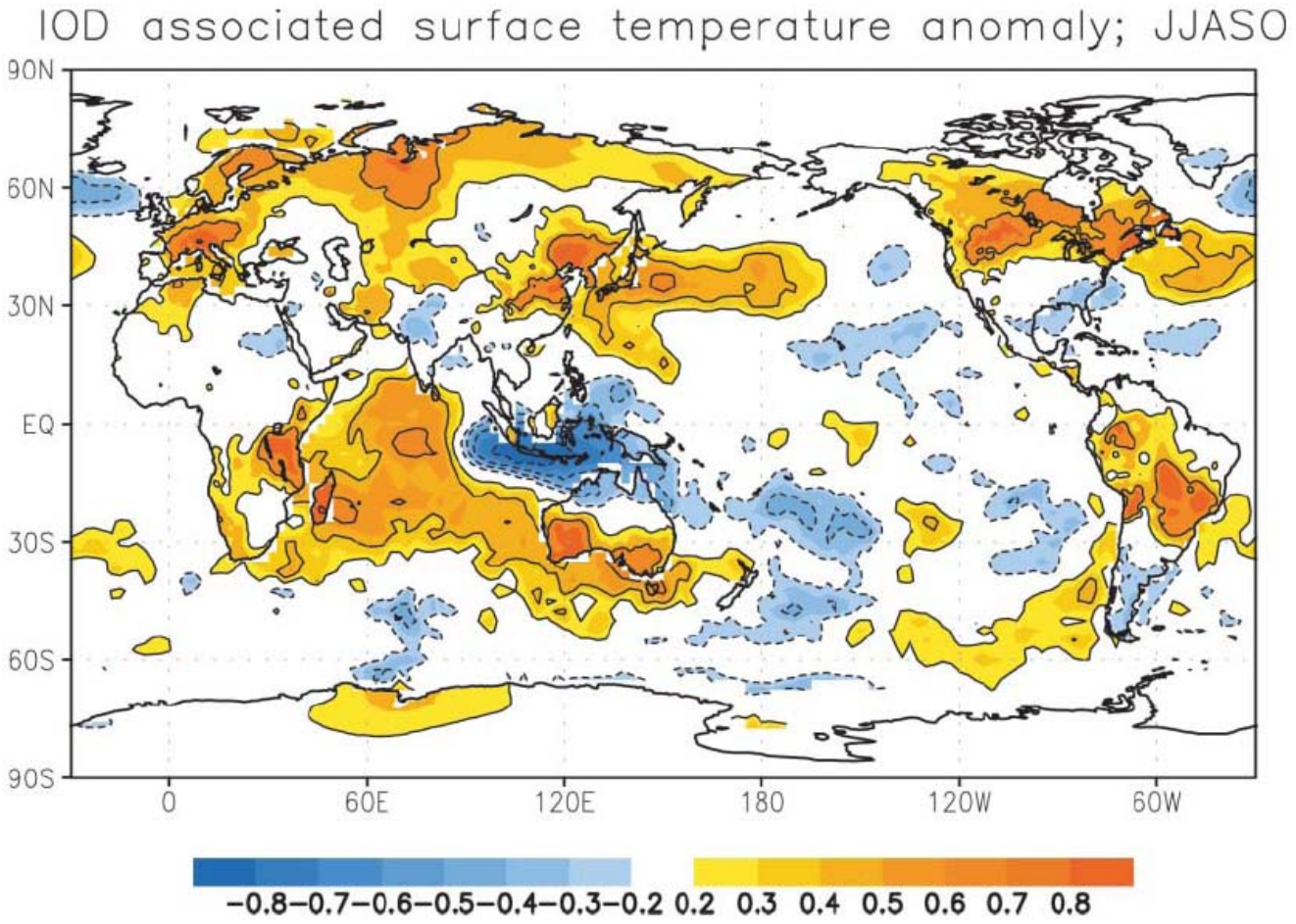

Fig. 21. Partial correlation of land and sea-surface temperature on DMI independent of Nino3 during JJASO

Saji and Yamagata, 2003

The relevance of the IOD to East Asia: The 1994 case study

IOD and ENSO impacts on East Asian temperature (Composite method; Saji and Yamagata, 2003)

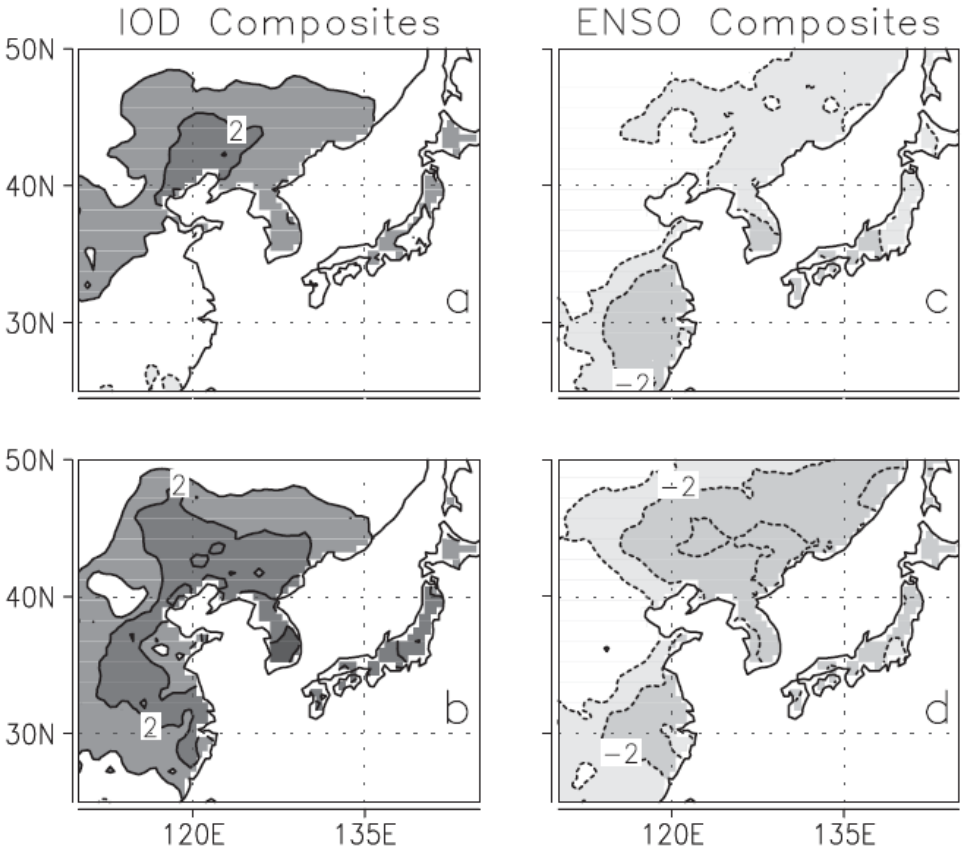

Fig. 2. Composite surface temperature anomaly over NE Asia during JJAS for (a) 19 IOD events, (b) 11 ENSO-independent IOD events, (c) 20 ENSO events and (d) 12 IOD-independent ENSO events. The composite anomaly was normalized by the standard deviation of rain during OND. Contours given at ±1, ±2, etc.

Table 1. Years of IOD and ENSO used in the study. Independent IOD and ENSO events and co-occurring IOD-ENSO events are given

Positive IOD	El Niño	Negative IOD	La Niña
Independent IOD and ENSO events			
1961	1965	1958	1967
1967[a]	1969	1960	1970
1977	1976	1974	1973
1983	1986	1989	1978
1994	1987	1992	1984
		1993	1985
			1988
Co-occurring IOD-ENSO events			
1963	1963	1964	1964
1972	1972	1971	1971
1982	1982	1975	1975
1997	1997	1996	1996

[a]Positive IOD event co-occurring with La Niña

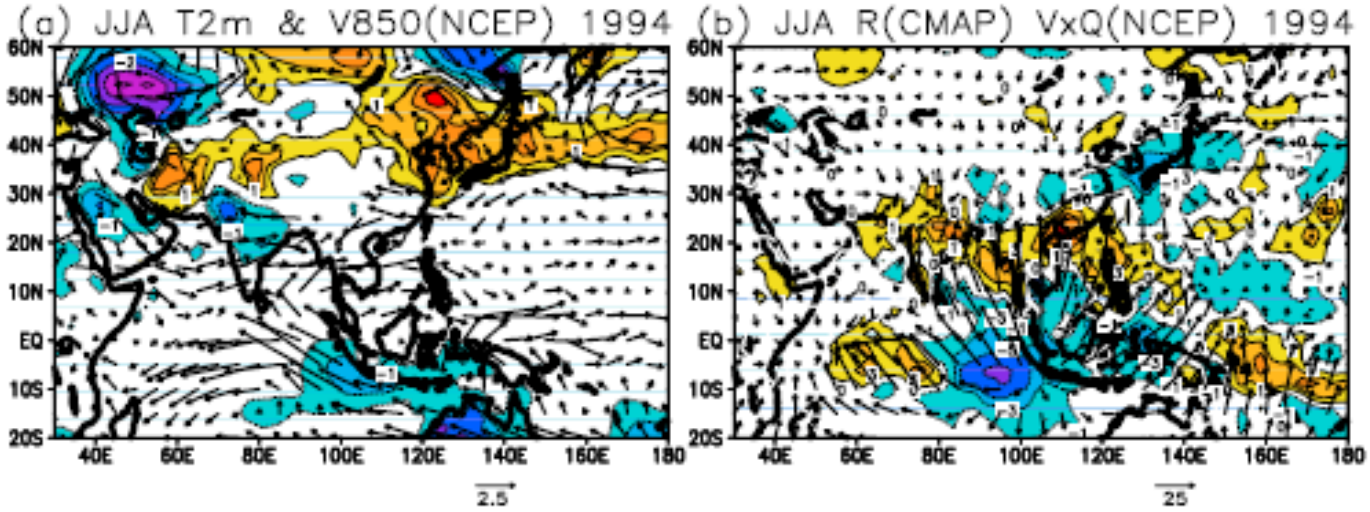

Figure 1. (a) The JJA mean anomalous air temperature at 2 m above the earth surface (contour intervals: 0.5°C), along with the wind at 850 hPa (in $m \cdot s^{-1}$) during 1994. (b) The anomalous precipitation (contour intervals: 1 $mm \cdot d^{-1}$) and the anomalous water vapor flux (in $Kg \cdot m^{-1} \cdot s^{-1}$) which is vertically integrated from the earth surface up to 300 hPa (shown with vectors).

Guan and Yamagata (2002)

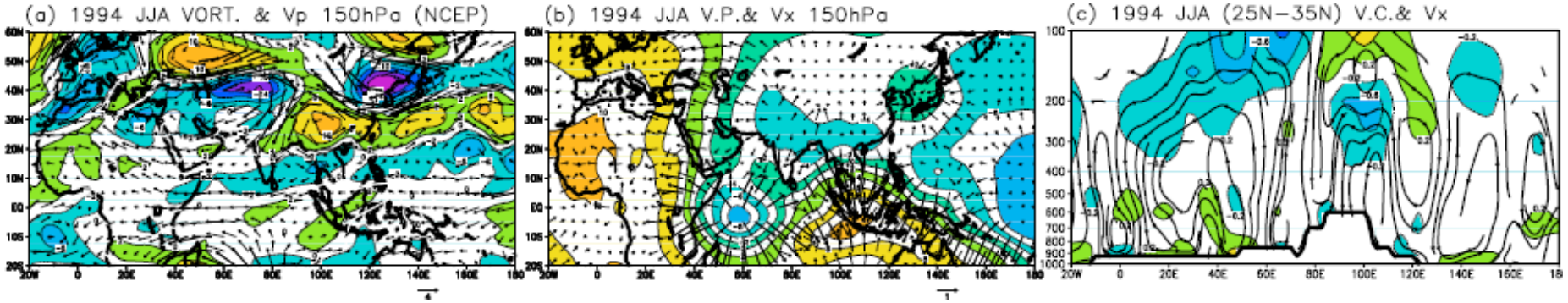

Figure 2. (a) JJA mean anomalous vorticity (to be multiplied by $1 \times 10^{-6}\ s^{-1}$) along with the rotational wind ($m \cdot s^{-1}$) at 150 hPa in 1994. (b) JJA mean velocity potential along with the divergent wind ($m \cdot s^{-1}$) at 150 hPa in 1994. The contour interval is $4 \times 10^{-5}\ m^2 \cdot s^{-1}$. (c) JJA mean zonal-vertical circulation averaged over (25°N–35°N). The contours denote the zonal component of the divergent wind with contour interval of $0.2\ m \cdot s^{-1}$.

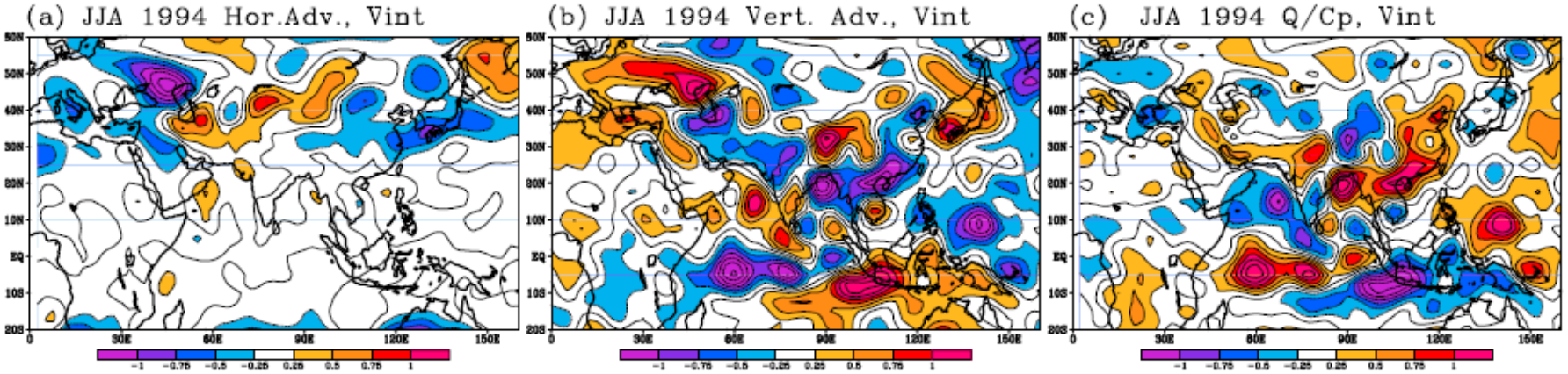

Figure 3. JJA mean vertically integrated quantities for 1994. (a) The anomalous horizontal advection of temperature, (b) the anomalous vertical advection of potential temperature, and (c) the anomalous diabatic heating rate. All these quantities are vertically averaged over pressure from surface to 100 hPa. The unit is $°C \cdot d^{-1}$.